UNCLASSIFIED

SECURITY CLASSIFICATION OF THIS PAGE *(When Data Entered)*

REPORT DOCUMENTATION PAGE

READ INSTRUCTIONS BEFORE COMPLETING FORM

1. REPORT NUMBER: AFFDL-TR-74-138	2. GOVT ACCESSION NO.
3. RECIPIENT'S CATALOG NUMBER	
4. TITLE *(and Subtitle)*: ANALYSIS AND SIMULATION OF VARIABLE THROTTLE/ENERGY MANAGEMENT CONCEPTS FOR FIGHTER AIRCRAFT	5. TYPE OF REPORT & PERIOD COVERED: Final 29 June 73 - 1 Oct 74
	6. PERFORMING ORG. REPORT NUMBER
7. AUTHOR(s): G. G. Grose, R. J. Landy, R. G. Marsh and R. D. Turner	8. CONTRACT OR GRANT NUMBER(s): F33615-73-C-3130
9. PERFORMING ORGANIZATION NAME AND ADDRESS: McDonnell Aircraft Company, McDonnell Douglas Corporation, P. O. Box 516, St. Louis, Mo. 63166	10. PROGRAM ELEMENT, PROJECT, TASK AREA & WORK UNIT NUMBERS: Project: 1987, Task: 02, Work Unit: 08
11. CONTROLLING OFFICE NAME AND ADDRESS: Air Force Flight Dynamics Laboratory, Air Force Systems Command, Wright-Patterson AFB, Ohio 45433	12. REPORT DATE: November 1974
	13. NUMBER OF PAGES
14. MONITORING AGENCY NAME & ADDRESS *(if different from Controlling Office)*	15. SECURITY CLASS. *(of this report)*: Unclassified
	15a. DECLASSIFICATION/DOWNGRADING SCHEDULE

16. DISTRIBUTION STATEMENT *(of this Report)*

Approved for public release; distribution unlimited.

17. DISTRIBUTION STATEMENT *(of the abstract entered in Block 20, if different from Report)*

18. SUPPLEMENTARY NOTES

19. KEY WORDS *(Continue on reverse side if necessary and identify by block number)*

Energy Management	Flight paths	Thrust control
Cruise	Control simulation	
Descent	Hybrid simulation	
Aircraft Interception	Displays	

20. ABSTRACT *(Continue on reverse side if necessary and identify by block number)*

The application of a modified Rutowski logic to mission throttle/energy management was extended, investigating additional types of mission segments and providing a means of logically integrating optimum segments into mission profiles. Measurable fuel savings through throttle modulation were predicted for a demonstration flight mission for the F-4E airplane. A flight path and throttle control system was designed for following the optimum paths. A hybrid simulation plan was prepared.

DD FORM 1 JAN 73 1473 EDITION OF 1 NOV 65 IS OBSOLETE

UNCLASSIFIED

SECURITY CLASSIFICATION OF THIS PAGE *(When Data Entered)*

FOREWORD

This report was prepared by McDonnell Aircraft Company, St. Louis, Missouri 63166 under USAF Contract Number F33615-73-C-3130. The objective of the investigation was to extend the application of the modified Rutowski logic for throttle/energy management, and to provide analytical and simulation studies of a throttle/energy management control concept which are needed for eventual flight test demonstration of a throttle/energy management control system.

This work was supported by the Control Systems Development Branch of the Flight Control Division of AFFDL, under Project No. 1987, "Develop Concept of Throttle/Energy Management by Analysis and Simulation". The work was performed as a part of task number 02 under the guidance of I. A. Carnegis, Major R. Limburg and R. E. Guth, AFFDL/FGL. This report was submitted by the authors in November 1974 and covers research in the period June 1973 to October 1974.

The program at McDonnell Aircraft Company was conducted by the Aerodynamics Department under the supervision of Mr. J. Pavelka, Branch Manager. Major contributors to the program were Messrs, G. G. Grose, Program Manager; Dr. R. J. Landy, Guidance and Control Mechanics, Group Engineer; R. G. Marsh, Guidance and Control Mechanics, Senior Engineer; Dr. R. D. Turner, Technical Specialist, Aerodynamics; and D. E. Kramer, Senior Group Engineer, Flight Test.

INTRODUCTION & SUMMARY

During a previous study conducted by MCAIR for the Air Force Flight Dynamics Laboratory (Reference 1) a mission throttle/energy management concept was developed. It was shown that throttle/energy management in the form of engine control and flight path selection can significantly improve performance of a mission segment in terms of fuel savings, time reduction, improved range, or a combination of any or all three. A method of determining the optimum throttle and flight path control was developed (the Modified Rutowski program, RUTO, Reference 2), and it was applied to a limited number of mission segments to show the performance benefits. Two throttle control system configurations were designed using onboard measured parameters to correlate propulsion performance.

The objectives of the present study are (a) to extend the application of the modified Rutowski logic by investigating additional types of mission segments and to provide means of logically integrating them into mission profiles, and (b), to provide analytical and simulation studies of a throttle/energy management control concept which are needed for eventual flight test demonstration of a throttle/energy management control system. These objectives were accomplished in five tasks:

Task I - Performance Comparison of Mission Profiles

Task II - Investigation of Throttle/Flight Path Control Techniques

Task III - Analysis of Flight Path and Throttle Control System

Task IV - Recommendation of Hybrid Simulation Study

Task V - Preparation of a Flight Test Plan and Program Schedule

The result of Tasks I-IV are reported in subsequent sections of this report. The results of Task V are covered in a separate Flight Test Plan report (Reference 3). In addition, a revised user's manual for the modified RUTO program with extended capabilities is published in Reference 4, and a user's manual for the program used for digital simulation of the throttle and flight path control systems designed in Task III is published in Reference 5.

In Task I (Section 1), the modified Rutowski logic (RUTO program) is extended for calculation of a complete mission history, including a succession of acceleration, cruise or dash, and descent segments. For long range intercept missions, involving a significant cruise or dash segment, a simple relation

is presented between the performance function to be optimized for cruise or dash segments and the performance function for the acceleration or descent segments. This is used to survey the range of possible range-time conditions at intercept for the F-4K, with the limitation of sufficient fuel for return. For long-range intercept of a specific incoming target, an optimum variable throttle mission can reach intercept over 100 nautical miles farther from base, but with the same combat fuel remaining, compared to a delayed takeoff followed by a minimum time acceleration at full throttle.

In Task II (Section 2) the F-4E airplane is selected for a study of control techniques which could be used for a possible flight test demonstration of a throttle/energy management control system. The F-15A aircraft would also be suitable, but the performance data for the F-4E was better documented at the time of this study. The control concept selected is to follow a precomputed, stored program of altitude, pitch angle and rate of change of specific energy, $\dot{E}_S$, as a function of specific energy, E_S. Flight demonstration cases are selected which will give an easily measurable fuel savings (over 650 pounds) for a variable throttle path compared to a fixed throttle path to the same final condition. For both good control and good performance, a procedure is defined to give as smooth a control program as will stay close to the optimum flight path.

In Task III (Section 3) a throttle/energy management control system is designed to follow the stored program for both flight demonstration cases with as few changes as possible to the existing F-4 control system and instrumentation. It uses the F-4E sensors, autopilot and radarscope display, and an autothrottle design used on the F-4J. It would require addition of a small digital computer and analog-digital interface units. A digital simulation of this system follows the desired path very closely (maximum altitude deviation of 300 feet in the transonic transition region). The desired end conditions are matched very closely, and the variable throttle case uses approximately 22% less fuel than the fixed throttle case.

In Task IV (Section 4) a plan for a manned simulator program is recommended, for selection of displays and evaluation of pilot workload and performance in partly automatic and fully manual control. The conclusions from this simulator study can then be used in design of the throttle/energy management system and displays.

The simulator could also be used to prepare for a flight test program by providing pilot familiarization with the displays and missions and testing of the software for energy management and display. A flight test plan has been recommended under Task V of this study and is published separately (Reference 3).

TABLE OF CONTENTS

TABLE OF CONTENTS (CONTD)

LIST OF ILLUSTRATIONS

LIST OF ILLUSTRATIONS (CONT'D.)

LIST OF ILLUSTRATIONS (CONT'D.)

LIST OF ILLUSTRATIONS (Cont'd)

LIST OF TABLES

SECTION 1

PERFORMANCE COMPARISON OF MISSION PROFILES (TASK I)

The modified Rutowski method developed in a previous contract (Reference 1) produced performance information for acceleration, cruise, dash and loiter mission segments, with the flight path and throttle control optimized to give the best value of a rather general performance function (ϕ) consisting of a weighted sum of fuel, range and time covered in the segment.

$$\phi = C_1 \ (\Delta \text{ Fuel}) - C_2 \ (\Delta \text{ Range}) + C_3 \ (\Delta \text{ Time})$$

Using the energy approximation, the computer program conducts a search at each energy level defined by combinations of altitude (h) and velocity (U) for a given value of specific energy (E_s), defined by

$$E_s = h + U^2/2g$$

The search determines the values of altitude and throttle setting index (S) for which the increment of ϕ to the next energy level will be as small as possible by finding the (h, S) values for a peak of $\dot{E}_s/\dot{\phi}$, where $\dot{E}_s$ is the rate of change of specific energy (also commonly called specific power, P_s). The flight path and throttle history connecting these optimum conditions will then give the optimum performance (defined by $\Delta\phi$ being a minimum) for acceleration between specified initial and final values of energy, E_s. Throttle/energy management consists of following optimum paths of this type, and it can give significant performance advantages compared to following "handbook" type paths.

Special cases which are well known are the "Rutowski" paths for minimum time to a given energy (max $\dot{E}_s$) and minimum fuel to a given energy (max $\dot{E}_s/w_f$), where w_f is fuel flow rate. These types of flight paths have been demonstrated by flight test, for fixed throttle operation. The modified Rutowski formulation provides a wider selection of optimum segments, and gives the additional benefits of variable throttle operation.

The modified Rutowski method is described in more detail in Reference 1. The reader should be familiar with that description, to understand the additional capabilities which are discussed in this section.

An objective of Task I, described in this Section, is to extend the applications of the modified Rutowski logic to complete the investigation of additional mission segments which will be components of complete missions. This includes optimum descent segments, from a higher to a lower energy level,

and additional cruise options, including optimum ϕ at specified Mach, at specified E_s, and Breguet cruise with a search for the optimum (h,M) for best specific range (max U/w_f) or best loiter (min w_f). The program was modified so that cruise, dash and loiter segments can be "flown", with time and range increments integrated by the program, and so that a succession of acceleration, cruise or dash, and descent segments can be calculated to give a complete mission history.

In Reference 1, the modified Rutowski method was applied to a limited number of mission segments to show the performance benefits for the F-4K airplane. In this study, additional segments and complete missions are calculated, using the same aerodynamic and engine data for the F-4K as in Reference 1.

Another objective of this task is to provide a rational method of joining optimum mission segments together to give complete mission profiles satisfying meaningful conditions on range, time or fuel at specified waypoints. Two approaches were investigated. In the first, the two (or more) mission segments that are to be joined are considered to be of equal rank. The logic that unites them is the statement of the overall problem in variational terms. The numerical technique selected was a parametric search by the Davidon method (Reference 6), with the parameters being the values of the cruise energy levels and durations, and the values of the weighting constants C_1, C_2, C_3 in the performance function, ϕ. The search would calculate a series of missions for trial values of these parameters to find the set giving optimum ϕ and specified end values of time, fuel or range. The program was modified for this purpose, but it was determined that the many mission calculations required would be excessively expensive.

In the second approach to mission profile integration, a cruise segment is regarded, on realistic grounds, as dominant and the acceleration or descent segments joining either end of it are considered to be "boundary layers". A very general formulation of this type was found for the "long-range intercept" problem of minimum fuel to a given range, time and energy. The formulation results in simple relations, with the basic information obtained from a curve of minimum fuel flow rate versus velocity for steady (cruise) conditions. It was applied to some rather complex mission cases.

All these additional capabilities have been incorporated into a new version of the RUTO program, documented in Reference 4.

1.1 Computation of Additional Mission Segments

A mission may consist of a series of mission segments which may be accelerations (increasing E_s), cruise or dash (constant E_s), and descent (decreasing E_s), with the particular combination of segments depending on the specified end conditions. In Reference 1, the optimization of accelerations was developed for a sufficiently general performance function that a variety of time, range and fuel end conditions could be satisfied. To optimize complete missions, a method of calculating descent and cruise segments with an equally general performance function was developed. The payoff function for descents is the same as for acceleration segments, a weighted sum of time, fuel and range, which is minimized for a given decrease in energy. Results are presented in Section 1.1.1. The payoff for cruise and descent segments is a weighted sum of time and range, to be minimized for a given amount of fuel used. Results are shown in Section 1.1.2, and a discussion is given of the relation of the weighting constants in cruise or dash to those in the acceleration and descent segments of a mission. Methods of combining segments into a complete mission will be discussed in Section 1.2.

1.1.1 Descent - The F-4K engine data has been extended to lower throttle settings and higher altitudes for calculation of descent segments. To reduce the table size with the additional engine data, values of the ratios of gross thrust, ram drag and fuel flow to atmospheric pressure are stored in the tables to permit accurate interpolation over larger altitude increments.

The method used to calculate optimal descent segments is illustrated in Figure 1. This example uses a performance function to be minimized:

$$\phi = (\text{Fuel})_{\text{Descent}} - \left(\frac{w_f}{U}\right)_{\text{Cruise}} * (\text{Range})_{\text{Descent}} = \left(\frac{\dot{\phi}}{\dot{E}}\right) dE$$

where $\dot{\phi} = (w_f)_{\text{Descent}} - \left(\frac{w_f}{U}\right)_{\text{Cruise}} * U_{\text{Descent}}$

The best ϕ is obtained when $(\dot{\phi}/\dot{E})$ is maximized, for negative $\dot{E}$. This gives the maximum range for a given amount of fuel used, when combined with an optimum cruise segment. This is the same performance function previously used t find optimum climbs to cruise. Figure 1 shows values of energy rate ($\dot{E}$) and performance function rate ($\dot{\phi}$) calculated by the RUTO program in the search for the best throttle setting (S) and altitude (h) for the F-4K airplane at an energy level of 60,000 feet.

The best descent is obtained at the condition where the ratio $(\dot{\phi}/\dot{E})$ is at the maximum for negative $\dot{E}$. The graphical solution for optimum descent would be at the tangent from the origin to the envelope of attainable values of $\dot{E}$ versus $\dot{\phi}$, as shown in the figure. (The corresponding condition used to find the best ascent condition is the maximum of $(\dot{E}/\dot{\phi})$, for positive $\dot{E}$). The RUTO program makes a series of one-dimensional peak searches versus altitude at constant throttle setting to give a set of peak $(\dot{\phi}/\dot{E})$ values. When the throttle setting is close to the optimum value, the peak at constant S is close to the envelope curve, and the locus of peaks gives the same optimum value as the envelope curve. A nonlinear interpolation of peak $(\dot{\phi}/\dot{E})$ versus S is made to determine the value of S for optimum $(\dot{\phi}/\dot{E})$, and an interpolated value of h is determined for that S value.

For the case shown in Figure 1, this method works very well, as the three S values around the optimum all have peaks close to the envelope curve. At higher S values, however, the peak at constant S is not close to the envelope, but is at the maximum altitude, corresponding to $C_{L_{MAX}}$. The change to this different type of peak occurs near $\dot{\phi} = 0$, as indicated in the figure. At lower values of E_s, the optimum occurs close to the abrupt change between the two types of peak. This causes difficulty in the interpolation for optimum S and h.

Figure 2 shows the descent flight path calculated for this example. The descent path is good down to an energy level near the optimum cruise condition. At lower energy levels, the path is a meaningless interpolation between the two types of peak. The solution to this difficulty is simple. Previously, the list of throttle settings (S) at which the program maximized the values of $\dot{\phi}/\dot{E}$ was limited to the S values at which data was stored in the engine tables, to avoid inaccuracies due to linear interpolation. The difficulty occurred because, at low E_s, the peak of $\dot{\phi}/\dot{E}$ at constant S was not close to the envelope of attainable values at enough S values to properly determine the optimum condition. It was found that if the peak search was made at additional intermediate S values, enough points close to the envelope were obtained to give a good solution for the optimum condition. This requires only a change in the input data.

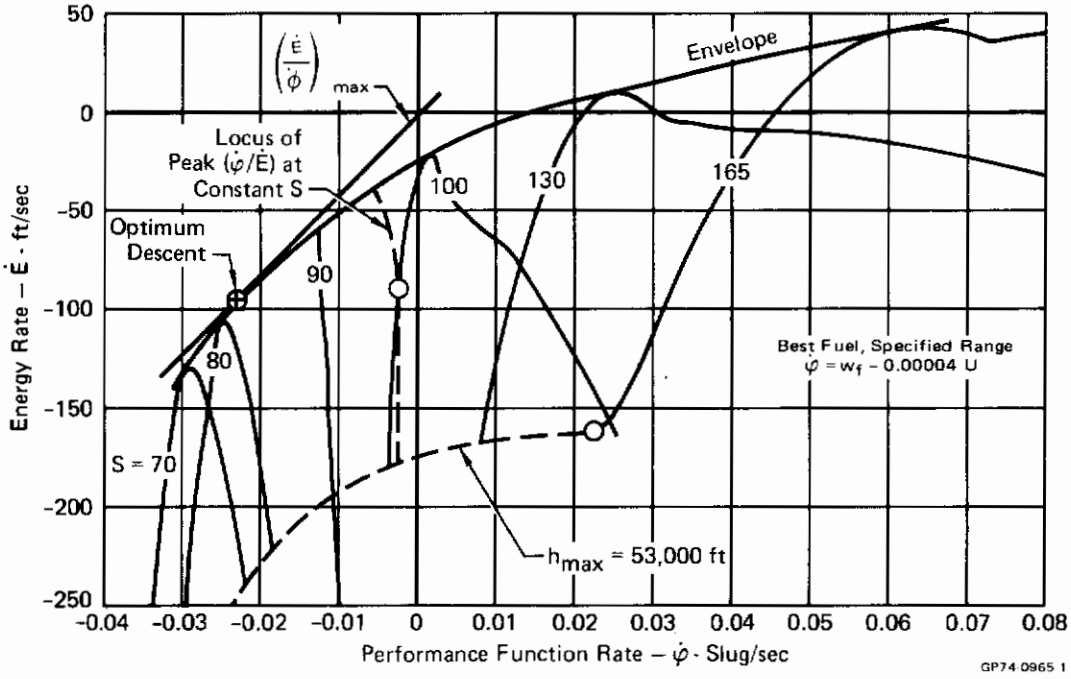

Figure 1 Graphical Solution for Optimum Descents S and h
F-4K
E_s = 60,000 ft

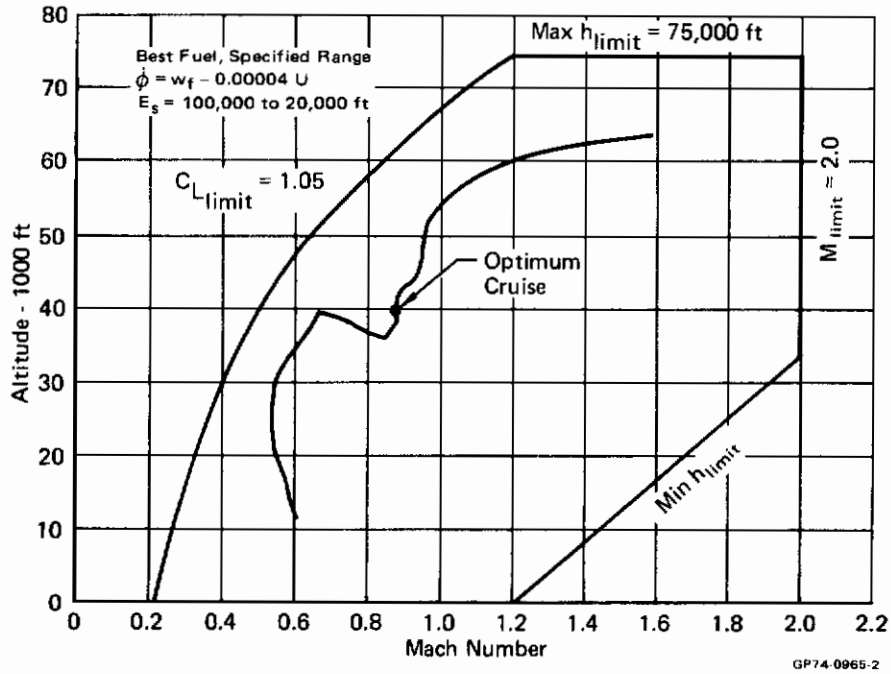

Figure 2 Optimum Descent Flight Path
F-4K

Figure 3 shows the weight versus range during descent from E = 100,000 ft for the maximum range-specified fuel case (solid curve) with the performance function ϕ of the previous example. Also shown for comparison (dotted line) is the case commonly used in fixed-throttle energy management of descents, where ϕ is selected to give maximum range for a specified change in E_s with the throttle setting fixed at idle. For this case

$$\dot{\phi} = -U$$

and the program maximizes $U/\dot{E}_s = W/(T-D)$. Note that for the power-off case, this gives the flight path for maximum L/D at constant E_s, a rule previously used in finding optimum descent for lifting reentry vehicles.

For evaluation of the benefit of variable throttle descent, the points at E_s = 5,000 in Figure 3 are joined to lines at the cruise specific range, to permit comparison at equal weight or range values. The maximum range-specified fuel case shows an advantage over the fixed throttle case, but it is only 35 pounds of fuel, or 4.4 miles range out of about 110 total, about 4% of the descent range. A similar comparison of the points at cruise E_s = 50,000 feet gives a 2 mile advantage, or again about 4% of the descent range. It is concluded that for conventional fighter aircraft, similar to the F-4K, there is no significant benefit from using variable throttle in descent. This conclusion may not apply to supersonic cruise aircraft such as the YF-12, however, as the range in descent is much larger.

Following the optimum flight path in descent is important. Figure 3 shows a curve for the extreme case, minimum range descent for a specified change in E_s. For this case

$$\dot{\phi} = U$$

and the path is at the minimum altitude limit and idle throttle setting. The descent does not use much fuel, but is inefficient at converting the initial energy into additional range. Patching on a cruise segment for a comparison at equal weight, this case has over 50 n. mi. less range, or a loss of nearly 50% of the available descent range.

Figure 4 compares the flight paths for the best fuel-spec. range case and the max. range-fixed throttle case. The Mach-altitude paths are identical

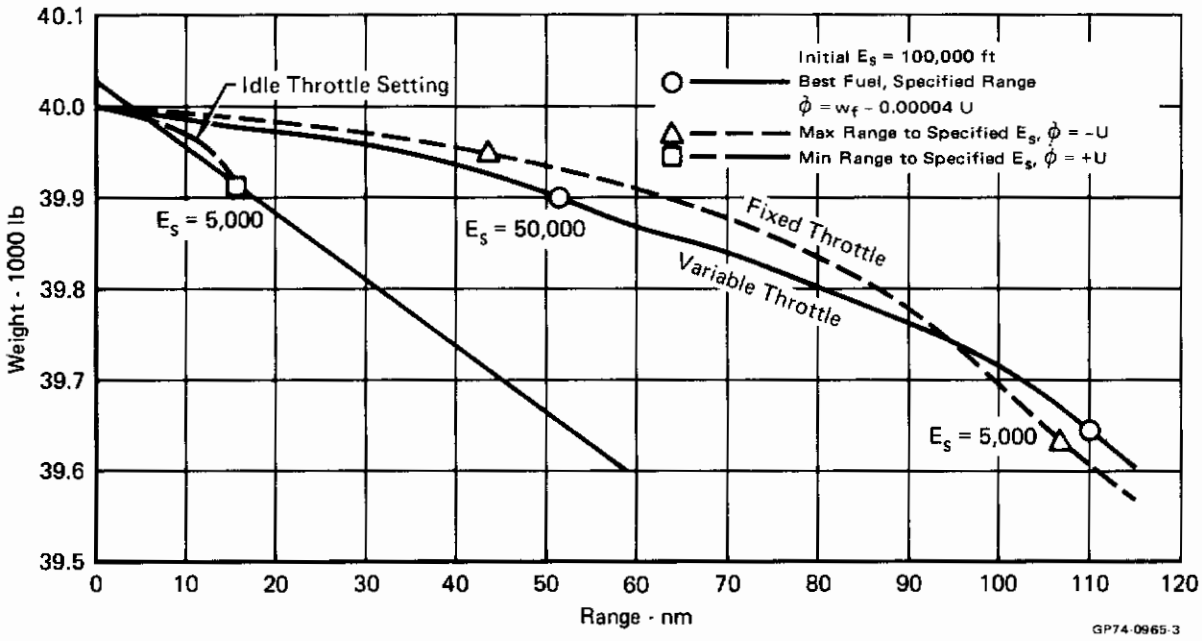

Figure 3 Optimum Descent Segments
F-4K
Weight vs Range

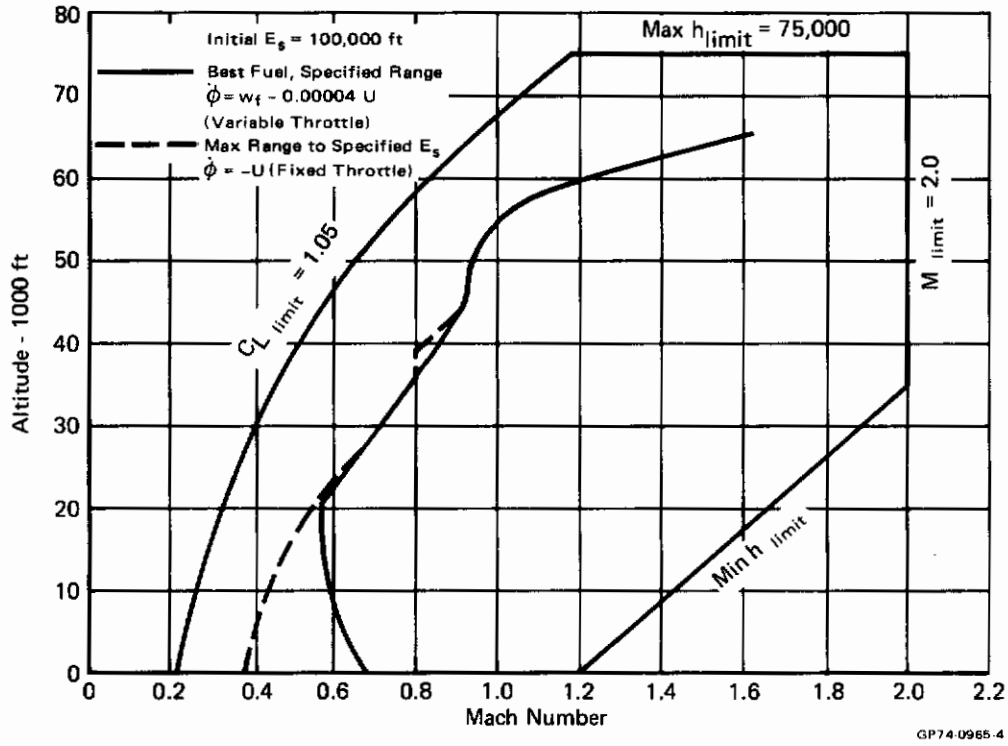

Figure 4 Optimum Descent Flight Paths
F-4K

except around 40,000 ft altitude, near optimum cruise energy, and at altitudes below 20,000 feet. The supersonic part of the path is above the A/B ceiling. The max range path below 40,000 ft altitude is quite close to the handbook descent at 250 knots EAS. For an actual F-4K airplane, the best fuel path at low altitudes would be closer to the max range path than shown, as the engine idle limit at low altitude is less than the value of S = 70 (70% rpm) which was the lower limit of the engine data used in the calculation. The Mach-altitude path for max L/D is a good approximation for optimum descent.

Figure 5 shows the optimum throttle setting variation for the best fuel-specified range case. The throttle varies at E_s values down to slightly below the cruise E_s = 50,000. The throttle is on the idle limit at low E_s. The mismatch in the two curves near E_s = 60,000 is the effect of the additional specified throttle settings on the search at low E_s, but there is no difference in the performance function ($\dot{E}/\dot{\phi}$) between the two curves.

Figure 6 shows the program for a potential throttle control parameter, flight path acceleration (FPA). The max range curve is for idle throttle, and the difference between the curves at high E_s is an indication of the measurement accuracy required to command the right throttle setting. At low E_s, the relatively large difference in FPA is due to the different flight paths, as both cases are on the idle throttle limit.

1.1.2 Additional Cruise Options - The following cruise options (for quasi-steady cruise, loiter or dash) which are now in the RUTO program are:

(a) INDSEL = 2 - Time history of flight produced; quasi-steady flight; Mach number and altitude chosen to maximize:

a. U/w_f (LOITER = 1)

b. $-w_f$ (LOITER =2)

c. $C_1W_f - C_2U + C_3$ (LOITER = 3)

(b) INDSEL = 3 - Point performance; for given altitude and weight, Mach number is chosen to maximize the payoff functions listed above; or, for given Mach and weight, altitude is chosen to maximize the payoff functions.

(c) INDSEL = 4 - Time history of flight produced; can be used only in conjunction with acceleration; for given weight and energy level, the altitude is chosen to maximize:

$$C_1w_f - C_2U + C_3$$

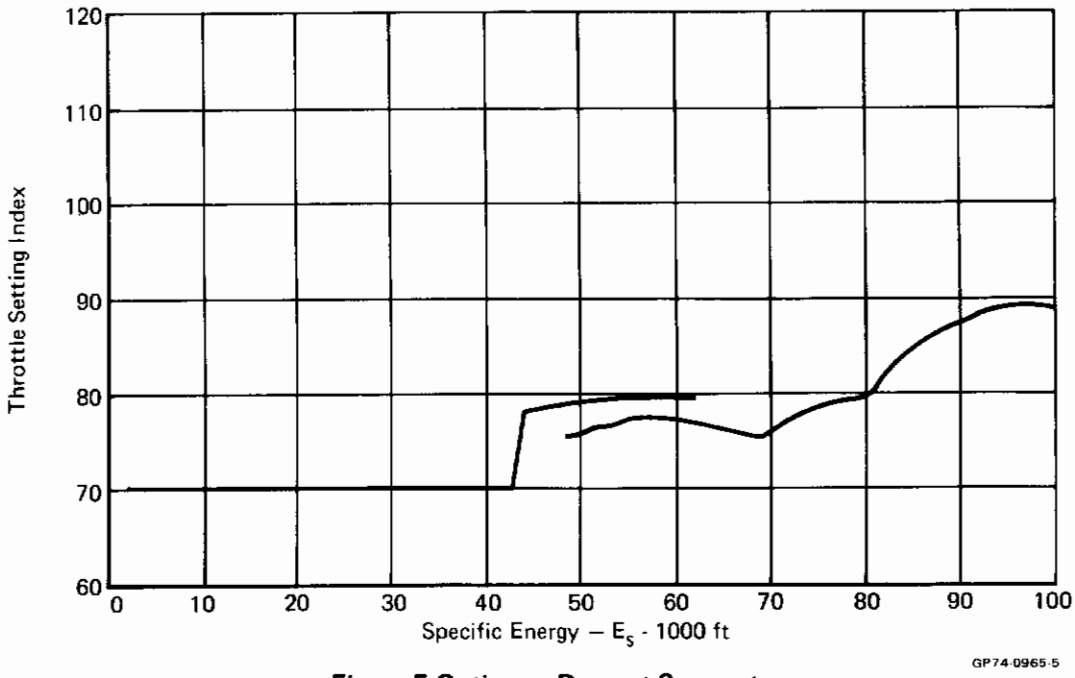

Figure 5 Optimum Descent Segment
F-4K
Throttle Setting
Best Fuel, Specified Range

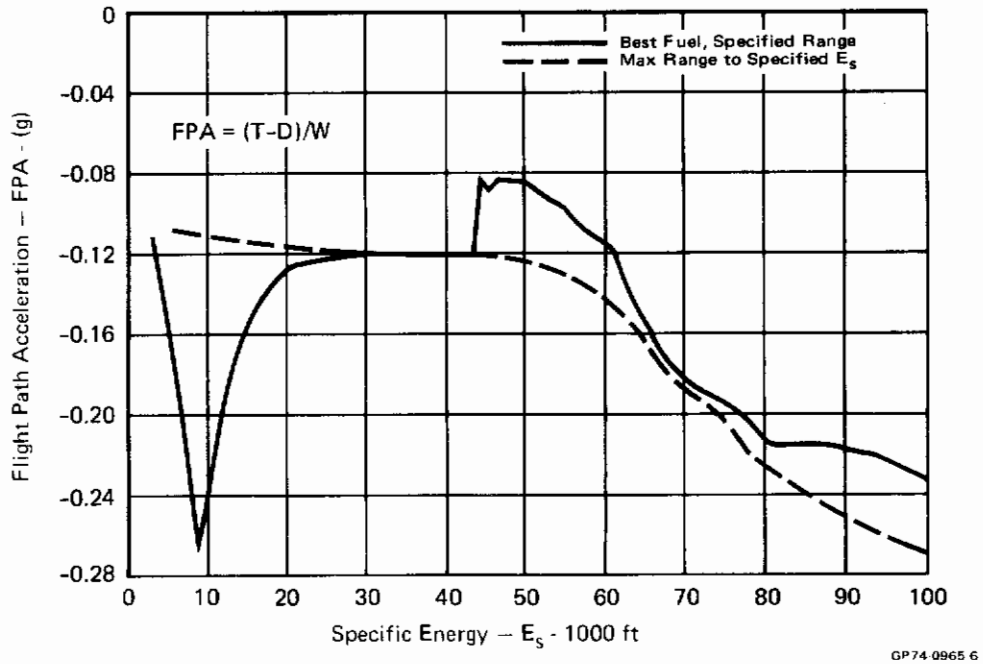

Figure 6 Optimum Descent Segment
F-4K
Flight Path Acceleration

The INDSEL = 2 option, particularly with the mixed performance function (LOITER = 3) is for use in the approach to integration of segments into mission profiles which considers the problem as dominated by the cruise or dash, so the acceleration segments are treated as boundary layers which inherit the weighting constants from a dash segment which reaches the desired end conditions. Figure 7 shows quasi-steady optimum dash performance generated by varying the C_2 constant in this option. This is the same as optimizing the flight condition for

$$\min \dot{\phi}_{cr} = \dot{w}_f - K_{cr} U_{cr}$$

for a range of values of K_{cr}. Any one of these dash segments of a selected duration, in combination with the appropriate acceleration segment, will give the resulting end conditions of range and time with minimum fuel used. It is shown in Section 1.2.1 that the appropriate acceleration segment to be combined with a given dash segment can be determined by optimizing the payoff function

$$\max PAY_E = \frac{\dot{E}}{\dot{\phi}} = \dot{E}/(C_{1_E} w_f - C_{2_E} U + C_{3_E})$$

with the values of the constants given by the dash segment performance as

$$C_{1_E} = \frac{1}{K_{cr}}, \quad C_{2_E} = 1, \quad C_{3_E} = -\dot{\phi}_{cr}/K_{cr}$$

The values of these weighting constants for the F-4K are given in Figure 8. A family of these optimum acceleration segments, with a final or combat energy of E_{sF} = 100,000 feet, have been calculated for the F-4K, to be matched with dash segments of special interest. These cases are:

a. K_{cr} = .00004 - The dash segment is at the flight condition for maximum specific range, and the overall acceleration-dash mission gives maximum range for a specified final weight. The constants of the performance function are: C_{1_E} = 25,000, C_{2_E} = 1, C_{3_E} = -90.

b. K_{cr} = .00019 - This corresponds to the straight line segment of Figure 7, connecting subsonic and supersonic dash conditions. A combination of subsonic and supersonic dash segment durations can be selected to give an average U_{cr} anywhere in the range of 900 to 1650 ft/sec. permitting intercept of a corresponding range of target conditions. The constants of the performance function are:

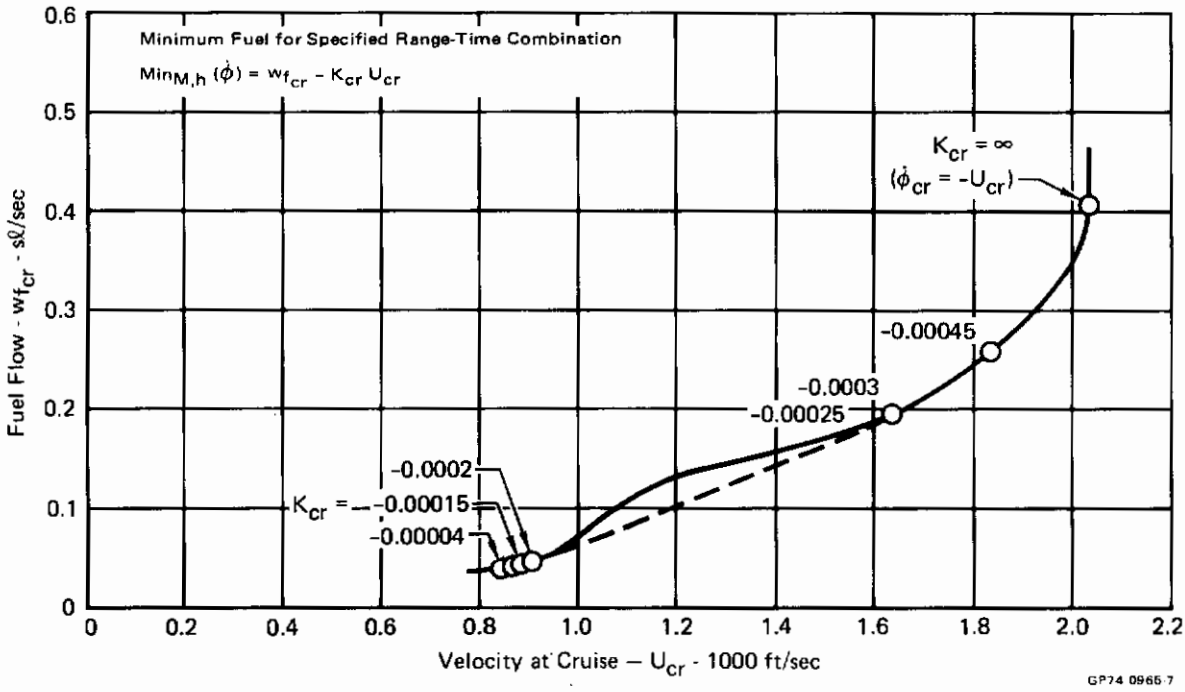

Figure 7 Quasi-Steady Optimum Dash
F-4K

$C_{1_E} = 5263$, $C_{2_E} = 1$, $C_{3_E} = 700$.

c. $K_{cr} = \infty$ - The dash segment is at U_{max}, and the acceleration-dash mission gives maximum range in a specified time. The constants of the performance function are: $C_{1_E} = 0$, $C_{2_E} = 1$, $C_{3_E} = 1985$.

The calculation of case b showed that it is necessary to account for the lower weight at which the higher U_{cr} conditions are reached. The previous dash performance calculations were for a constant weight. The constants of case b account for this, and differ slightly from those given in Figure 8.

Figure 9 shows the acceleration flight path for these cases. The dash conditions are indicated by the symbols. Case a is essentially identical to the optimum climb-to-cruise case calculated in Reference 1, with a subsonic climb to cruise at intermediate throttle, then increasing to a supersonic acceleration at max A/B. Case c is close, but not identical, to the max range-specified time case calculated in Reference 1, with a max A/B acceleration to dash at U_{max} at the final energy. Case b is an essentially new type of path, with a modulated A/B climb to a subsonic dash condition, a max A/B acceleration to a supersonic dash at 1.7 Mach and ceiling altitude, and a max A/B acceleration to final energy.

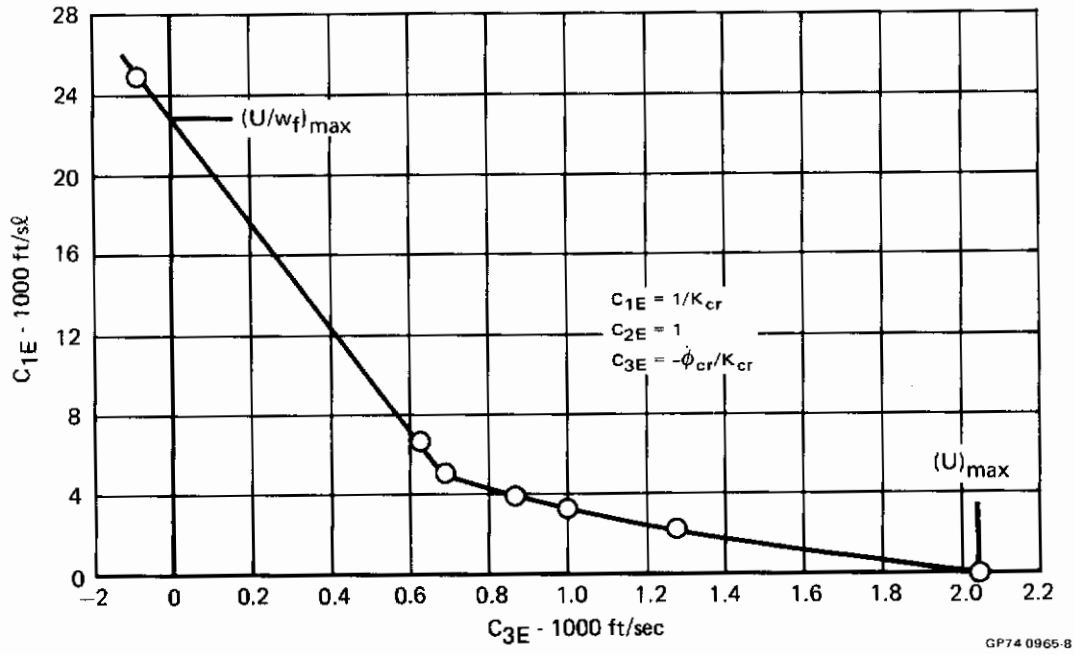

Figure 8 Weighting Constants for Optimum Energy Transition
F-4K
Long-Range Intercept Mission
Weight = 40,000 lb

The use of the family of matching dash and acceleration segments to give the total mission performance to specified target conditions is described in Section 1.2.

The INDSEL = 4 option is for use in the approach to integration of segments into mission profiles which uses a parameter search method (Davidon) to vary the segment lengths and weighting constants for optimum mission performance. One parameter varied is the energy level at dash; this option optimizes the altitude of the dash segment at the given energy level.

1.2 Integration of Segments into Mission Profiles

1.2.1 Long Range Intercept - A class of missions of current interest is the long range intercept, for which the requirement is to intercept a target aircraft at a long enough range that a combination of a dash or cruise segment and an acceleration segment to the combat energy level is required. It is desirable to reach the intercept point with as much fuel remaining as possible, in order to increase the time in combat, and to increase the range at inter-

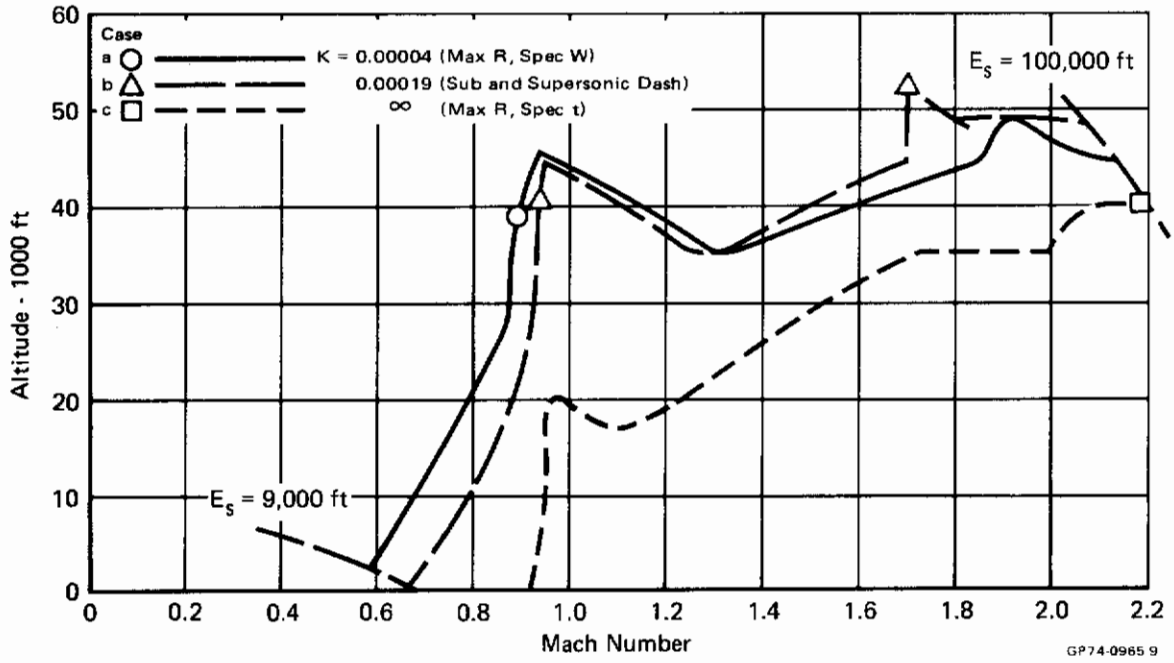

Figure 9 Flight Paths for Optimum Acceleration to E_s = 100,000 ft
F-4K
Long Range Intercept

cept of targets (specified by initial range, speed and altitude) that could be intercepted with fuel remaining for combat and return to base.

In the past, no technique was available for solving this problem directly in the general case. Instead, two special cases were usually solved:

a. Time-critical, consisting of a minimum time acceleration to combat energy, followed by a max A/B dash at U_{max}. This is for fast, short-range targets.

b. Fuel-critical, consisting of a cruise at best specific range, followed by a minimum fuel acceleration to combat energy. The acceleration might have a two-position throttle schedule, with an intermediate power subsonic climb and a max A/B supersonic acceleration. This is for slow or long-range targets.

For intermediate cases, one of the two types of missions was selected, and the cruise or dash was continued long enough to reach intercept, but the fuel used was not optimized. This is the type of information that has been available from handbooks and from studies of on-board computation and display of energy management paths.

The long range intercept problem is the type that is dominated by the quasi-steady cruise or dash segment. The energy transition (climb or acceleration) segments at either end can be treated as boundary layers on the dash segment, which take the values of the Lagrange multipliers or the weighting constants in the performance function from the quasi-steady arc solution which satisfies the end conditions of range and time with minimum fuel used. This is one of the two types of mission profile integration investigated in this task.

The condition for optimum matching of the energy transition and dash segments is based on geometric reasoning.

The set of quasi-steady or dash solutions which give the least fuel used (ΔF_{cr}) for a given range (ΔR_{cr}) and time (ΔT_{cr}) are found by optimizing the function, ϕ_{cr}, for the appropriate weighting constant, K_{cr}, where

$$\min \phi_{cr} = \Delta F_{cr} - K_{cr} \Delta R_{cr}$$

This occurs at the Mach-altitude condition for

$$\min \dot{\phi}_{cr} = w_{f_{cr}} - K_{cr} U_{cr}$$

The RUTO cruise option for INDSEL = 2, LOITER =3 maximizes the function

$$\max PAY_{cr} = + C_{1_{cr}} w_f - C_2 U + C_3$$

Since $\min \dot{\phi}_{cr} = \max (-\dot{\phi}_{cr})$, we may set

$$\dot{\phi}_{cr} = -PAY_{cr}$$

and the values of the constants are

$$C_{1_{cr}} = -1,\ C_{2_{cr}} = -K_{cr},\ C_{3_{cr}} = 0$$

Figure 7 shows the optimum dash solutions for the F-4K at 40,000 lb gross weight. By comparing the above equation for $\dot{\phi}_{cr}$ with Figure 7, it is seen that K_{cr} is the slope of a straight line tangent to the envelope of cruise solutions from below, and $\dot{\phi}_{cr}$ is the intercept of this line with the vertical ($w_{f_{cr}}$) axis. The curve is generated from the solutions for various values of K_{cr}. Special cases are loiter or min w_f ($K_{cr} = 0$), max specific range or U/w_f ($\dot{\phi}_{cr} = 0$), and U_{max} dash ($K_{cr} = \infty$). (For U_{max}, the constraints are

$$C_{1_{cr}} = 0,\ C_{2_{cr}} = -1,\ C_{3_{cr}} = 0$$

and the value of $PAY = -\dot{\phi}_{cr}/K_{cr}$).

The envelope of possible cruise solutions can also be found by minimizing $w_{f_{cr}}$ versus altitude at constant values of U_{cr}, using the INDSEL = 3 option. It is found that the envelope is not convex from below for the F-4K, and a better solution is obtained by a straight line tangent to the envelope curve at two points spanning the concave section as in Figure 7, between U_{cr} = 950 and 1600, and for a slope of K_{cr} = .000205. The performance at a point on this straight line segment is obtained by flying two dash segments, at the subsonic and supersonic velocities at either end of the line, with the time at each velocity ratioed to give the selected average U_{cr}.

The mission from the initial loiter or takeoff energy level to the final combat energy will consist of two energy transition segments, with a dash segment between them at the dash value of E_s. Exceptions are: (a) for $U_{cr} = U_{max}$, for which the dash E_s = combat E_s, and the dash is at the end of a single energy transition segment, and (b) for U_{cr} on the straight line segment of Figure 7, for which there will be three energy transition segments, with subsonic and supersonic dash segments between them at the proper energy levels.

To simplify the cruise calculations, it is assumed that cruise performance is a sufficiently weak function of gross weight that the results in Figure 7 can be used for all the dash segments, without predetermining the weight at the start of the dash. It is further assumed that the effect of the weight change during the dash can be neglected, and a particular cruise segment will be a straight line in a coordinate system with axes ΔF_{cr}, ΔR_{cr}, ΔT_{cr}. The family of optimum cruise solutions will form a conical surface, with a vertex at the origin. A plane ($\Delta F_{cr} = 1$) cuts the conical surface to form a curve of

$$\left[\frac{\Delta R_{cr}}{\Delta F_{cr}} = \left(\frac{U}{w_f}\right)_{cr}\right] \quad \text{versus} \quad \left[\frac{\Delta T_{cr}}{\Delta F_{cr}} = \left(\frac{1}{w_f}\right)_{cr}\right]$$

A tangent straight line $\dot{\phi}_{cr} = w_{f_{cr}} - K_{cr}\, U_{cr}$ transforms to the tangent straight line in this plane

$$\left(\frac{U}{w_f}\right)_{cr} + \frac{\dot{\phi}_{cr}}{K_{cr}} \left(\frac{1}{w_f}\right)_{cr} = \frac{1}{K_{cr}}$$

The equation for the plane tangent to the conical surface along the corresponding dash solution is

$$F_{cr} - K_{cr}\, \Delta R_{cr} - \dot{\phi}_{cr}\, \Delta T_{cr} = 0$$

It is assumed that the final or combat value of E_{s_F} is the same for all cases, and is the largest value attainable in a reasonable time, to maximize the effective range of a launched missile. It will also be assumed that the effect of the weight change during the dash on the succeeding energy transition segment performance can be neglected, so that the complete energy transition to E_{s_F} can be calculated as a single segment, without knowing the dash solution. The envelope of all the energy transition solutions to E_{s_F} forms a surface in a coordinate system of fuel used (ΔF_E), range (ΔR_E) and time (ΔT_E) which is found by optimizing the performance function

$$\text{Max PAY}_E = \frac{\dot{E}}{\dot{\psi}} = \dot{E}/(+C_{1_E}\, w_f - C_{2_E}\, U + C_{3_E})$$

for various values of C_{1_E}, C_{2_E}, C_{3_E}, using the RUTO program.

Since the assumptions of independence of weight changes permit dash and energy transition segments to be calculated separately, the total mission performance ΔF_F, ΔR_F, ΔT_F is the sum of the two parts. The condition for optimization of the sum is that a plane tangent to the surface of optimum dash solutions along a particular K_{cr} line should be parallel to the plane which is tangent to the surface of final values from optimum energy transition solutions at the particular end point of the matching energy transition. That is, the energy transition solution should be optimized for a performance function

$$\min \phi_E = (\Delta F_E - K_{cr} \Delta R_E - \dot{\phi}_{cr} \Delta T_E)$$

This is found by optimizing along the path

$$\max (\dot{E}/\dot{\phi}_E) = \dot{E}/(w_f - K_{cr} U - \dot{\phi}_{cr})$$

and the correct values of the constants in the PAY_E function are

$$C_{1_E} = 1, \; C_{2_E} = K_{cr}, \; C_{3_E} = - \dot{\phi}_{cr}$$

An equivalent form, which gives reasonable values for the constants for dash conditions from max U/w_f to U_{max}, is

$$C_{1_E} = \frac{1}{K_{cr}}, \; C_{2_E} = 1, \; C_{3_E} = - \dot{\phi}_{cr}/K_{cr}$$

The values of these weighting constants for the F-4K are shown in Figure 8, for the complete range of cases of interest. The break in the curve at C_{3_E} = 700 ft/sec is between the subsonic and supersonic dash solutions, corresponding to the cruise cases on the straight line segment in Figure 7.

As expected, the energy transition "boundary layer" segments get their weighting constants from the matching dash segment. This is a one-parameter family of solutions, corresponding to variations of K_{cr}, so the data storage for all the cases of interest may not be too large for on-board selection of the optimal path. Interpolation versus K_{cr} of simple equations for the end conditions will be the basis for selection.

The class of long range intercept missions for the F-4K has been calculated using the family of dash and acceleration segments discussed above, and their properties are illustrated in Figures 10 to 14. The calculation proce-

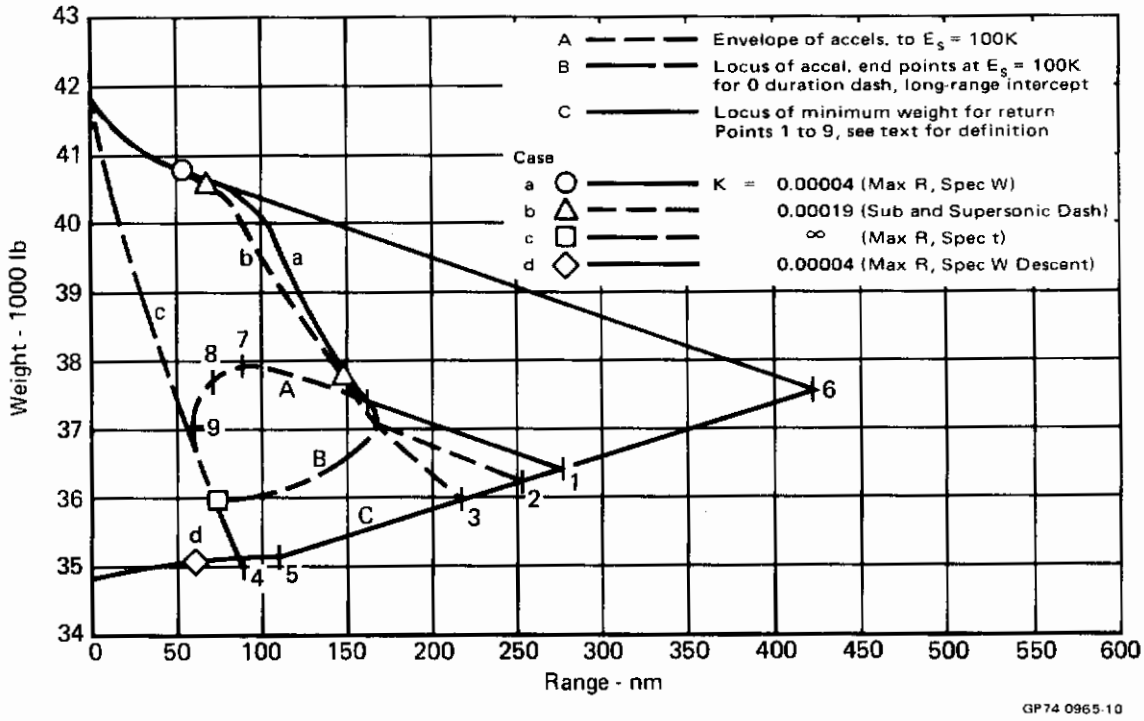

Figure 10 Weight-Range Variation for Long Range Intercept Missions
F-4K

dure assumes that the problem is dominated by the dash segment, so the acceleration segments can be treated as boundary layers on the dash segment which are a sufficiently weak function of gross weight that the effect of the weight change during the dash can be neglected. The only change required is an allowance for the lower weight at which the dash energy level of the higher U_{cr} dash cases is reached, as described above.

Figure 10 shows the weight-range variation of the acceleration cases a, b, c described in Section 1.1, ending at line B, which is the locus of acceleration end points at E_s = 100,000 feet for zero duration dash. Consistent with the assumptions, the dash segment is shown connected to the end point. The dash lines are the locus of intercept conditions for various dash durations,

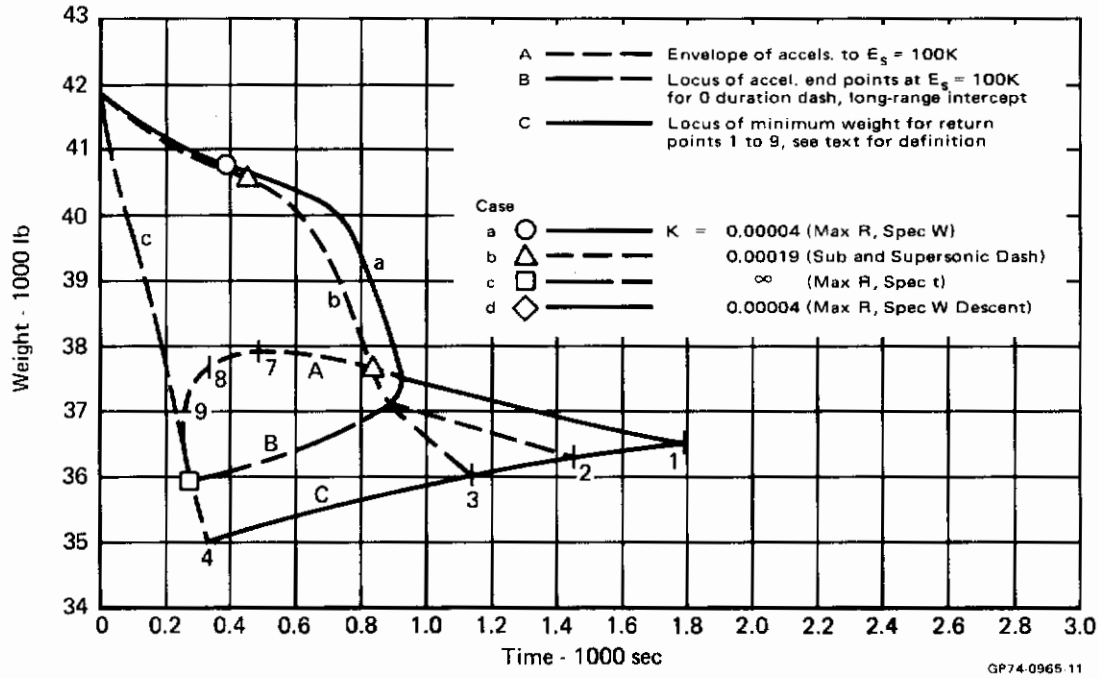

Figure 11 Weight-Time Variation for Long-Range Intercept Missions
F-4K

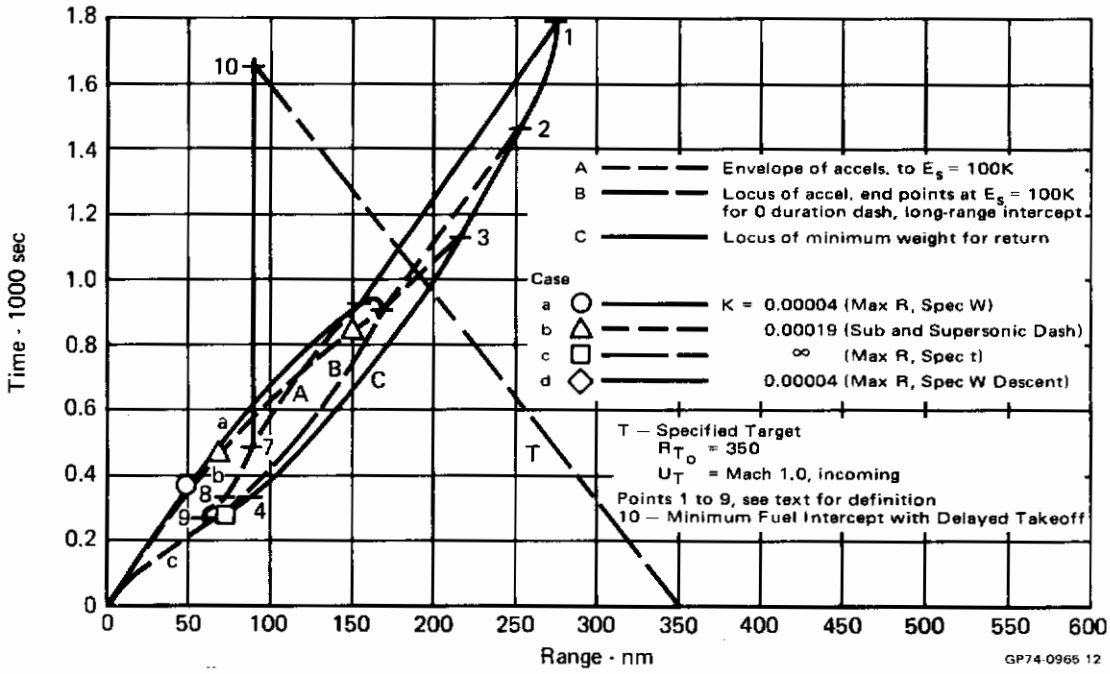

Figure 12 Range-Time Variation for Long Range Intercept Missions
F-4K

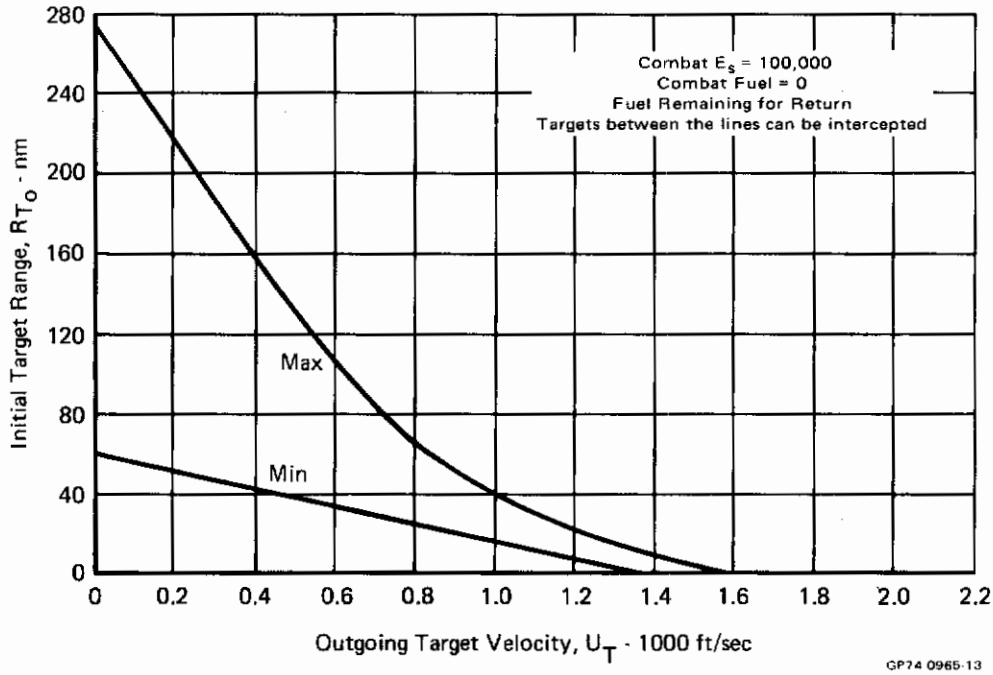

Figure 13 Outgoing Targets That Can Be Intercepted
F-4K

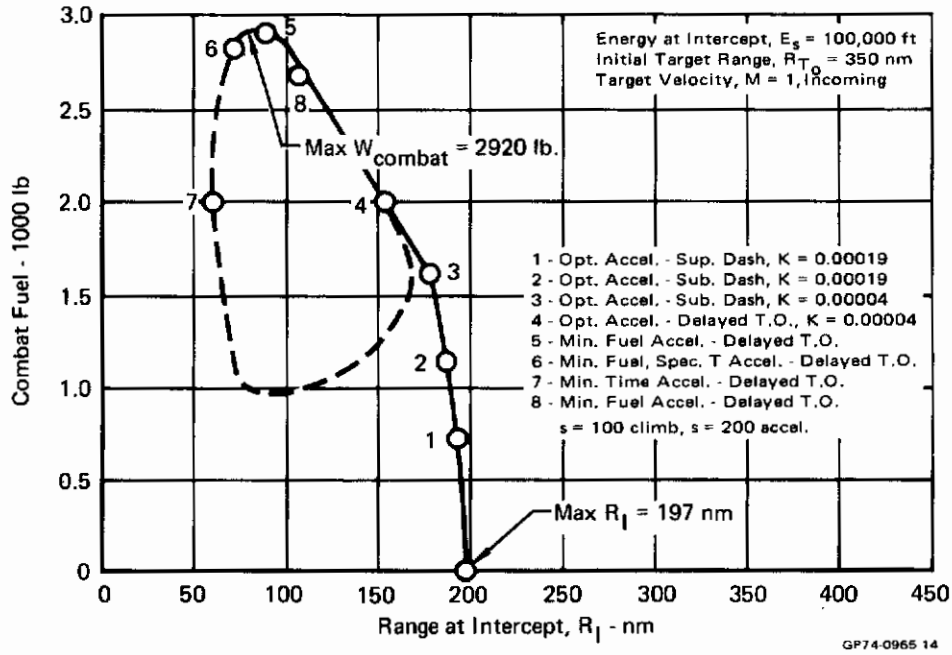

Figure 14 Optimum Intercept of Specified Target
F-4K

although the dash segments would actually be joined to the acceleration line at the conditions shown by the symbols, followed by the remainder of the acceleration.

Also shown as line A is the envelope of end conditions for acceleration to E_s = 100,000 ft, determined in Reference 1 - Point 7 is the minimum fuel (or max weight), 8 is min time - specified weight, and 9 is min time accel. Points on line A to the right of 7 are max range for specified fuel. Points on line A give the maximum combat fuel remaining at E_s = 100,000, for the specified time or range. As shown later, they are complementary to the accel - dash solutions in defining the attainable intercept conditions.

Line d is the max range-specified fuel descent segment presented above, starting from E_s = 100,000 at Point 5, and ending at the minimum return weight with landing reserves. Line C is the locus of minimum weight vs. range for start of the return descent and cruise, drawn at cruise specific range slope. Conditions between lines B and C are the long range intercept solutions.

Point 1 is the maximum range at E_s = 100,000 with sufficient fuel to return (276 n.mi.), reached by accel. and dash for case a (K_{cr} = .00004). Point 2 is for case b with subsonic dash. Point 3 is for case b with supersonic dash and points between 2 and 3 are reached by a combination of subsonic and supersonic dash. Point 4 is the case c, with dash at U_{max}. This point actually requires a shorter range descent than line d, with no return cruise segment. For reference, Point 6 is the maximum mission range (421 n.mi.) without specified E_s, and is obtained by max. range climb and cruise (case a) without a supersonic accel. Conditions between Points 1 and 6 can be reached at reduced energy levels, with a penalty in combat capability.

Figure 11 shows the weight-time variation for long range intercept missions, with the same legend as Figure 10. Figure 12 shows the most significant result, the range-time variation. A specific target is a straight line on this figure, defined by an initial target range, R_{T_0}, and a slope equal to the target velocity, U_T.

$$R_T = R_{T_0} \pm U_T \, t$$

with + sign for outgoing targets. Line T is an example. The intersection between the target and interceptor lines is the intercept point (actually the earliest missile launch point, the missile range has been subtracted from the actual target range to obtain line T). As indicated in Figure 12, this is

easily solved as the intersection of two straight lines, for conditions between lines B and C.

Line C is the envelope of attainable intercept range, with the specified value of E_s and sufficient fuel for return. Similar lines could be constructed for lower energy levels. For outgoing targets, line C defines the limits on maximum initial target range and velocity that permit intercept before the fuel remaining for combat reaches zero, again for the specified combat E_s. Point 9 (minimum time accel. to E_s = 100,000) defines the minimum target range that leaves time to accelerate to the specified E_s. These limits are shown on Figure 13. Point 1 on Figure 12 is the maximum intercept range (276 n.mi.). Incoming targets which would pass to the right of Point 1 can be intercepted at this range by delaying takeoff.

For the specified target shown by line T on Figure 12, the fuel remaining at combat is shown on Figure 14. The maximum intercept range, with zero combat fuel, is 197 n.mi. Points 1 to 3 are combined accel.-dash missions. Points 4 to 6 are accelerations with delayed takeoff. The maximum combat fuel is 2920 lb, close to the minimum fuel accel. case, Point 5, but with only 80 n.mi. intercept range. Note that points 7 and 8 are the only two intercept solutions which are usually available from energy management studies. Note, for example, Point 4, which has the same combat fuel as Point 7, but with over twice the intercept range.

The procedure for solving the long range intercept problem illustrated here is quite simple, covers most of the interesting cases in a clearly visible way, and is apparently as suitable for on-board computation as the cases treated in previous energy management studies. On the other hand, the Davidon search procedure for matching mission segments described in Section 1.2.2 would take many times as much calculation to give the solution for a single target case. Therefore, it is recommended that this procedure be used in preference to the Davidon search procedure of paragraph 1.2.2 whenever possible.

1.2.2 Davidon Parameter Search - The second method of matching mission segments to form a complete mission is a parameter search, where the parameters varied are the time duration and specific energy in each dash segment, and the weigting constants (C_1, C_2, C_3) in the payoff function.

$$\dot{\phi} = C_1 w_f - C_2 U + C_3$$

The parameter values are selected to maximize $(\dot{E}/\dot{\phi})$ in the accelerations and descent segments, and to minimize $\dot{\phi}$ in the dash segments, with a constraint

of specified final value of energy and the final values of any one or two of the variables range, time and fuel.

A general mission profile has been defined consisting of the following segments:

- Increasing or decreasing energy transition from initial energy E_1 to energy E_2.
- Dash for time ΔT_1 at energy E_2.
- Increasing or decreasing energy transition from energy E_2 to energy E_3, with sign of energy change same as or opposite to first and last segments.
- Dash for time ΔT_2 at energy E_3.
- Increasing or decreasing energy transition from energy E_3 to final energy E_4, with sign of energy change same as first segment.

The energy increments and dash times may be chosen so as to omit given segments and give simpler missions of interest.

The parameters available to be varied are (E_2, ΔT_1, E_3, ΔT_2, C_1, C_2, C_3), with up to 3 end constraints of specified E_4, T_{Final}, R_{Final} or W_{Final}. A little experimentation showed that the values of the end conditions are related to the values of the parameters in a very sensitive and nonlinear way. With so many possible parameters to be varied, a very efficient nonlinear search procedure was needed. Based on successful application in other problems, the Davidon search method was selected. This method has quadratic or second-order convergence properties, and is described in Reference 6. A computer program for this method was taken from one of the options in the AESOP program for function optimization developed for NASA, Ames, and documented in Reference 7. The Davidon logic was combined with the RUTO program. A complete mission is calculated for a given set of parameter values. The Davidon method then changes the value of the parameters and new missions are calculated until additional changes of the parameter values do not improve the result. The use of the method is described in Reference 4.

As many complete missions will be calculated in the process of the search, the calculation can be very expensive (several cycles, with the initial cycle requiring up to 14 complete mission calculations) unless good judgement is used in stating the problem in the most efficient way possible. In particular, the number of parameters to be varied must be kept small, as each one in turn is varied twice in a given cycle to determine a combined step in all parameters

that should be closer to the optimum. A number of cycles of this type could be required to locate the optimum, requiring hours of computer time. This is probably not justified as a routine performance calculation method. Instead, the Long-Range Intercept method of Section 1.2.1 should be used whenever possible.

1.3 Demonstration Case

A complete mission was calculated, including the return segments, to demonstrate the use of the various options available in the RUTOA program. The outgoing leg was of the type of Case b in Figure 9, with three acceleration segments, joining to subsonic and supersonic dash segments. The Davidon option was used for this part of the calculation, but only the initial mission was calculated, as the parameter values required for the mission could be guessed accurately enough from the previously calculated results for Case b, in Figures 7 through 12. The dash durations were selected to give about half the dash range (42 n.mi.) in the subsonic segment and half in the supersonic segment. The end conditions, at combat energy of E_s = 100,000 ft, leave enough fuel for return, and are about half way between points 2 and 3 on Figure 10, at 227 n.mi. range.

The return leg was from the end conditions of the outgoing leg, with a supersonic descent segment as in Figure 4 for best fuel, specified range, a Breguet cruise using the cruise option (INDSEL = 2, LOITER = 1), and a subsonic descent also shown in Figure 4. The end conditions of the return leg were designed to be at an energy of E_s = 5,000 ft, a weight of 34,800 lb (empty weight + reserves), and at a return range equal to the outgoing range of 227 n.mi. In fact, the end conditions were off by only 53 lb weight and 2.5 n.mi. range. This verifies that the assumption in Section 1.2.1 of a weak dependence of performance on the weight change in cruise is sufficiently accurate. The effect of the weight change in cruise was accounted for in an approximate way, by multiplying the previously calculated fuel used in a segment by the ratio of the estimated new average weight to the average weight in the previous calculation. That is, the fuel consumption was assumed proportional to weight, a well established rule in performance estimation.

In the supersonic part of the acceleration, it was found that too few throttle settings gave valid values of $(\dot{E}/\dot{\phi})$ to correctly determine the optimum throttle setting. This was similar to the problem previously described in the

descent calculation, and it was solved in the same way, by adding enough throttle setting values to get a good answer. The effect was that full throttle was used earlier in the supersonic acceleration, and less fuel was used. Because of this, and the lower weight following dash, the performance came out slightly better than the previous calculations, with about 7 n.mi. more range for a given time and fuel used than shown on Figure 12. This indicates that the mission segment matching by the method of Section 1.2.1 is slightly conservative.

The input data and output results of the demonstration case are listed in Reference 4. This case took 4415 sec. CP time on the CDC 6500 computer.

Figure 15 is a Mach-altitude trace of the demonstration case. Notice the subsonic dash point, the transonic acceleration and the supersonic dash point. The bump in the trace near the supersonic dash point is caused by the relationship of the weighting constants in the payoff function to the performance figure of the aircraft at the dash point. The smoothing process would continue the constant Mach number climb to the dash point.

A transition is made at maximum energy from U_{max} to the start of the optimal descent. Notice the cruise point, which is part of the descent path. The increase in Mach number at low energies is due to not having true idle throttle setting available.

Figure 16 is the throttle setting history for the demonstration case. It begins at 9000 ft energy and a throttle setting index, $, of about 100. The spike at about 53,000 ft energy is the throttle modulation for the subsonic dash, the vertical line at about 95,000 ft energy is the throttle modulation for the supersonic dash.

Figure 17 shows gross weight versus energy for the demonstration case. The dash segments and the cruise segments are easily discerned; notice the slight energy increase in the Breguet cruise.

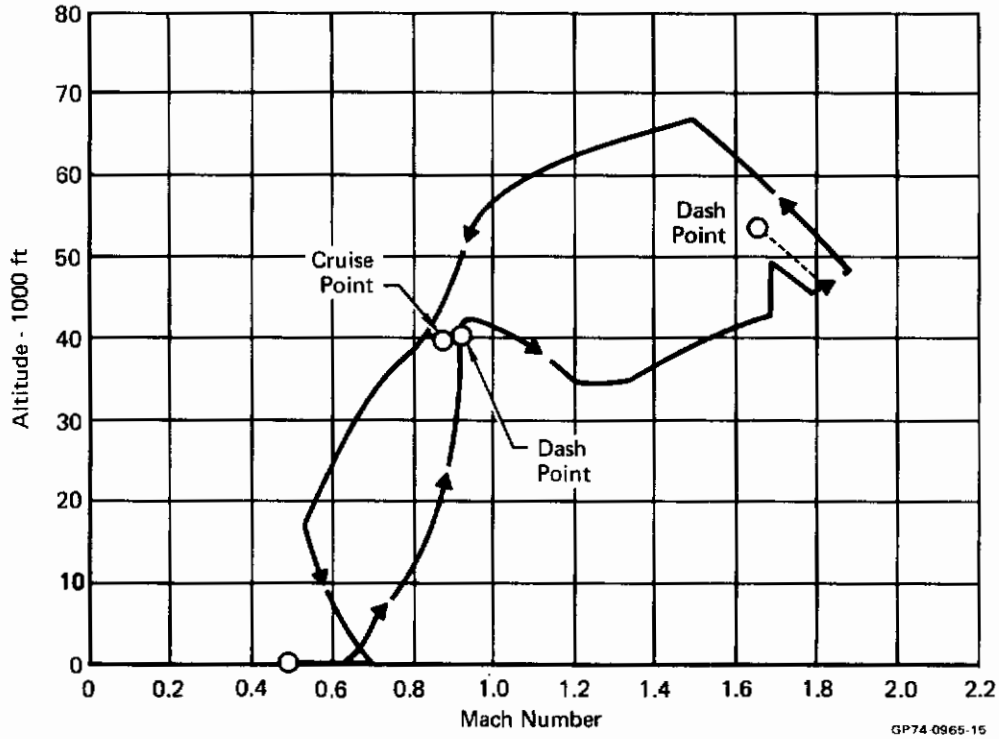

Figure 15 Demonstration Case Flight Path
F-4K

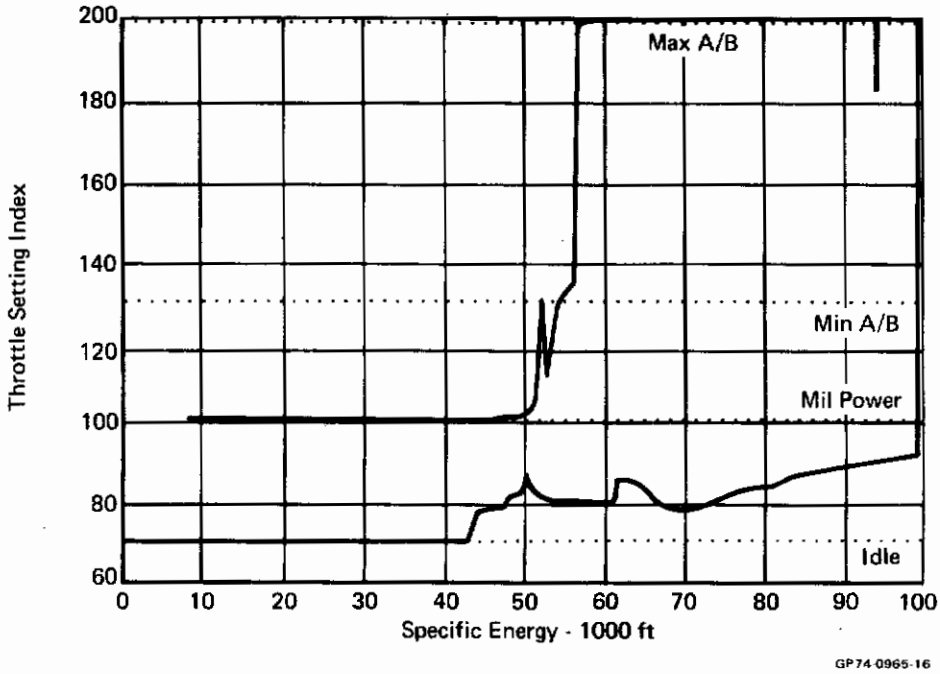

Figure 16 Demonstration Case Throttle History
F-4K

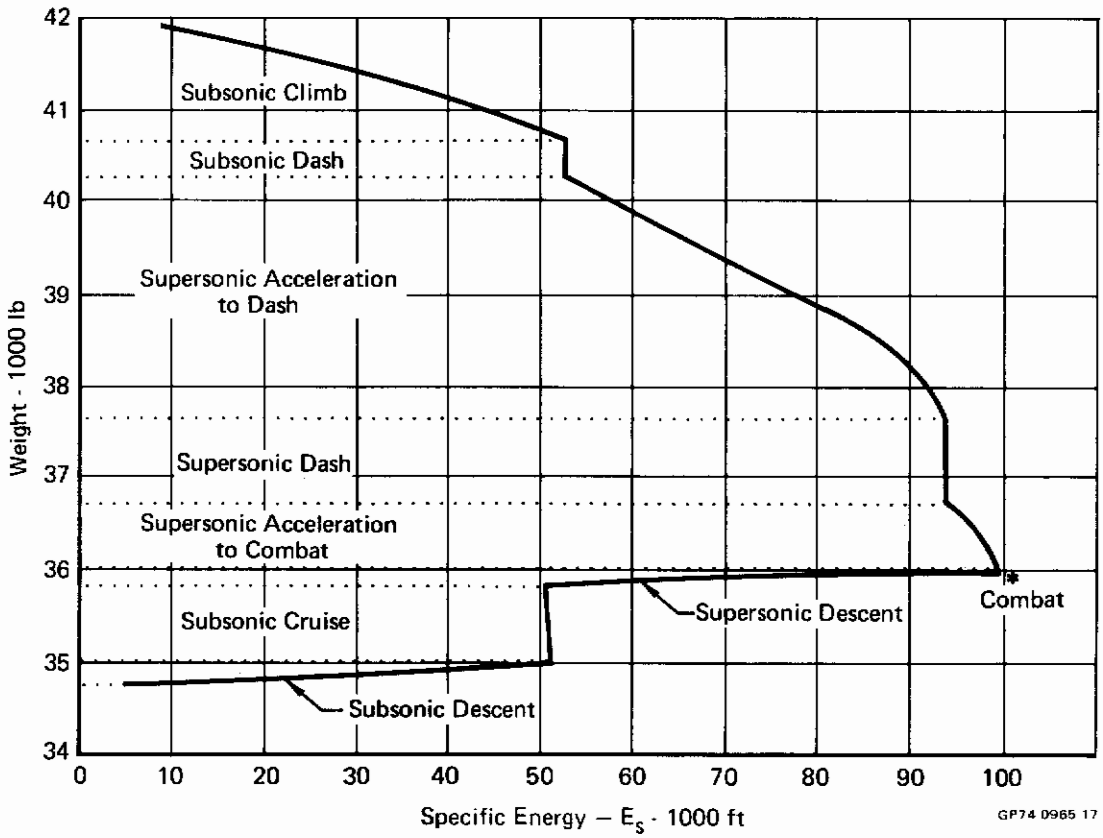

Figure 17 Demonstration Case Weight vs Energy
F-4K

SECTION 2
INVESTIGATION OF THROTTLE/FLIGHT PATH CONTROL TECHNIQUES (TASK II)

2.1 Selection of Flight Test Aircraft and Mission

2.1.1 Comparison of Candidate Aircraft - A comparison of the F-4E, F-111, and F-15 as candidate aircraft for flight test demonstration of the benefits of throttle/energy management has led to the selection of the F-4E as the one to be used for further study in this contract. A discussion of the investigation leading to this conclusion follows.

Available F-111 data reports (References 8 and 9) have been used to set up a data deck for RUTO calculations. A wing sweep schedule was selected which gives low drag at lift coefficients used in acceleration, and drag polars were selected at each Mach number according to this schedule. Engine data tables were also set up. However, it should be noted that the data provided are for the TF-30-8 engine. It is understood that this engine has been superseded by later models with significantly improved performance, and the later models have been retrofitted on all the existing aircraft. Therefore, the engine data is not really useful for flight test planning. The drag tables may be useful for F-111 studies if later engine data can be obtained. However, no calculations were made with the F-111 data deck.

Sufficient energy management calculations are presented in the F-111 reports that no additional calculations are needed for this evaluation. These calculations were made by the tedious process of comparing contours of $\dot{E}$ and $(\dot{E}/w_f)$ for various throttle settings and sweep angles. Recommended schedules of sweep and throttle setting with Mach number are given for minimum time and minimum fuel acceleration.

The calculations show the F-111 must go to max A/B operation at supersonic Mach at a much lower energy level than the F-4, because of the low thrust to weight ratio. The benefits of throttle modulation will, therefore, be smaller for the F-111. Also, automatic control of the modulated afterburner will be very difficult for the F-111 because the engine performance reports indicate that there are stepwise variations between thrust levels (or "zones") rather than the smooth thrust variation of the F-4E and F-15 engines in afterburner setting. These facts, plus the lack of available current engine data, led to rejection of the F-111 for study as a flight test aircraft.

Difficulties also were encountered in setting up a RUTO data deck for the F-15 airplane. The only data available at the time of this study were frozen at a preflight-test point in time, and this was the only data approved for release.

The engine data are for an F-100 "A" engine, which does not correspond to any engine now flying in F-15 aircraft. In Figures 19, 20, and 21, calculations based on this preliminary preflight-test data are identified as for an air superiority fighter aircraft (ASF), to emphasize that the applicability to the actual F-15 aircraft is only qualitative. The performance differences due to throttle modulation that can be predicted with this data set are less dependable than for the F-4, and are not considered as good a basis for flight test planning.

The data set for the F-4E was readily obtained, as it is in current use. The drag data is identified as Drag Status (DS) 120472A, and is for the slatted F-4, as all the F-4E's are being converted to the slatted configuration. The engine data is for either the J-79-10 or -17 as used in the F-4E and F-4J, and is reported in MDC reports A1158 (Reference 10) and A1216 (Reference 11). The throttle dependent drag is not in the engine data. Instead, two sets of drag data were defined from flight test, to match the measured acceleration at intermediate and maximum A/B throttle when used with the engine thrust predictions. The difference between these two drag levels may be considered a flight measurement of the throttle dependent drag at intermediate throttle.

For the computer programs implemented, the basic drag polar data are for maximum A/B, and a curve of ΔC_{D_T} versus Mach number gives the additional drag at intermediate throttle setting. The additional drag is assumed to vary linearly with thrust from zero at maximum A/B to the ΔC_{D_T} from the curve at intermediate thrust, and to be constant at the ΔC_{D_T} value for reduced thrust. The afterbody drag data from the ESIP contract (MDC A1333, Reference 12) was used as a guide in the variation of ΔC_{D_T} with Mach number. The linear drag variation with thrust level is based on the fact that the nozzle boattail aft facing area varies approximately in this way, and boattail drag is the main source of throttle dependent drag in afterburner operation. For the J-79 engine, there is very little variation of jet total pressure with afterburner modulation (Figure 18).

Note that the variation of inlet spill drag with mass flow at reduced throttle is not included in the F-4E data, as it was not defined by the flight test data. This, and the use of a ΔC_{D_T} to define throttle dependent drag, are differences from the F-4K data, for which the various sources of throttle dependent drag were estimated and included in the ram drag tables. This requires minor differences between the RUTO programs for the F-4K and the F-4E.

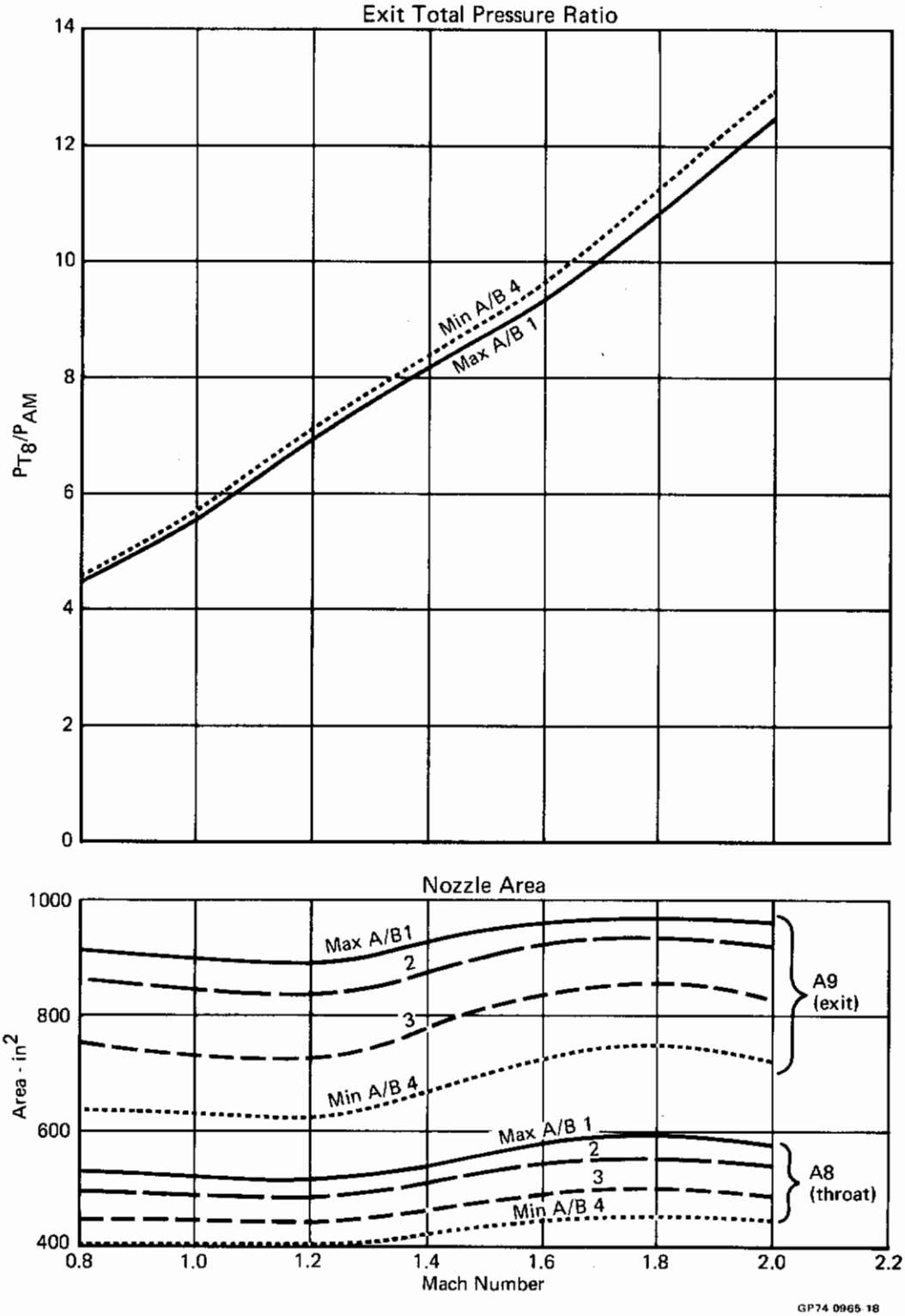

Figure 18 Exhaust Nozzle Characteristics
J79-GE-17 Engine
Standard Day Altitude 36,089 ft

The variation of excess thrust with fuel flow is compared for the candidate aircraft F-4E, F-111 and F-15(or ASF), as well as for the F-4K in Figures 19, 20, and 21. The flight conditions are:

a. .8 Mach, 10,000 feet - near the start of subsonic climb, E_s = 21,000.
b. .9 Mach, 40,000 feet - near optimum cruise for the F-4, E_s = 52,000.
c. 1.6 Mach, 40,000 feet - in the middle of the supersonic acceleration.

The values are normalized by the atmosphere pressure ratio, δ (where $\delta = p/p_{\text{sea level}}$), and the static, sea level gross thrust, F_{G_o}. One noticeable difference between the curves is the much larger range of afterburner modulation for the F-111 engine. This is probably related to the use of fan air in the afterburner.

The dash performance of the F-4E has been calculated as a step in determining the performance benefit of throttle modulation. The conditions for optimum dash are at the altitude and throttle setting for minimum fuel flow at a selected dash velocity. Figures 22 and 23 show the dash altitude and throttle setting for a range of dash Mach numbers, and for several values of gross weight. The variation of dash altitude with weight shown in Figure 22 corresponds to a single value of W/δ at a given dash Mach number. Figure 23 shows the dash throttle setting is essentially independent of weight. It is significant that the supersonic dash requires modulated afterburner throttle setting at Mach numbers up to 2.0.

The effect of weight on specific range is shown in Figure 24. This variation corresponds to a constant value of fuel flow rate/gross weight (w_f/W). To determine the slopes (K_{cr}) and intercept (ϕ_{cr}) of a line tangent to the curve of minimum $w_{f_{cr}}$ versus U_{cr}, it is necessary to account for the lower weight at which the higher U_{cr} conditions are reached. A method of doing this was developed and applied to the F-4E dash performance.

Figure 25 shows the dash specific energy, $E_{s_{cr}}$, calculated from the dash altitude for 40,000 lb. weight from Figure 22. Figure 26 shows the estimated weight at which the dash energy is reached based on the acceleration segments calculated for the F-4K. From these figures, the weight (W_{cr}) at a given U_{cr} was determined, and used to correct the dash $w_{f_{cr}}$ curve to the estimated W_{cr} (Figure 27). Tangents to this curve, as shown, determine the various acceleration segments which match with a given dash segment for best mission performance.

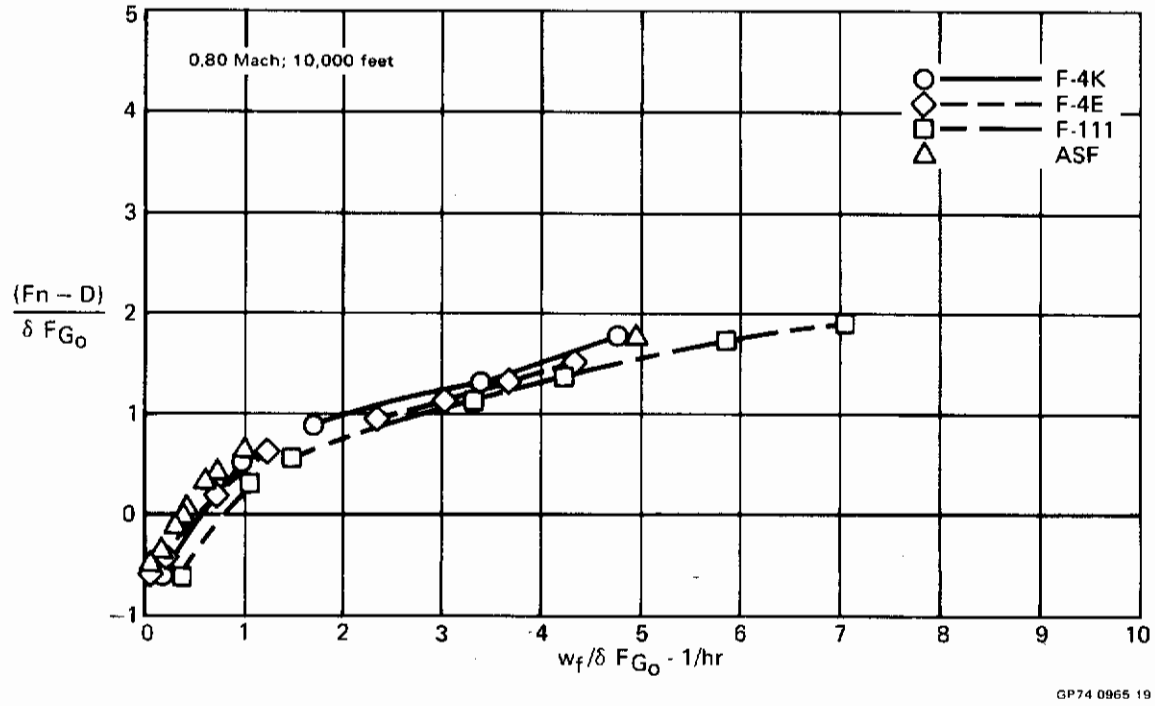

Figure 19 Comparison of Candidate Aircraft

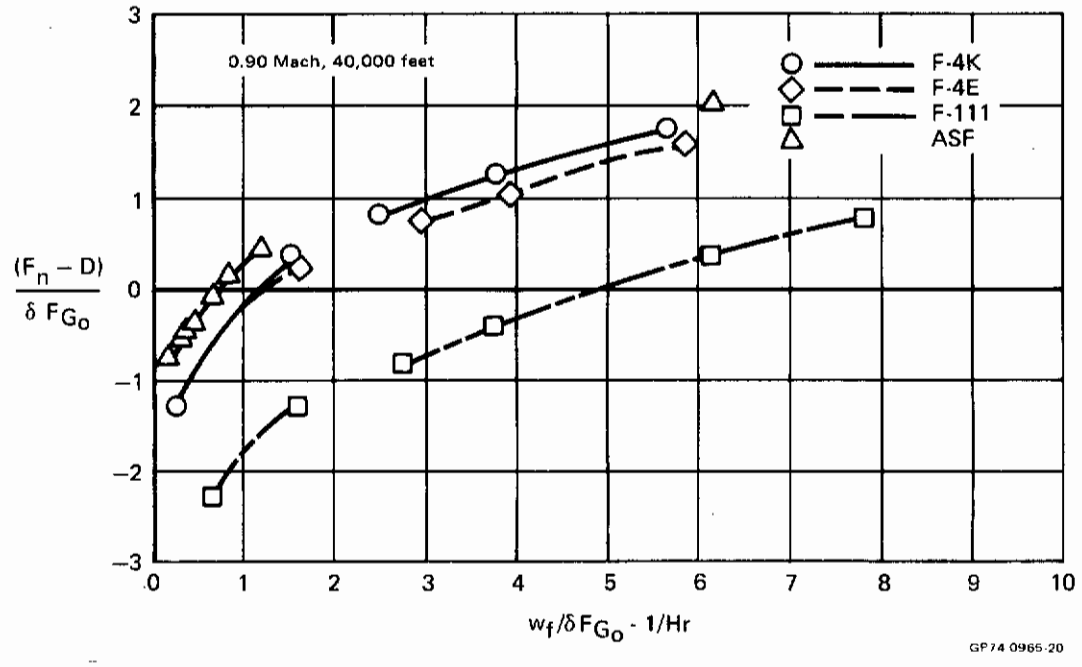

Figure 20 Comparison of Candidate Aircraft

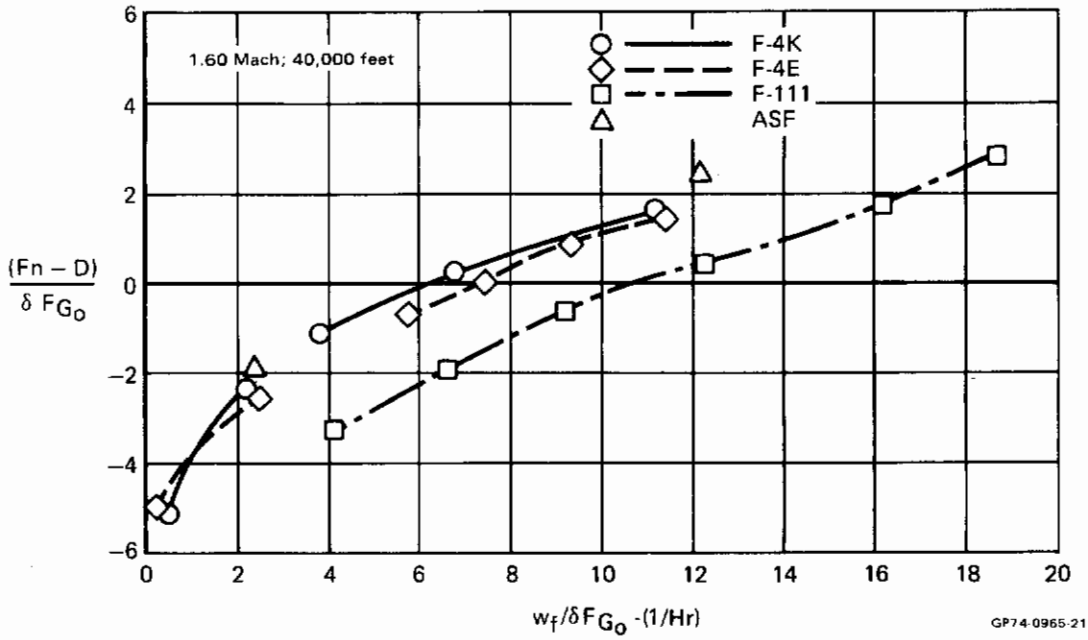

Figure 21 Comparison of Candidate Aircraft

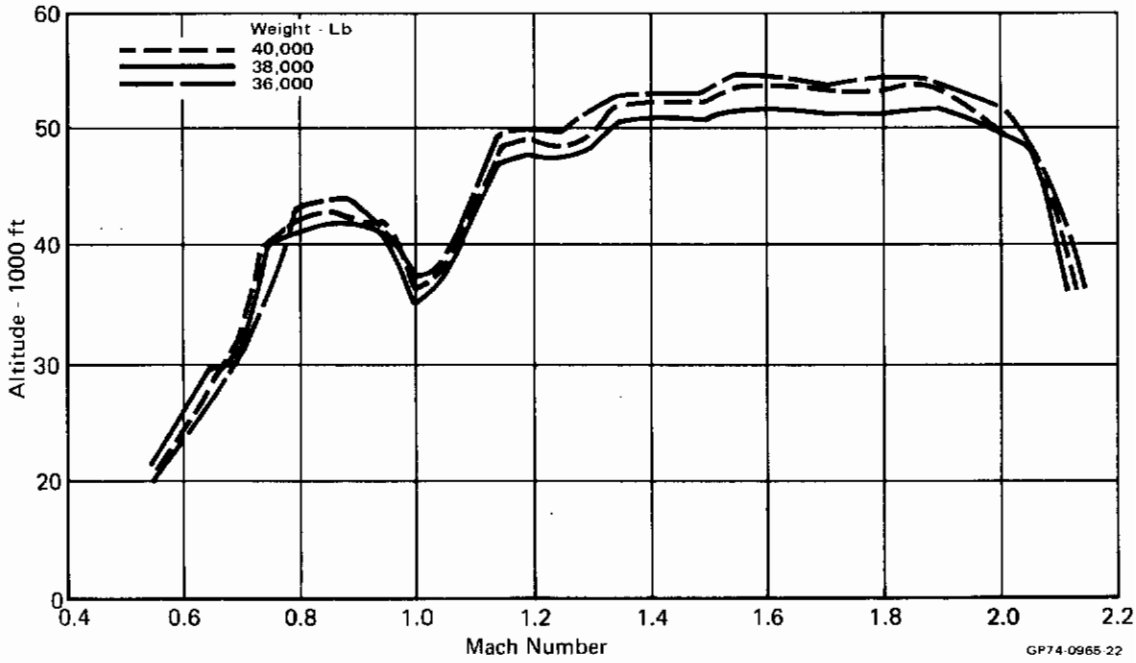

Figure 22 Dash Altitude for Minimum w_f
F-4E

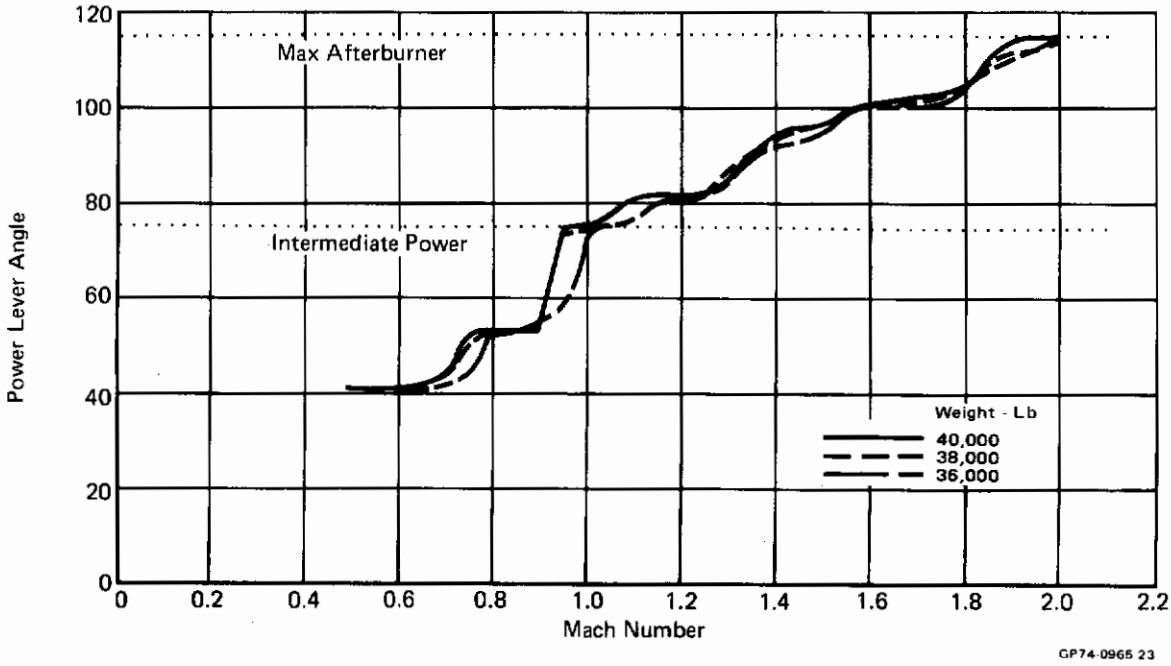

Figure 23 Dash Throttle Setting
F-4E

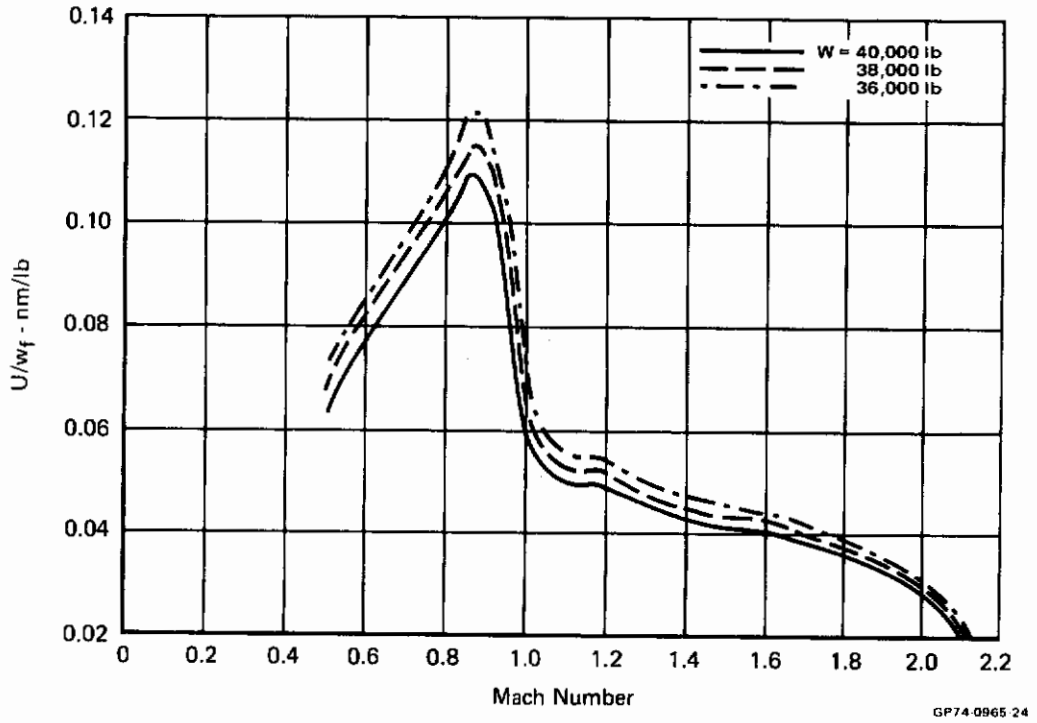

Figure 24 Cruise Specific Range
F-4E

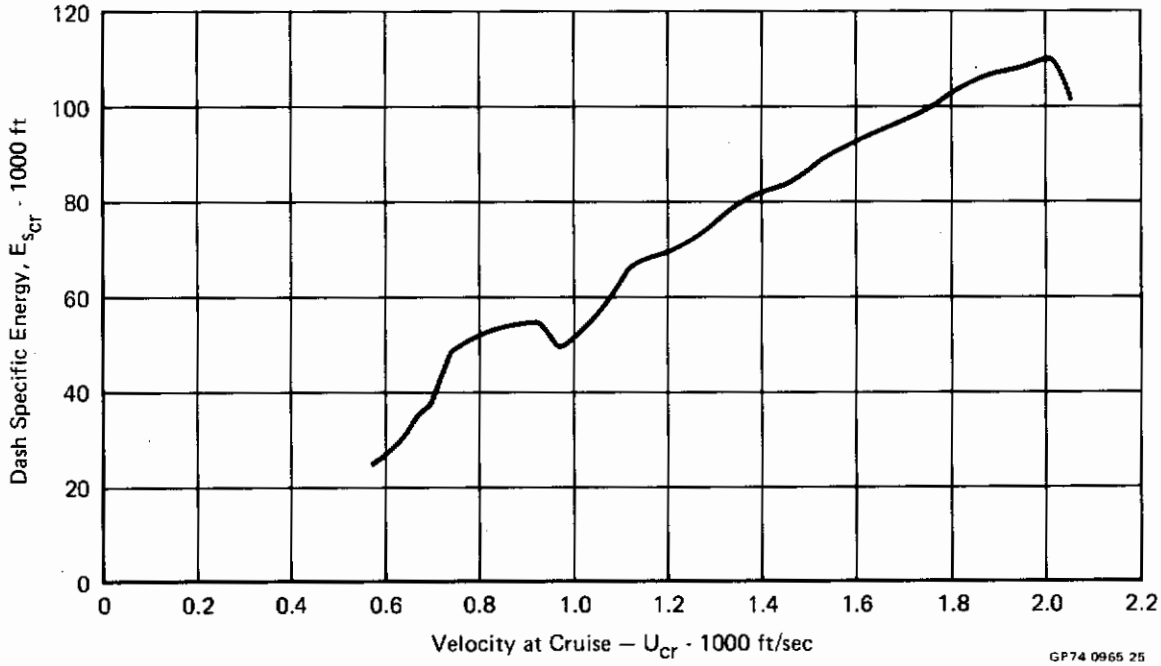

Figure 25 Dash Specific Energy
F-4E
W = 40,000 lb

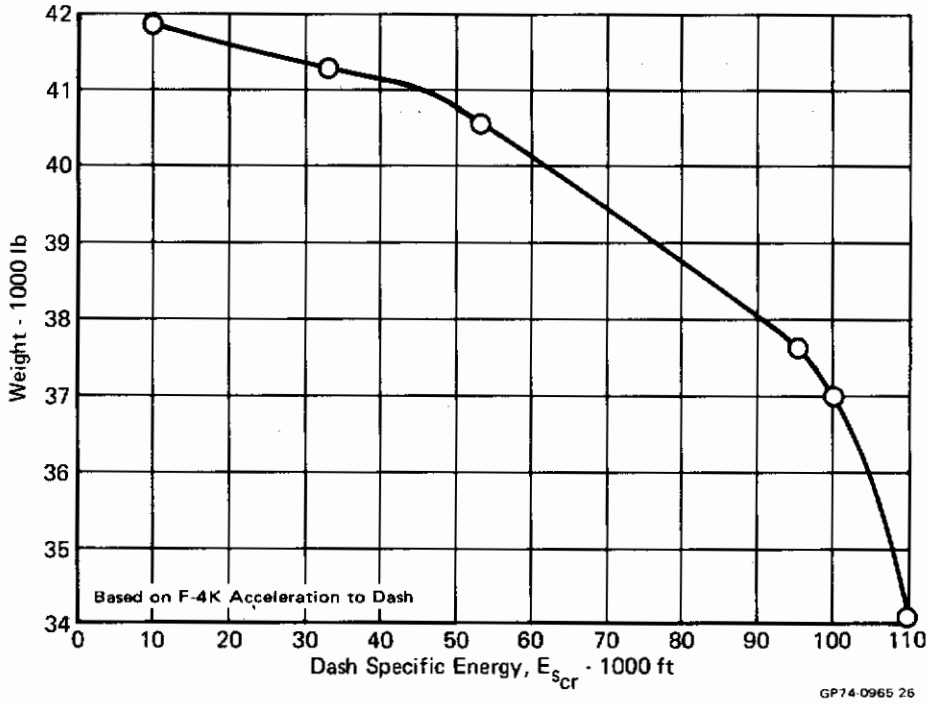

Figure 26 Estimated Weight at Dash
F-4E

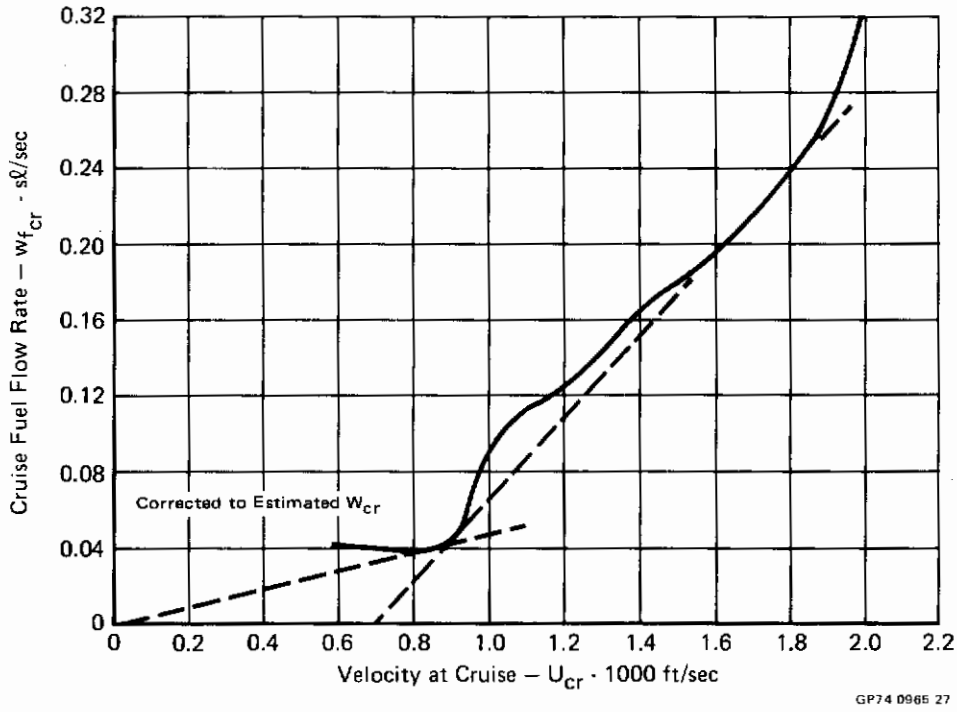

Figure 27 Quasi-Steady Optimum Dash
F-4E

2.1.2 Flight Test Mission Definition - Flight test missions for demonstration of the benefits of throttle/energy management should consist of a fixed throttle and a variable throttle case which will have easily measured differences in fuel used, if followed closely, but will be comparable in other respects. An additional condition desired is that the missions not require an unreasonable amount of range or fuel.

The RUTO program was used to calculate various fixed and variable throttle segments for the F-4E. The flight paths were found to be very similar to those previously calculated for the F-4K (Reference 1). The throttle histories versus E_s were different, with the F-4E showing a more abrupt jump from intermediate throttle to a setting slightly less than maximum A/B (Figure 28), in contrast to the more gradual variation for the F-4K. This is due to the different variation of thrust with fuel flow, as shown in Figures 19 and 21.

The flight mission selected is an acceleration for minimum fuel to a given energy with variable throttle, to be compared to a fixed throttle (maximum A/B) acceleration, also on a minimum fuel path, matched to a cruise segment selected to give the same time and range end conditions as the variable

throttle case. The difference in fuel used to the same end conditions is then a clear measure of the benefits of optimum control of both the throttle and flight path. The altitude-range paths for these two demonstration missions are compared in Figure 29, with the flight segments identified.

As shown in Figure 30, this mission has a large fuel savings of about 570 pounds for acceleration from E_s = 9,000 ft. to 65,000 ft., or 29% of the optimum fuel required. The fuel difference will be the same to any supersonic point on the flight path, as the supersonic part of the path is the same for both cases. The case shown (final E_s = 65,000) requires only about 50 n.mi. total range. Continuing the acceleration to E_s = 100,000 ft. would require about 100 n.mi. total range.

2.2 2-Degree of Freedom Simulation

2.2.1 Point-Mass Simulation Program - A point-mass simulation program (2 DOF) has been developed for calculation of ideal and baseline (fixed throttle) performance. It uses a flight plan programmer subroutine to follow a tabular control variation of pitch angle and throttle setting with energy during the smooth part of the energy transition segments. A prescribed load factor is used during the dive onto or zooms off the Rutowski path to specified end-point or

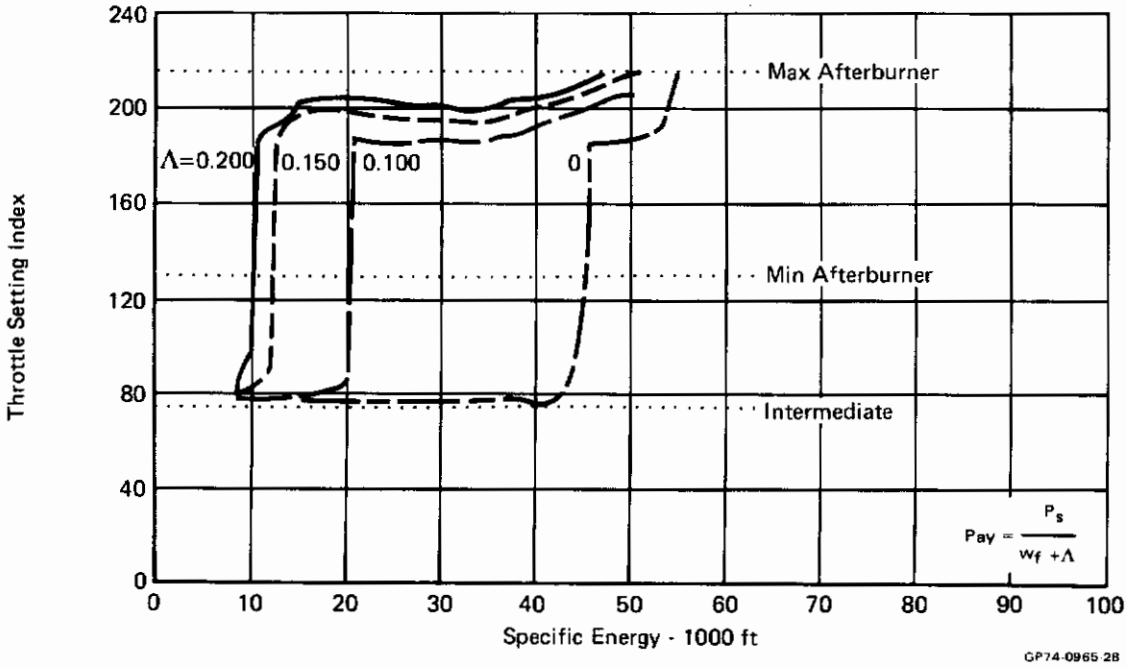

Figure 28 Throttle Variation for Optimum Acceleration
F-4E
Minimum Fuel for Specified Time

dash flight conditions, and during pullups or pushovers at the corners and at the transonic constant energy arc of the Rutowski path. MCAIR simulation studies have shown that with fixed throttle a pilot can fly these parts of the path accurately and repeatedly, using constant load factor arcs with a time cue for starting the pullup or pushover.

2.2.2 Calculation of Optimum Control Program - The following sequence of calculations is to be used to calculate the optimum control program of altitude (h_c), pitch attitude (θ_c), and energy rate ($\dot{E}_{s_c}$):

a. Calculate the optimum path by the RUTO program.

b. Smooth the RUTO histories of h, θ, and throttle setting (S) versus energy (E_s).

c. Use the flight plan programmer options of the 2-Degree-of-Freedom (2 DOF or point mass) program to calculate paths following tables of the smoothed RUTO histories of Step b.

d. Use the point mass histories of h, θ, and $\dot{E}_s$ versus E_s, with any smoothing needed, as the control program for testing the control laws in the point mass program and the nonlinear control simulation program (MITCON) described in Section 3.2.

The control programs used in Step d would be stored on tape or in computer memory for the flight test demonstration.

The RUTO program generates values of h, θ and $\dot{E}_s$ versus E_s, and it was originally thought these could be used as the optimum control program. Attempts to follow the RUTO data with both the 2 DOF and 4 DOF programs showed that the control laws were not able to accurately follow irregularities in the RUTO data. Also, increased drag due to large load factors used in an attempt to follow these irregularities caused a reduction in the average value of $\dot{E}_s$ and a continually increasing time lag behind the RUTO performance. When a smoothed control program was used, the load factor was reduced and the commanded path was followed much more accurately. It is clear that both good control and good performance depend on use of as smooth a control program as will stay close to the optimum flight path.

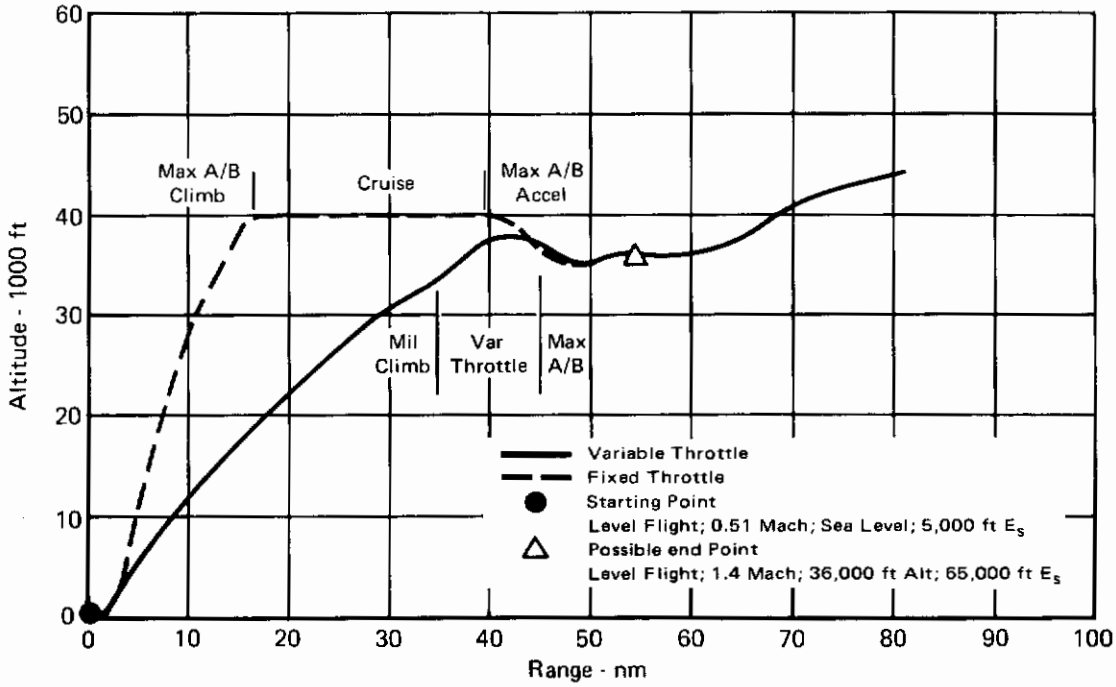

Figure 29 Comparison of Demonstration Flight Paths
F-4E

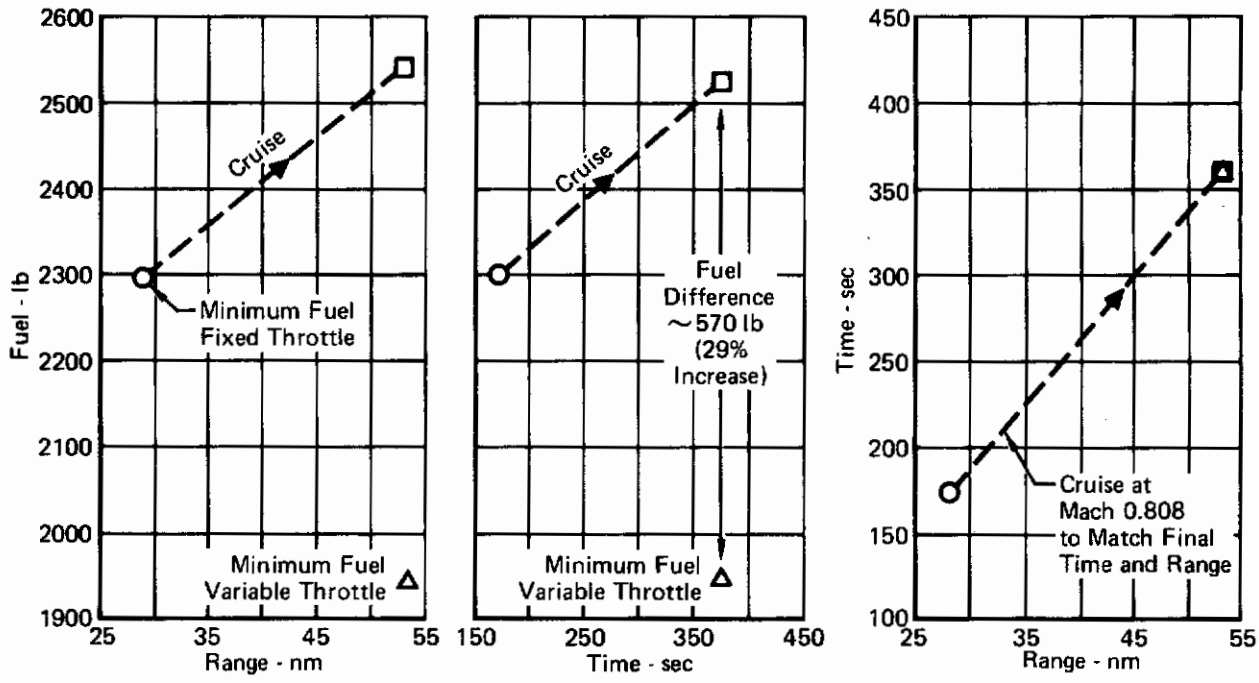

Figure 30 Flight Demonstration Mission
F-4E
E_S = 9,000 ft to 65,000 ft

The irregularities in the RUTO data are due to a combination of the following causes:

a. Linear interpolation of the aerodynamic and engine data tables produces corners in the variation of performance which cause the calculated optimum values of h, M, and S to tend to follow piecewise constant paths. Small variations of the data from a smooth variation with h or M also have this effect.

b. The tolerances selected to reduce the number of trials in the iterative search for the optimum altitude.

c. Small steps of energy (E_s) of 1,000 feet are used to improve the accuracy of the integration of fuel, time and range. Small irregularities in the variation of h with M thus give large variations in the values of θ_c calculated from:

$$\theta_c = \alpha + \sin^{-1}\left[\frac{\dot{E}_s}{U}\quad\frac{dh}{dE}\right] = \alpha + \gamma$$

The irregularities in the RUTO calculations are small enough that the performance values are quite accurate. It was noted that the values of $\dot{E}_s$ and α have fairly smooth variations with E_s. The values of h versus E_s are somewhat irregular, but can be fitted closely by a series of straight line segments. The values of path angle (γ) are very irregular, and are the main source of the irregularities in θ. On this basis, a method of smoothing the data was selected.

The variation of (E_s - h) with E_s is visually fitted by straight line segments where possible. Where the slope changes, cubic connecting segments are used which match the value and slope at each end. Where there is a step change in throttle setting and $\dot{E}_s$ (as in the step from intermediate to min A/B throttle), a change in the slope of (E_s - h) with E_s is selected which makes the values of γ and θ continuous. The RUTO values of $\dot{E}_s$ and α are used in calculating θ from

$$\theta = \alpha + \sin^{-1}\left[\frac{\dot{E}_s}{U}\left(1 - \frac{d(E_s - h)}{dE_s}\right)\right]$$

using the analytic values of the slope of $(E_s - h)$ with E_s from the linear and cubic segments. Values of θ are calculated at large intervals of E_s, up to 5,000 feet in the linear segments. Instead of the discontinuous step in h at constant E_s between the subsonic and supersonic segments, a more gradual linear variation is used following Boyd's rule of thumb

$$\Delta E_s = K\Delta h$$

where K = -1 for dives and 1/2 for zooms. In terms of $(E_s - h)$, Boyd's rule becomes:

$$\frac{d(E_s - h)}{dE_s} = \pm 2$$

with the + sign for dives and - sign for zooms.

The optimum control programs calculated by these rules for the variable throttle and fixed throttle flight test missions are shown in Figure 31. The h and θ variations in the pullup at sea level and the pushover and pullup at the transonic dive are not defined by these rules. Neither are the transitions to and from the cruise segment of the fixed throttle mission. These are to be defined by the 2 DOF and MITCON programs.

Note that the value of γ depends on the slope of $(E_s - h)$ with E_s. $\dot{\gamma}$, and hence load factor, depends on the curvature or second derivative, $\frac{d^2(E_s - h)}{dE_s^2}$. Hence the straight line segments will have load factors very close to 1 g and the cubic segments will have nearly constant load factor, which tends to give the minimum performance loss due to load factor fluctuations.

The flight plan programmer options of the 2 DOF program which are used to follow the smoothed RUTO data are:

a. Throttle command - S_c vs E_s input as a table.

b. Pitch command - θ_c vs E_s input as a table. The angle of attack is computed as

$$\alpha = \theta_c - \gamma + K\,(h - h_c)$$

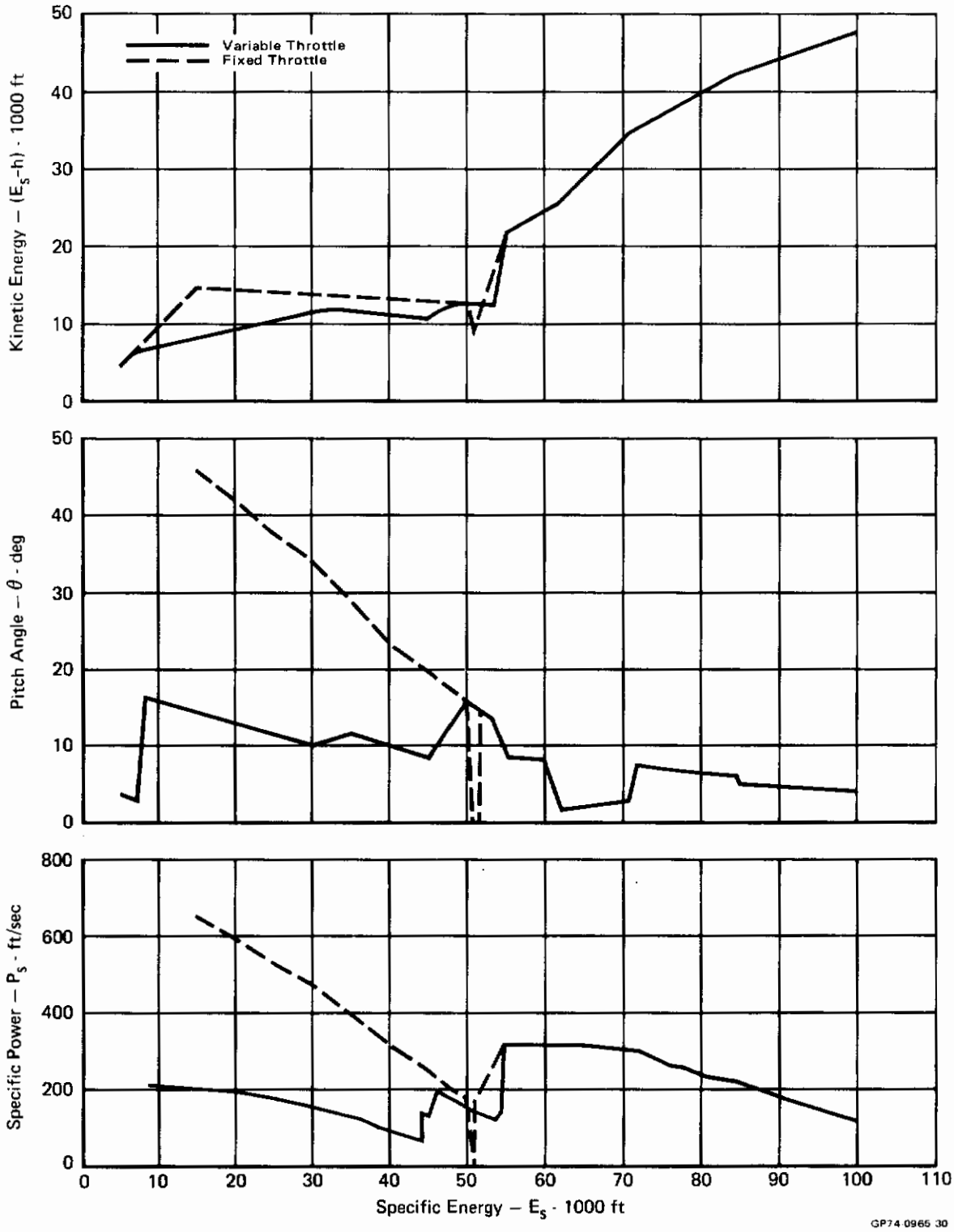

Figure 31 Optimum Control Programs for Flight Demonstration Missions
F-4E
Smoothed RUTO Data

c. Load factor command - N_{Z_c} vs time input as a table. C_L is computed from

$$C_L = \frac{1}{qA_{ref}} [N_{Z_c} \cdot W - F_G \sin (\alpha + \lambda_T)]$$

and the value of α computed from a table of α as a function of C_L and M, produced by inverting the table of C_L as a function of α and M in the aerodynamic data.

The pitch command and throttle command programmers are used to follow the smoothed RUTO segments. The load factor command programmer is used to input a constant load factor, and the time of beginning and end of the pullup or pushover are adjusted by trial to match the altitude and γ of the RUTO data at each end. Load factor limits of 1.5 and 0.5g are selected. Exceptions are at pullup at sea level or to a zoom, where a load factor limit of 4g will be used.

A consequence of the need for smoothing discussed above is that an energy management control scheme using on-board computation of the control program by a RUTO calculation would need special attention to the requirements for smoothness. The smoothing procedure which has been developed is suitable for a flight test demonstration of a single, pre-selected mission, but some other scheme would be needed for on-board computation. The present RUTO program is quite satisfactory for performance prediction, but some modification will be required for direct generation of smooth control programs.

The following RUTO modifications might be used for on-board calculation of a smoother control program:

a. Remove the irregularities due to the aerodynamic and engine data tables by using nonlinear (e.g., cubic spline) interpolation instead of the present linear interpolation. This will also permit storage of data at larger intervals of h and M.

b. Engine data normalized by total pressure and temperature would smooth the computed variation with altitude and Mach number. Other benefits would be less engine data to be stored to give a good representation, and a method of calculating the effects of non-standard atmosphere properties without new tables for each model

atmosphere. (Some of these benefits were realized by normalizing the F-4K engine data by ambient atmospheric pressure.)

c. Use calculated flight path data at larger increments of E_s than the present 1,000 feet, to smooth the calculated values of γ and θ. This would also reduce the amount of data to be stored.

d. Use spline interpolation of the h_c and $\dot{E}_{s_c}$ control programs to give smoother values, and to generate the slope $\frac{dh_c}{dE_s}$ for calculation of γ_c, rather than storing a separate table of θ_c. (The calculation of γ_c from the slope of the h_c table has been used in the 4 DOF program.)

e. Develop a logic for smoothing the h_c variation at corners and transonic transitions of the RUTO path which will require acceptable load factors and give continuous variations of θ_c or γ_c.

f. Apply load factor corrections to the RUTO (1 g) values of $\dot{E}_{s_c}$ on segments of the path where pullups or pushovers are required.

2.2.3 Flight Performance Benefits of Throttle Management - Figures 32 through 34 show a comparison of the performance predicted by RUTO for the two flight demonstration cases with the performance calculated by the 2 DOF programs, following the smoothed RUTO control programs. The results show that the performance predictions from the RUTO method are very good, in spite of the use of load factors different from 1.0 during pullups and pushover maneuvers. This is attributed to the use of constant load factor maneuvers in the range of 0.5 to 1.5 g. The times from the two methods differ by less than 10 sec., the range by less than 2 n.mi., and the fuel savings due to use of variable throttle are almost exactly the same, 675 lbs by the RUTO method versus 678 lbs by the 2 DOF program. The 2 DOF flight paths are shown later (Figures 77 and 78) in the comparison with the MITCON path produced by the control system.

2.3 Systems and Display Requirements

In this section, consideration is given to the requirements and suggested approaches to design and mechanization of the throttle/energy management system developed in this study for flight test demonstration on a single mission profile. A discussion is also given of the limitations of this concept for multimission applications, for a more comprehensive system evaluation test or for operational use.

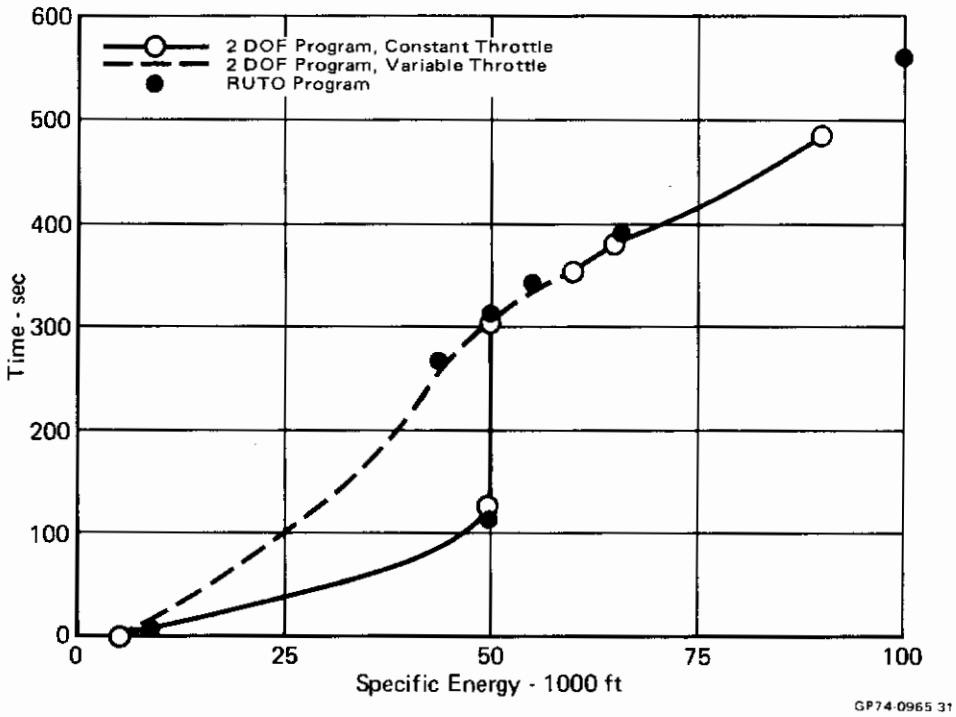

Figure 32 Comparison of RUTO and 2 DOF Performance
Time vs Energy

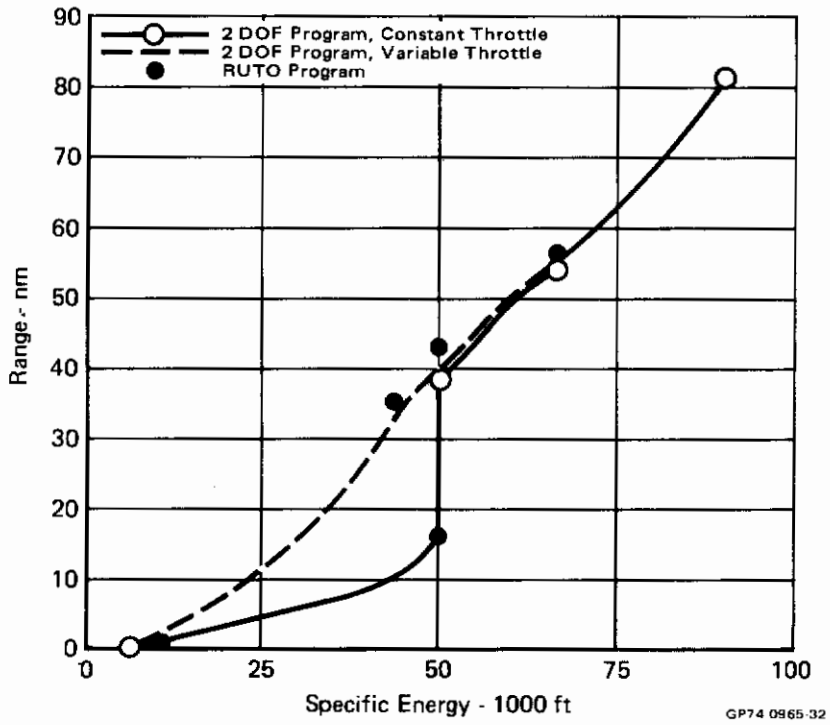

Figure 33 Comparison of RUTO and 2 DOF Performance
Range vs Energy

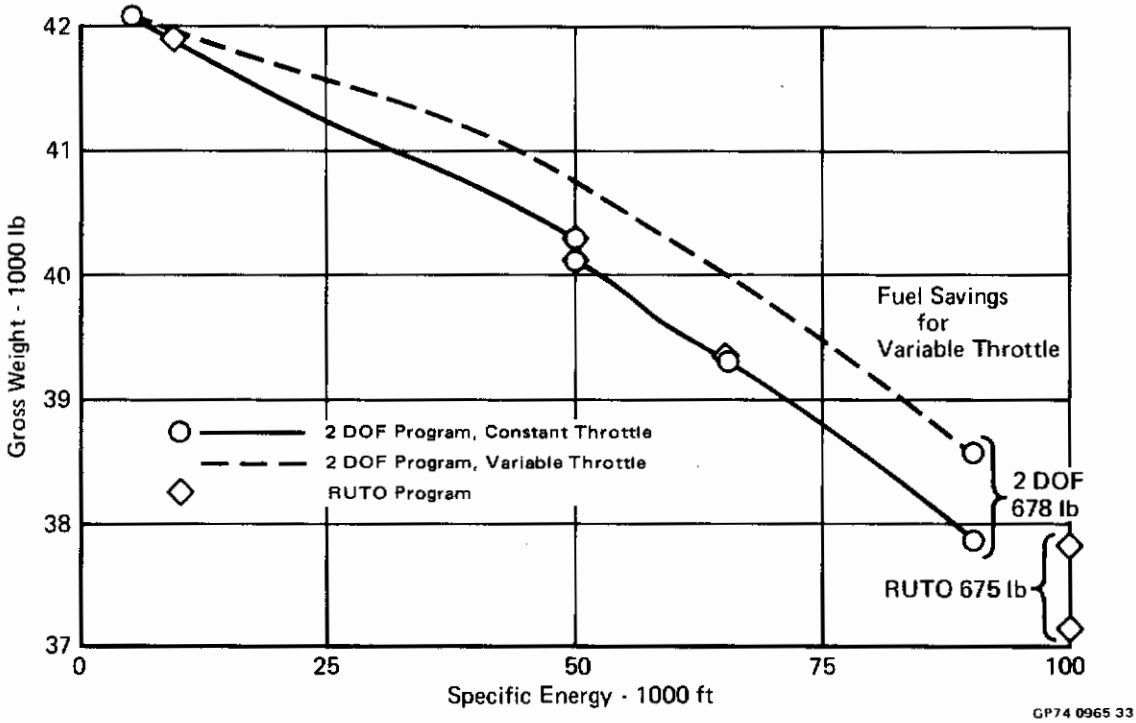

Figure 34 Comparison of RUTO and 2 DOF Performance
Weight vs Energy

Both the F-4E and F-15A are considered on test vehicles in this section, as the better definition of the performance data set which led to selection of the F-4 for this analysis effort may not be a factor in the near future, when the F-15 test program has been completed. The most significant differences between the aircraft concerning a throttle/energy management test are:

a. The systems and sensors of the F-4E are analog type, requiring development and installation of digital interface units and a digital EM (Energy-Management) computer. The F-15A has digital flight test instrumentation, INS and CADC, and the CCC (Central Computer Complex) provides a programmable digital computer already interfaced with the INS and CADC.

b. The F-4J automatic landing autothrottle system could be adapted to the F-4E, with some modification for use at modulated A/B settings. The F-15 would require development of a new autothrottle system for demonstration of an automatic variable throttle mission.

Flight Instruments for Energy Management - Standard instruments are all that is required (altitude, velocity, pitch or flight path angle, throttle setting). The digital interface problem for the F-4, mentioned above is the only major factor to consider.

Engine Instruments and Autothrottle System - The F-4J autothrottle system, which uses an engine-mounted servo, is adaptable to the F-4E, which uses the same engine. A digital interface unit to the throttle command signal from the E/M computer must be added. In the F-4J, the servo authority limits are Idle to Mil power, but the authority can probably be extended to Max A/B. The throttle quadrant has a detent on A/B position which may need a manual input to permit a servo-driven quadrant to follow the autothrottle servo on the engine. There is a jump in thrust between Mil and Min A/B setting. This is accounted for in the control system design of Section 3 by computing a throttle switch point, before which the upper limit on throttle command is Mil setting, and after which the lower limit is Min A/B. In either automatic or manual operation, the switch point signal could be used in a display to alert the pilot to move the quadrant to A/B setting. The type of power-lever angle (PLA) sensor used on the F-15 can be added, for input to the display and the E/M computer. It is digital and needs no interface unit.

A cam in the F-15 throttle quadrant permits use of a servo-driven quadrant with full authority. There is no sensible gap in thrust at A/B lightoff, allowing a smooth transition into modulated A/B. An alternate type of autothrottle would have the pilot set a nominal PLA to match a display command, and input a digital

signal for an incremental PLA from the EM computer direct to the engine trim control, which has a limited authority of about 10° PLA. No additional actuator would be needed, and this system might reduce the need for continuous attention to the throttle control sufficiently that the pilot workload of operating both the throttle and flight path control would be acceptable.

Measurements of fuel quantity and fuel flow rate are not used in the EM control system, but an accurate measurement of fuel used is very important to a successful test of variable throttle/energy management, as the fuel savings on the mission (compared to a fixed throttle flight) will be used to evaluate the performance benefit of variable throttle control. The flowmeter system used for F-15 performance tests meets this requirement. It consists of a low capacity flowmeter in the primary fuel line, a high capacity flowmeter in the total fuel line (primary plus augmentor fuel), Carrier electronics that generate pulses at the flowmeter frequency to measure volume flow rate, and a totalizer that sums the pulses to measure primary and afterburner fuel volume used. By recording the totalizer signal and a time code, the fuel volume used between any two time points can be measured to an accuracy of better than one percent. Fuel density depends on the fuel temperature and its source. By sampling the fuel density as it is put into the tanks before the flight and recording the temperature in the fuel lines during the flight, the fuel weight used is determined in post-flight data reduction. Some F-15 test aircraft have this system installed, and it can be added to an F-4 or other F-15 aircraft. The fuel rate and fuel quantity signals are digital and do not require a digital interface unit.

Energy Management Computer - The F-15 has the CCC programmable digital computer installed, with enough spare capacity for the throttle/energy management control and display functions. The F-4 needs a small digital computer to be added, preferably a programmable one.

Energy Management Display - On the F-4, the radar CRT or a TV picture of the CRT projected on a helmet sight might be used for display. Preprogrammed read-only memories (ROMs) can be prepared to generate the fixed part of the display, and a symbol generator would be needed for the moving part. An alternative is to use a transparent overlay of the optimal flight path (as in Figure 82) with only a moving dot, representing the current aircraft Mach-altitude condition, to be generated by the CRT. This approach has the advantage that the commanded path can be easily changed by changing overlays.

The F-15 has programmable displays on the Heads-Up-Display (HUD), radar, and Vertical Situation Display (VSD) CRTs , with data for the display generated by the CCC computer. Replaceable, preprogrammed ROMs would be needed for the different types of display. Changes in the CRT data, or replaceable overlays could be used to change the commanded path.

The measured and commanded throttle setting could be displayed for either aircraft by a dial or CRT display.

Flight Test Performance Measurement - Flight performance instrumentation is needed because different aircraft of the same type can differ significantly (up to 8%) in drag and thrust, so a drag and thrust basis from previous tests is not sufficient. The type of performance instrumentation and data recording used on the F-15 is desirable. This is described in Reference 3. It requires measurement of flight path acceleration and the engine data needed for input to an engine deck. Comparable performance instrumentation installations have been used on the F-4. If possible, an aircraft already equipped for performance testing should be used.

For comparison of performance on different flights it will be necessary to make corrections for differences in weight and atmosphere conditions (winds and temperature) between flights. The initial weight and CG location can be determined on the ground from properly calibrated fuel tank gages, and the weight estimate can be updated inflight from the pitch angle in steady level flight. The weight variation between updates is given by the fuel totalizer. The variation in atmosphere conditions is reduced by testing on successive days at the same time of day. Meteorological soundings should be made. Energy management studies by MCAIR show that the optimum flight path and performance vary significantly with nonstandard atmosphere temperature profiles, so it may be advisable to use stored path data designed for the temperature profile measured or expected at the time of test, rather than standard day data.

With the present state of test technology, the necessary accuracy of the energy management measurements (weight, drag, thrust, fuel flow) is obtained by post-flight data corrections and analysis. If methods of making in-flight measurements of comparable accuracy are used, they would help the test program by providing the pilot quicker evaluation of the performance. Another benefit of using and evaluating in-flight performance measurement methods is that an operational energy management system may need such data to present the pilot with an accurate prediction of mission performance and selection of the optimum path.

Multimission Energy Management - The energy management control concept selected in this study, which is to follow a stored flight path program based on a previous trajectory calculation, is best suited to demonstration of a single mission profile between preselected initial and final conditions, with a small on-board computer capability, on the order of a few hundred words of memory. If the test objective is expanded to include evaluation of the benefits in operational flexibility promised by an energy management system (that is, getting near-optimum performance on a variety of missions); considerably more computing capability and a more complex control scheme would be required. The CCC computer in the F-15 may be large enough. Some change in the control concept would also be needed, because it is not practical to store path data for all the different missions and initial and final conditions of interest.

SECTION 3

THROTTLE/ENERGY MANAGEMENT CONTROL SYSTEM DESIGN (TASK III)

The F-4E was chosen as the aircraft for this throttle/energy management control system design and analysis effort (Task III). Since flight test is considered a logical follow-on activity, a primary design goal was to define control laws which would require minimal changes to the existing F-4 control system and instrumentation.

The chapter is divided into three sections. The first two sections cover the linear and nonlinear analyses and are roughly chronological in tracing the evolution of the control system design. Recommendations for certain refinements in the design prior to flight test are made; however, full evaluation of these suggestions was beyond the scope of this program. The third section presents a discussion of the performance benefits obtained using the throttle/energy management control system to follow the two flight test demonstration flight paths defined in Section 2.1.2.

3.1 Linear Analyses

3.1.1 Preliminary Analysis and Design - A fundamental assumption in this preliminary analysis was that the aircraft was flying some "optimal" flight path for which the desired rate of change of aircraft specific energy was small relative to the time required to null out perturbations in the aircraft velocity, altitude, and throttle setting from desired values associated with the optimal flight path.

Linear perturbation equations were written for the F-4E defining deviations from a desired flight path. Two flight conditions consistent with typical RUTO-generated optimal flight paths were selected and the airframe coefficients and control component math models corresponding to these flight conditions were evaluated for use in the preliminary linear analysis and computer simulations. A root locus deck and a time history simulation CSMP (Continuous System Modeling Program) deck incorporating the throttle servo, engine dynamics, and engine thrust as a function of throttle setting were used to develop and evaluate several trial designs of the combined flight path/throttle control system. The root locus computer program was used to select control law candidates which exhibited satisfactory pole-zero configurations and the time history computer program was used to evaluate how well the control system performed in nulling out deviations from the optimal flight path.

The two flight conditions chosen for preliminary linear analysis were .85 Mach at 25,000 feet and 1.5 Mach at 35,000 feet. Consistent with the design goal of minimal modification to the existing F-4 control system, the flight path control system configuration was selected to be the F-4E attitude/altitude hold control system. The primary modification to the existing F-4E control system was the addition of an automatic variable throttle control law. This control law continuously compares the aircraft specific energy with that associated with the optimal flight path and feeds the difference back to the throttle servo. Under the fundamental assumption mentioned at the beginning of this section, this control system configuration corrects deviations from the flight path along a constant specific energy contour. Several types of throttle loop compensation were investigated including lead-lags, pure integrators, etc., but root loci analysis which included variation of the flight path angle showed that a simple gain was the most satisfactory. This conclusion was later modified as discussed in Section 3.2.3 for reasons not placed in evidence by the linear analysis.

The small perturbation block diagram of the F-4E with stability augmentation, flight path control and variable throttle loops is shown in Figure 35. Rate gyros, accelerometers and other "high frequency" dynamics were omitted since they were beyond the frequency range of interest for this throttle/energy management investigation. The system shown in the figure was used for all preliminary root loci and time domain studies.

Several linear time history simulations were made at the two flight conditions using a throttle loop gain $K_E = -.02$. These simulations included cases in which the phugoid derivatives (X_u, X_h) were modified to reflect the effect of thrust acceleration. In all cases the aircraft was assumed to be initially perturbed from the optimal flight path along a constant energy contour (i.e., the aircraft was initially at the correct specific energy level but at the wrong Mach-altitude point). The initial conditions for the two flight conditions are tabulated below:

	.85 Mach @ 25 K ft	1.5 Mach @ 35 K ft
Altitude Error [$\Delta h(0)$]	- 268 ft.	-298 ft
Velocity Error [$\Delta U(0)$]	- 10 ft/sec.	10 ft/sec.
Pitch Angle Error [$\Delta\theta(0)$]	- 3 deg.	-3 deg.

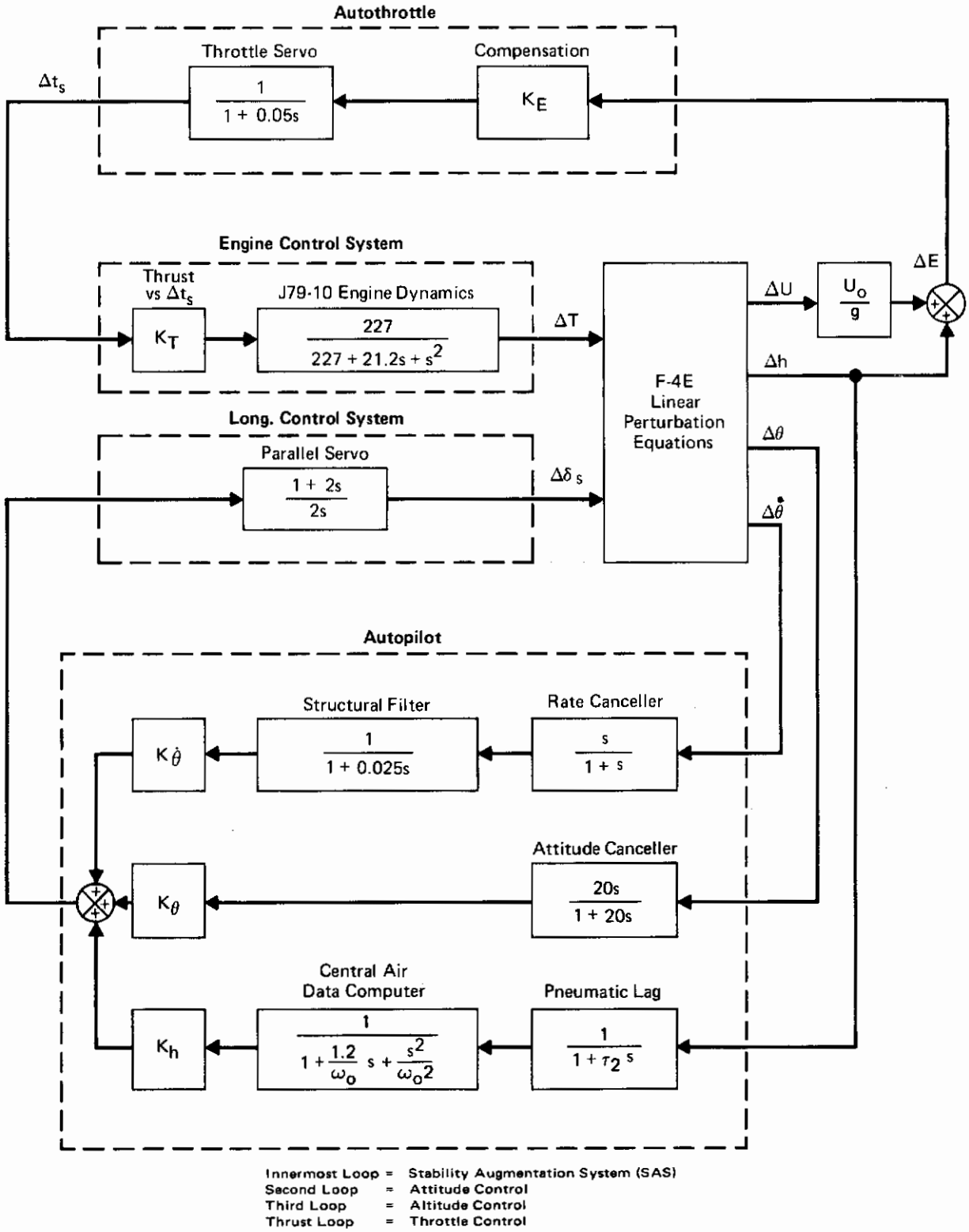

Figure 35 Linear Flight and Throttle Control System Model
F-4E

GP74-0965-34

Time histories of altitude, velocity, and pitch angle errors along with the corresponding stabilator deflection and thrust correction for a typical run at the flight condition of .85 Mach at 25,000 feet are shown in Figures 36 through 40. The initial pitch angle error, $\Delta\theta(0)$, causes the correction of the initial perturbation from the optimal flight path not to occur along a constant energy contour. Corresponding time histories for the flight condition of 1.5 Mach at 35,000 feet are very similar and so are not presented.

3.1.2 Throttle Control System: Peak Hunting Methods - An investigation was made of a "peak hunting" method to determine the feasibility of using such a method to automatically control the throttle to optimize a given performance index. The inherent advantage of this method is that optimal performance can be preserved in the presence of off-nominal conditions such as nonstandard days or engine performance. The F-4E linearized airframe, engine, and flight path control system shown in Figure 41 were used for this analysis. Also, the analysis was performed only for the throttle control system, assuming the flight path control system (or pilot) stabilator action to be "perfect" and the optimum aircraft attitudes achieved with very little angular rate variation.

Sinusoidal Perturbation Method

This method is documented in References 13, 14, and 15. Consider the problem of maximizing the performance index $f(x)$ with respect to the "control" x as represented in Figure 42.

Let the control be given a sinusoidal perturbation

$$x = x_o + A\cos\omega_p t$$

$$f(x) = f(x_o + A\cos\omega_p t)$$

Assuming $f(x)$ to be an analytical function, write a Taylor series expansion about x_o as follows:

$$f(x) = f(x_o) + f^{(1)}(x_o)\ (x-x_o) + \frac{1}{2!} f^{(2)}\ (x_o)(x-x_o)^2 + \frac{1}{3!} f^{(3)}\ (x_o)(x-x_o)^3 + \ldots$$

where

$$f^{(i)}(x_o) = \left.\frac{\partial^i f}{\partial x^i}\right|_{x=x_o}$$

Substitute $A\cos\omega_p t$ for $(x - x_o)$ and multiply both sides by $A\cos\omega_p t$:

$$f(x)A\cos\omega_p t = f(x_o)A\cos\omega_p t + f^{(1)}(x_o)A^2\cos^2\omega_p t + \frac{1}{2!} f^{(2)}(x_o)A^3\cos^3\omega_p t$$

$$+ \frac{1}{3!} f^{(3)}\ (x_o)A^4\cos^4\omega_p t + \ldots$$

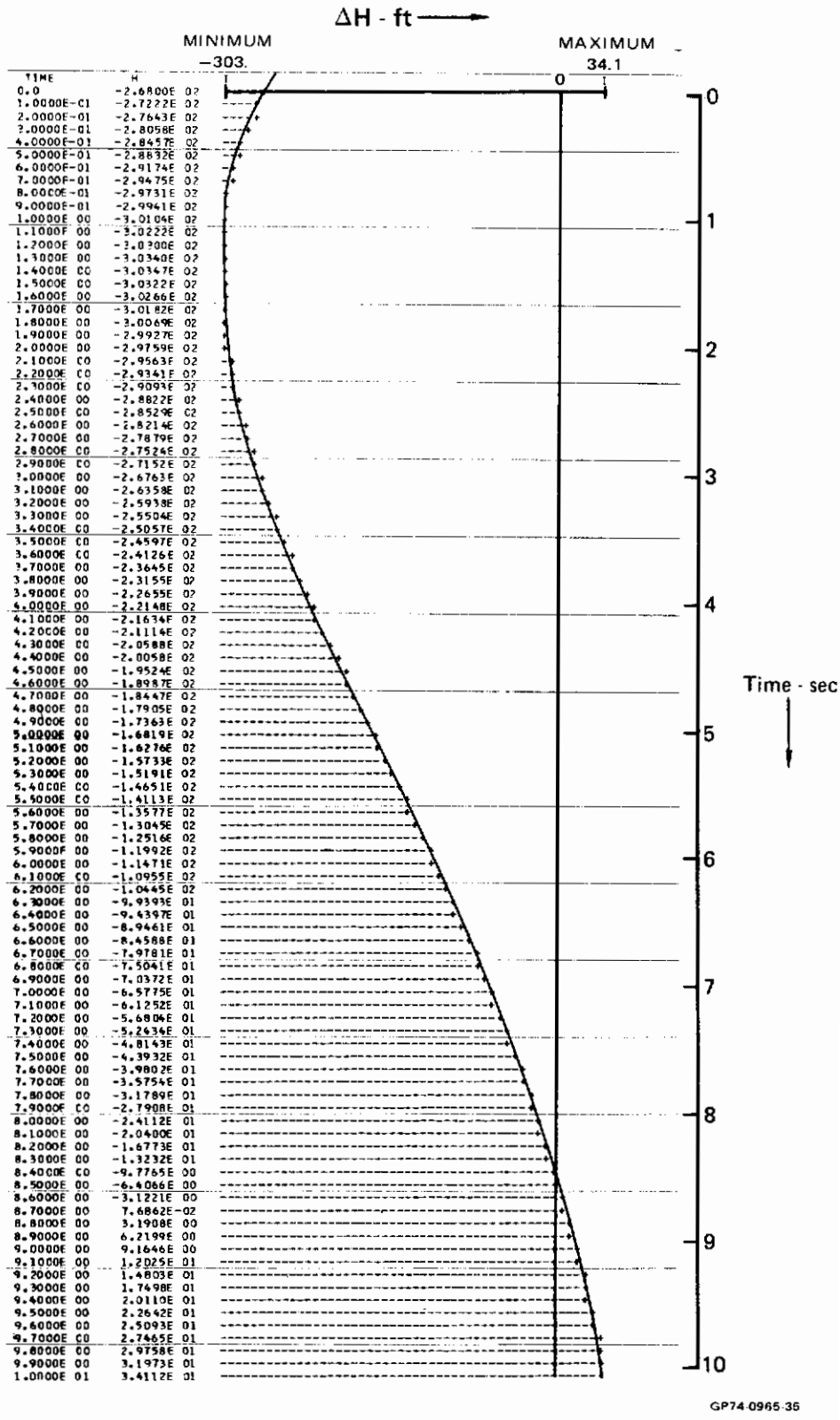

Figure 36 Altitude Error
0.85 Mach at 25,000 ft

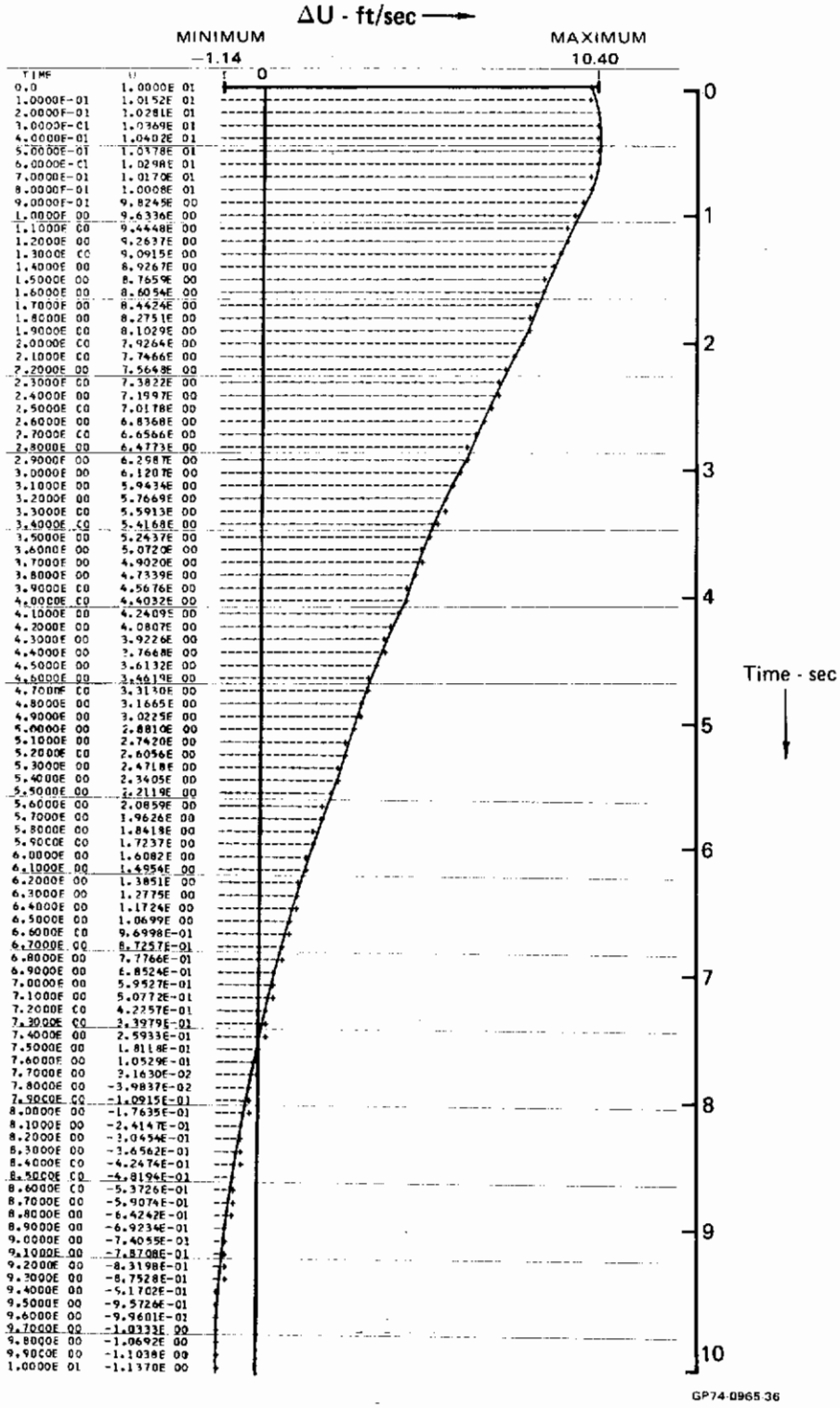

Figure 37 Velocity Error
0.85 Mach at 25,000 ft

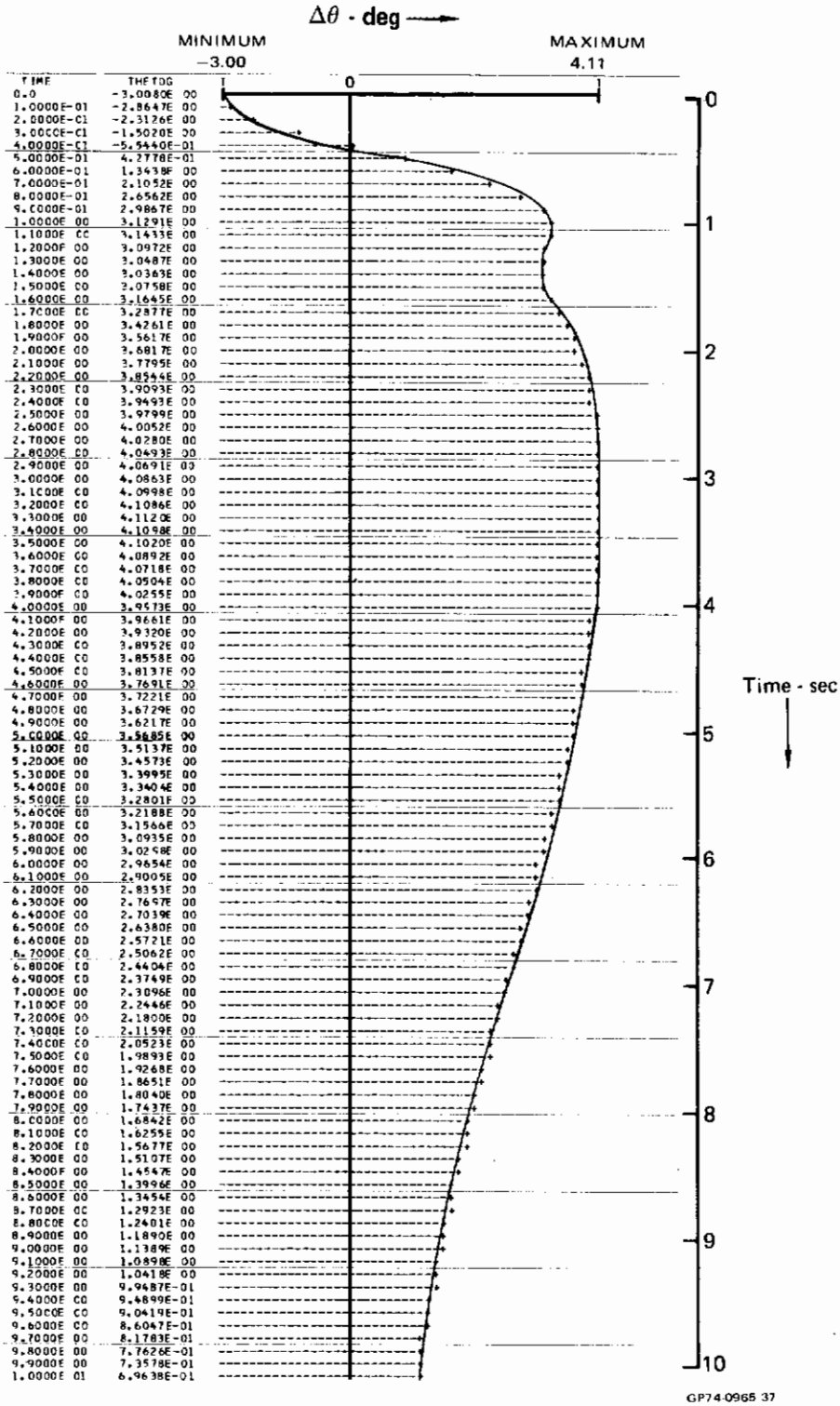

TIME	THETDG
0.0	-3.0080E 00
1.0000E-01	-2.8647E 00
2.0000E-01	-2.3126E 00
3.0000E-01	-1.5020E 00
4.0000E-01	-5.5440E-01
5.0000E-01	4.2778E-01
6.0000E-01	1.3438E 00
7.0000E-01	2.1052E 00
8.0000E-01	2.6562E 00
9.0000E-01	2.9867E 00
1.0000E 00	3.1291E 00
1.1000E 00	3.1433E 00
1.2000E 00	3.0972E 00
1.3000E 00	3.0487E 00
1.4000E 00	3.0363E 00
1.5000E 00	3.0758E 00
1.6000E 00	3.1645E 00
1.7000E 00	3.2877E 00
1.8000E 00	3.4261E 00
1.9000E 00	3.5617E 00
2.0000E 00	3.6817E 00
2.1000E 00	3.7795E 00
2.2000E 00	3.8544E 00
2.3000E 00	3.9093E 00
2.4000E 00	3.9493E 00
2.5000E 00	3.9799E 00
2.6000E 00	4.0052E 00
2.7000E 00	4.0280E 00
2.8000E 00	4.0493E 00
2.9000E 00	4.0691E 00
3.0000E 00	4.0863E 00
3.1000E 00	4.0998E 00
3.2000E 00	4.1086E 00
3.3000E 00	4.1120E 00
3.4000E 00	4.1098E 00
3.5000E 00	4.1020E 00
3.6000E 00	4.0892E 00
3.7000E 00	4.0718E 00
3.8000E 00	4.0504E 00
3.9000E 00	4.0255E 00
4.0000E 00	3.9573E 00
4.1000E 00	3.9661E 00
4.2000E 00	3.9320E 00
4.3000E 00	3.8952E 00
4.4000E 00	3.8558E 00
4.5000E 00	3.8137E 00
4.6000E 00	3.7691E 00
4.7000E 00	3.7221E 00
4.8000E 00	3.6729E 00
4.9000E 00	3.6217E 00
5.0000E 00	3.5685E 00
5.1000E 00	3.5137E 00
5.2000E 00	3.4573E 00
5.3000E 00	3.3995E 00
5.4000E 00	3.3404E 00
5.5000E 00	3.2801E 00
5.6000E 00	3.2188E 00
5.7000E 00	3.1566E 00
5.8000E 00	3.0935E 00
5.9000E 00	3.0298E 00
6.0000E 00	2.9654E 00
6.1000E 00	2.9005E 00
6.2000E 00	2.8353E 00
6.3000E 00	2.7697E 00
6.4000E 00	2.7039E 00
6.5000E 00	2.6380E 00
6.6000E 00	2.5721E 00
6.7000E 00	2.5062E 00
6.8000E 00	2.4404E 00
6.9000E 00	2.3749E 00
7.0000E 00	2.3096E 00
7.1000E 00	2.2446E 00
7.2000E 00	2.1800E 00
7.3000E 00	2.1159E 00
7.4000E 00	2.0523E 00
7.5000E 00	1.9893E 00
7.6000E 00	1.9268E 00
7.7000E 00	1.8651E 00
7.8000E 00	1.8040E 00
7.9000E 00	1.7437E 00
8.0000E 00	1.6842E 00
8.1000E 00	1.6255E 00
8.2000E 00	1.5677E 00
8.3000E 00	1.5107E 00
8.4000E 00	1.4547E 00
8.5000E 00	1.3996E 00
8.6000E 00	1.3454E 00
8.7000E 00	1.2923E 00
8.8000E 00	1.2401E 00
8.9000E 00	1.1890E 00
9.0000E 00	1.1389E 00
9.1000E 00	1.0898E 00
9.2000E 00	1.0418E 00
9.3000E 00	9.9487E-01
9.4000E 00	9.4899E-01
9.5000E 00	9.0419E-01
9.6000E 00	8.6047E-01
9.7000E 00	8.1783E-01
9.8000E 00	7.7626E-01
9.9000E 00	7.3578E-01
1.0000E 01	6.9638E-01

Figure 38 Pitch Angle Error
0.85 Mach at 25,000 ft

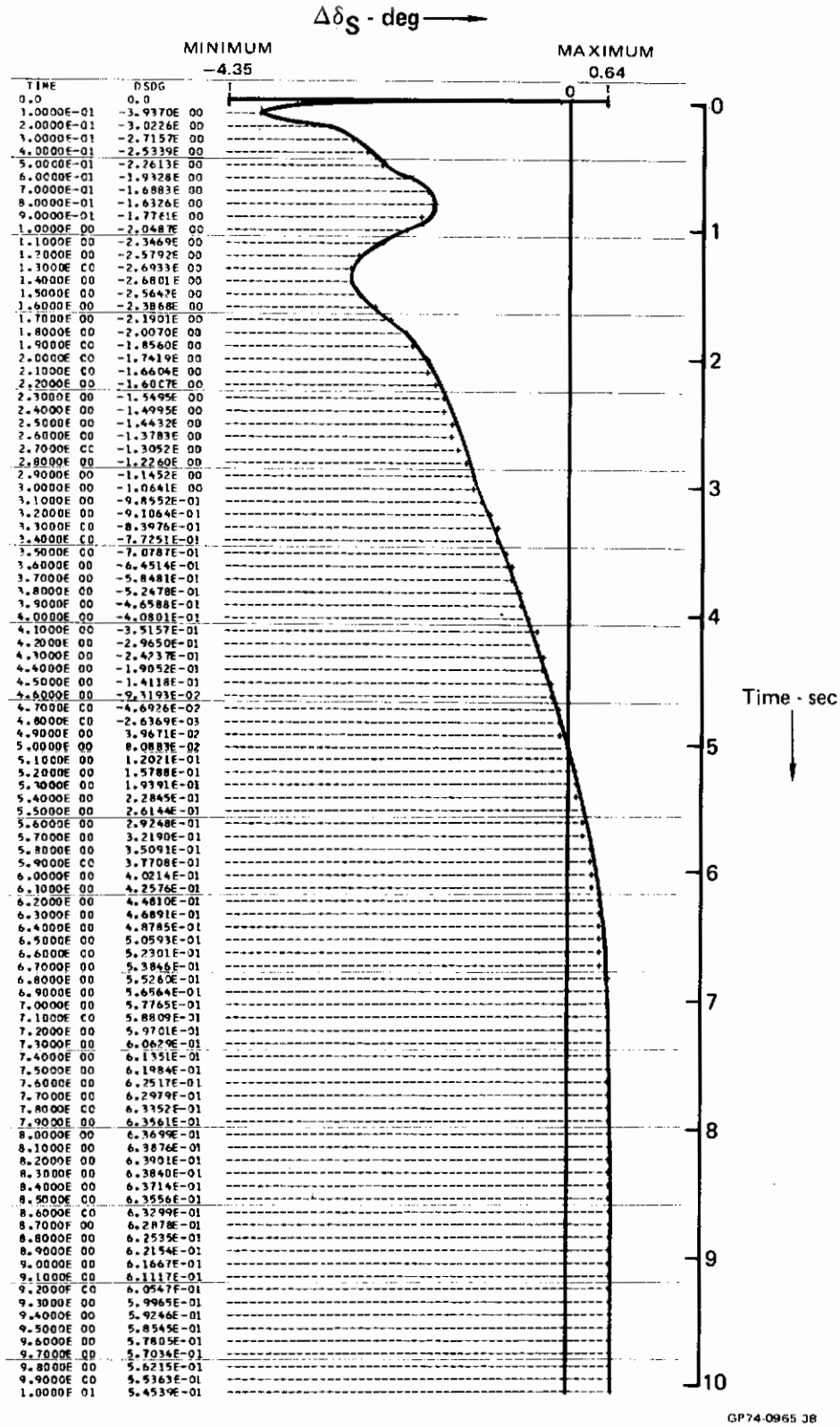

Figure 39 Stabilator Deflection
0.85 Mach at 25,000 ft

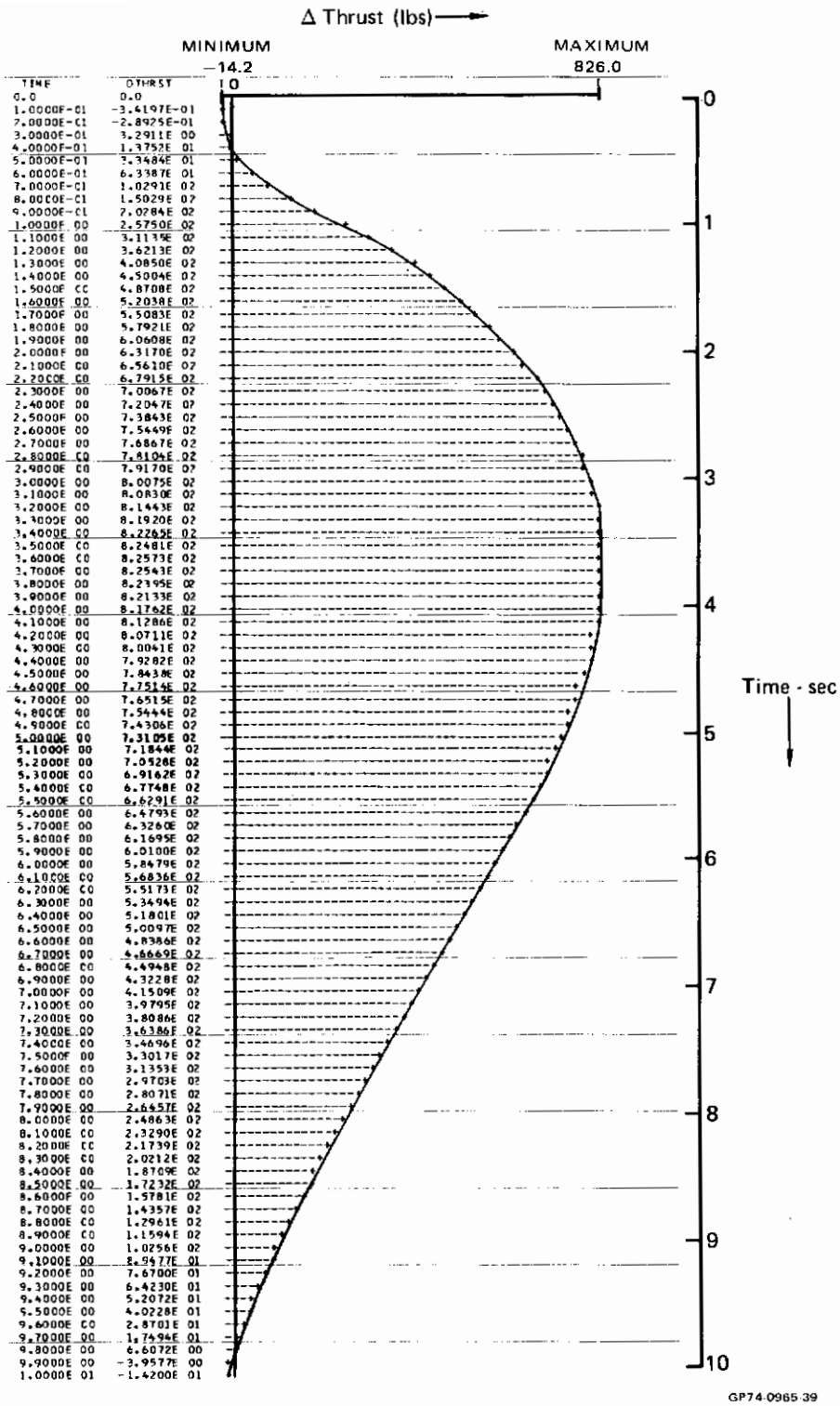

TIME	DTHRST
0.0	0.0
1.0000E-01	-3.4197E-01
2.0000E-01	-2.8925E-01
3.0000E-01	3.2911E 00
4.0000E-01	1.3752E 01
5.0000E-01	3.3484E 01
6.0000E-01	6.3387E 01
7.0000E-01	1.0291E 02
8.0000E-01	1.5029E 02
9.0000E-01	2.0284E 02
1.0000E 00	2.5750E 02
1.1000E 00	3.1135E 02
1.2000E 00	3.6213E 02
1.3000E 00	4.0850E 02
1.4000E 00	4.5004E 02
1.5000E 00	4.8708E 02
1.6000E 00	5.2038E 02
1.7000E 00	5.5083E 02
1.8000E 00	5.7921E 02
1.9000E 00	6.0608E 02
2.0000E 00	6.3170E 02
2.1000E 00	6.5610E 02
2.2000E 00	6.7915E 02
2.3000E 00	7.0067E 02
2.4000E 00	7.2047E 02
2.5000E 00	7.3843E 02
2.6000E 00	7.5449E 02
2.7000E 00	7.6867E 02
2.8000E 00	7.8104E 02
2.9000E 00	7.9170E 02
3.0000E 00	8.0075E 02
3.1000E 00	8.0830E 02
3.2000E 00	8.1443E 02
3.3000E 00	8.1920E 02
3.4000E 00	8.2265E 02
3.5000E 00	8.2481E 02
3.6000E 00	8.2573E 02
3.7000E 00	8.2543E 02
3.8000E 00	8.2395E 02
3.9000E 00	8.2133E 02
4.0000E 00	8.1762E 02
4.1000E 00	8.1286E 02
4.2000E 00	8.0711E 02
4.3000E 00	8.0041E 02
4.4000E 00	7.9282E 02
4.5000E 00	7.8438E 02
4.6000E 00	7.7514E 02
4.7000E 00	7.6515E 02
4.8000E 00	7.5444E 02
4.9000E 00	7.4306E 02
5.0000E 00	7.3105E 02
5.1000E 00	7.1844E 02
5.2000E 00	7.0528E 02
5.3000E 00	6.9162E 02
5.4000E 00	6.7748E 02
5.5000E 00	6.6291E 02
5.6000E 00	6.4793E 02
5.7000E 00	6.3260E 02
5.8000E 00	6.1695E 02
5.9000E 00	6.0100E 02
6.0000E 00	5.8479E 02
6.1000E 00	5.6836E 02
6.2000E 00	5.5173E 02
6.3000E 00	5.3494E 02
6.4000E 00	5.1801E 02
6.5000E 00	5.0097E 02
6.6000E 00	4.8386E 02
6.7000E 00	4.6669E 02
6.8000E 00	4.4948E 02
6.9000E 00	4.3228E 02
7.0000E 00	4.1509E 02
7.1000E 00	3.9795E 02
7.2000E 00	3.8086E 02
7.3000E 00	3.6386E 02
7.4000E 00	3.4696E 02
7.5000E 00	3.3017E 02
7.6000E 00	3.1353E 02
7.7000E 00	2.9703E 02
7.8000E 00	2.8071E 02
7.9000E 00	2.6457E 02
8.0000E 00	2.4863E 02
8.1000E 00	2.3290E 02
8.2000E 00	2.1739E 02
8.3000E 00	2.0212E 02
8.4000E 00	1.8709E 02
8.5000E 00	1.7232E 02
8.6000E 00	1.5781E 02
8.7000E 00	1.4357E 02
8.8000E 00	1.2961E 02
8.9000E 00	1.1594E 02
9.0000E 00	1.0256E 02
9.1000E 00	8.9477E 01
9.2000E 00	7.6700E 01
9.3000E 00	6.4230E 01
9.4000E 00	5.2072E 01
9.5000E 00	4.0228E 01
9.6000E 00	2.8701E 01
9.7000E 00	1.7496E 01
9.8000E 00	6.6072E 00
9.9000E 00	-3.9577E 00
1.0000E 01	-1.4200E 01

Figure 40 Thrust Change
0.85 Mach at 25,000 ft

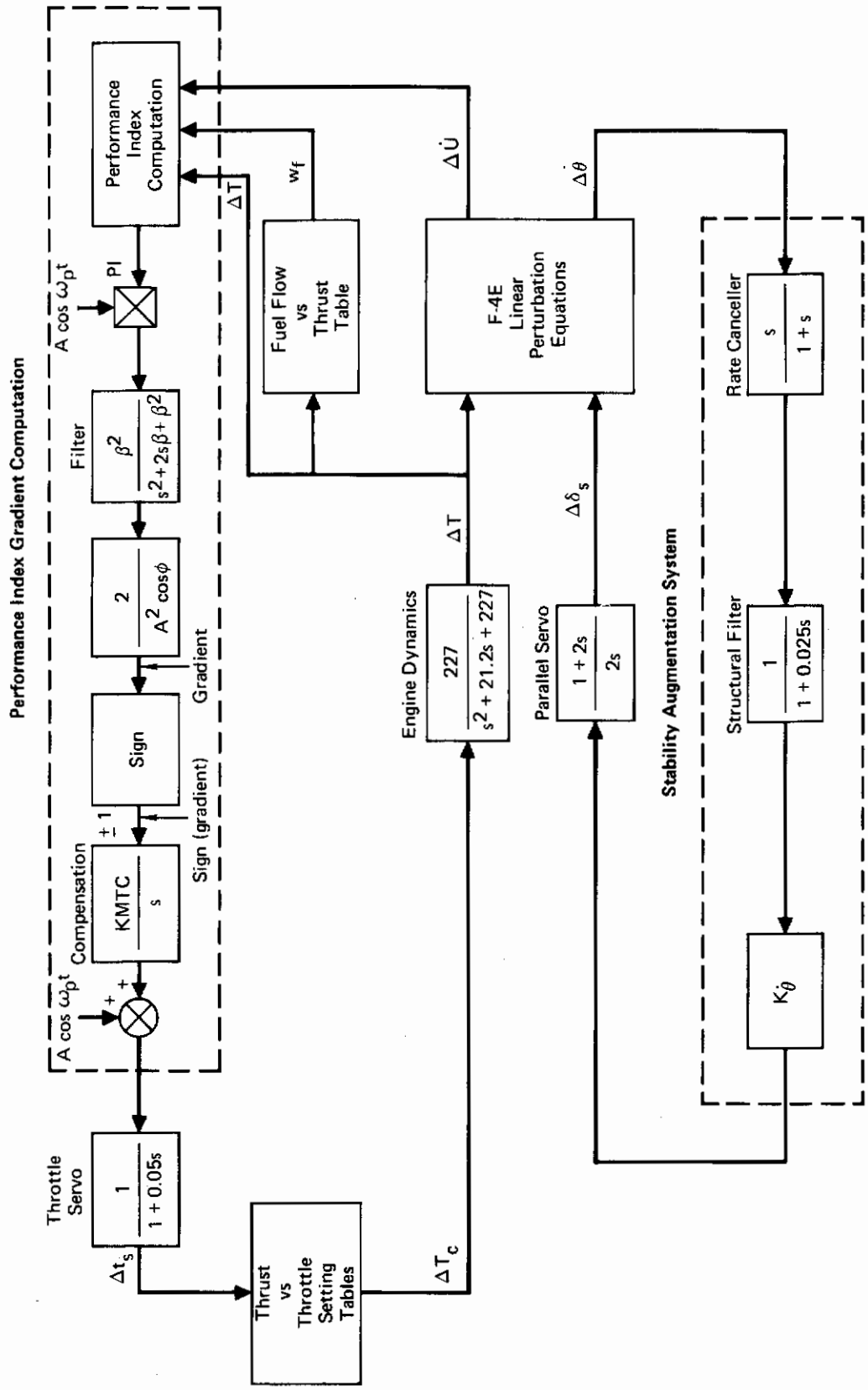

Figure 41 F-4E with Peak-Hunting Throttle Control System

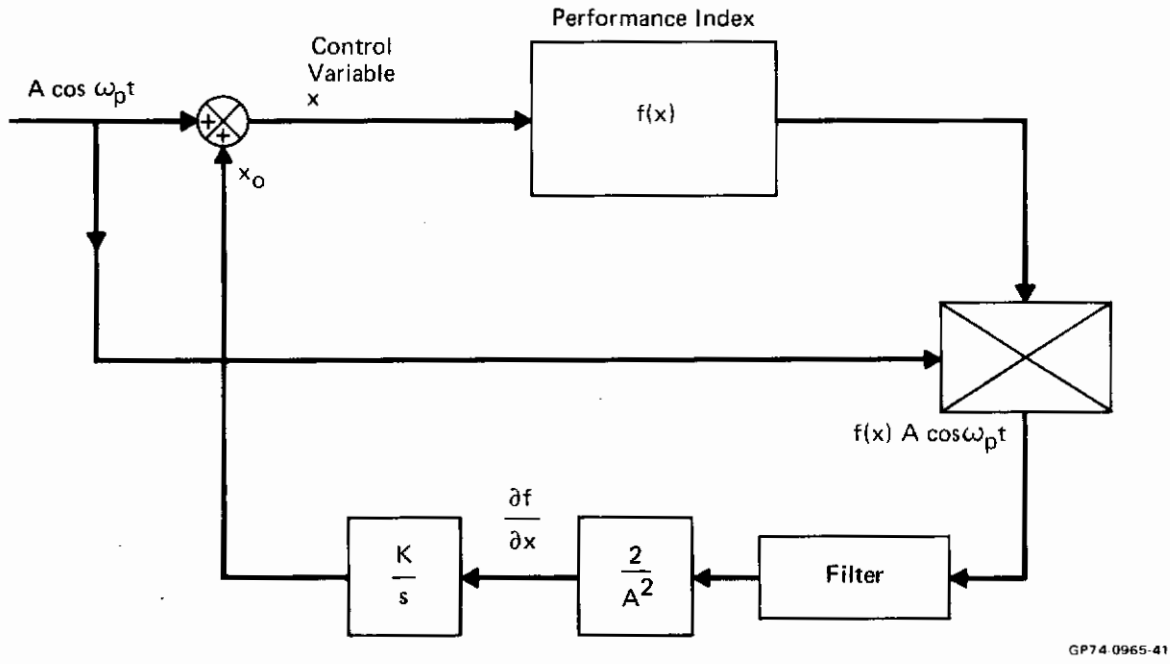

Figure 42 Sinusoidal Perturbation Method

Express the powers of $\cos\omega_p t$ in first order terms:

$$\cos^2\omega_p t = \frac{1}{2}(1 + \cos 2\omega_p t)$$

$$\cos^3\omega_p t = \frac{1}{4}(3\cos\omega_p t + \cos 3\omega_p t)$$

$$\cos^4\omega_p t = \frac{1}{8}(3 + 4\cos 2\omega_p t + \cos 4\omega_p t)$$

$$\vdots$$

Substitute these relationships into the $f(x)\ A\cos\omega_p t$ equation:

$$f(x)A\cos\omega_p t = f(x_o)A\cos\omega_p t + f^{(1)}(x_o)A^2\left[\frac{1}{2}(1 + \cos 2\omega_p t)\right]$$
$$+ \frac{1}{2!} f^{(2)}(x_o)A^3\left[\frac{1}{4}(3\cos\omega_p t + \cos 3\omega_p t)\right]$$
$$+ \frac{1}{3!} f^{(3)}(x_o)A^4\left[\frac{1}{8}(3 + 4\cos 2\omega_p t + \cos 4\omega_p t)\right]$$
$$+ \ldots.$$

Now if all terms which include $\cos(n\omega_p t)$, n = 1, 2, 3, ... are filtered out of the $A\cos\omega_p t$ equation, the filtered signal will be

$$\left[f(x)A\cos\omega_p t\right]_{\substack{\text{Ideally}\\ \text{Filtered}}} = \frac{A^2}{2} f^{(1)}(x_o) + \frac{A^4}{16} f^{(3)}(x_o) + \ldots$$

Choosing A < 1

$$[f(x)A\cos\omega_p t]_{\substack{\text{Ideally}\\ \text{Filtered}}} \cong \frac{A^2}{2} f'(x_o)$$

Hence the gradient of the performance index with respect to the control x has been obtained:

$$\frac{\partial f(x)}{\partial x}_{x=x_o} \cong \frac{2}{A^2} [f(x)A\cos\omega_p t]_{\substack{\text{Ideally}\\ \text{Filtered}}}$$

Using the method of steepest ascent for maximizing f(x) with respect to x (steepest descent for minimizing), we obtain:

$$x_{i+1} = x_i + K \frac{\partial f(x)}{\partial x}_{x=x_o}$$

where K is some positive number to be chosen by "cut and try" to give good system operation. For the case of a continuous control variable x, it has been found that the following expression works well:

$$\frac{dx}{dt} = KMTC \left.\frac{\partial f(x)}{\partial x}\right|_{x=x_o}$$

Here and in the sequel the positive number K is denoted as KMTC.

Modification must be made to the above derivation for two reasons. The first is that there are dynamics which cause phase shifts between the input sinusoid ($A\cos\omega_p t$) and the performance index f(x). This is due to the throttle servo and engine dynamics. The second reason is that physically realizable filters are not "ideal".

In the presence of phase shifts between the input and f(x) an ideal filter would remove all periodic terms leaving the "DC" terms unaffected. This is described by the equation:

$$\frac{A^2}{2} |G(j\omega_p)| \cos\phi \left.\frac{\partial f(x)}{\partial x}\right|_{x=x_o} = [f(x)\cos\omega_p t]_{\substack{\text{Ideally}\\ \text{Filtered}}}$$

where:

G(s) is the transfer function of the throttle servo/engine dynamics;

$|G(j\omega_p)|$ is the magnitude of $G(j\omega)$ at the perturbation frequency ω_p.

ϕ is the phase angle of $G(j\omega)$ at the perturbation frequency ω_p.

Note that because the proposed control system uses only the sign of the

gradient, it is unnecessary to explicitly account for $|G(j\omega_p)|$. If the filter is not ideal, the right hand side of the equation above is attenuated and phase shifted as expressed by the equation:

$$\frac{A^2}{2}|G(j\omega_p)|\cos\phi\left.\frac{\partial f(x)}{\partial x}\right|_{x=x_o} = [f(x)\cos\omega_p t]_{\substack{\text{Ideally}\\ \text{Filtered}}} |F(j\omega_p)|\cos\phi_F$$

where $F(j\omega_p)$, ϕ_F are the magnitude and phase angle, respectively, of the non-ideal filter at the perturbation frequency. This is the form of the performance index gradient equation which was used in the investigation of certain specific cases which are discussed below. A block diagram of the implemented system is shown in Figure 41.

Peak Hunting Method - Implementation

Two performance indices were selected for study of the peak hunting method in optimizing the throttle setting. The indices include both nominal and perturbed aircraft variables as defined below.

Performance Indices

$$PI_1 = \frac{T}{w_f} = \frac{T_{nom}+\Delta T}{w_f}$$

$$PI_2 = \frac{P_s}{w_f} = \frac{\dot{E}_s}{w_f} = \frac{1}{w_f}\left[\frac{U_{nom}}{g}(\dot{U}_{nom} + \Delta\dot{U}) + (\dot{h}_{nom} + \Delta\dot{h})\right]$$

where:

w_f = fuel flow

T_{nom} = nominal thrust

ΔT = thrust perturbation

U_{nom}, $\dot{U}_{nom}$ = nominal longitudinal velocity and acceleration

$\dot{h}_{nom}$ = nominal altitude time rate of change

$\Delta\dot{U}$ = longitudinal acceleration perturbation

$\Delta\dot{h}$ = altitude time rate of change perturbation

The object is to maximize the performance index with respect to the throttle setting. The indices chosen can be optimized by hand calculation so that the "correct" answers were known in advance for the nominal flight conditions selected.

The optimal throttle settings, which happen to be the same for both performance indices at the nominal flight condition selected for the investigation, are shown in Table I to be $t_{s_{opt}} = 61.0^o$.

Nominal Flight Conditions

The nominal flight condition for the first performance index, PI_1, was selected as trimmed unaccelerated flight at Mach .8 and 15,000 feet. The corresponding throttle setting (power lever angle) is 49.1°. This was used

as the starting point in the gradient search to optimize the performance index PI_1. In the case of PI_2, the nominal flight condition was modified to $\dot{U}_{nom}$ = 6 ft/sec^2, $\dot{h}_{nom}$ = 147 ft/sec, γ = 10 deg, T_{nom} = 21,000 lbs, $t_s(0)$ = 80°. As in the first case, the aircraft linearized perturbation equations were based upon a nominal flight condition of .8 Mach at 15,000 feet.

Filter Parameters and Dynamic Phase Shifts

The filter was initially selected to be a two pole Butterworth configuration. A modest parameter study yielded satisfactory filter natural frequency and damping parameters as well as perturbation signal frequency and amplitude parameters as tabulated below:

Perturbation Signal Parameters

Amplitude (A) = .5 deg.

Frequency (ω_p) = 4 Hz.

Filter Parameters

Natural Frequency (β) = .2 Hz.

Damping (ζ) = .707

At the selected perturbation frequency, ω_p, the throttle servo and engine dynamics lags were approximately 45° and 150°, respectively. These two lags comprise the lag parameter denoted as ϕ in Figure 41. Note that the selected

Table I Performance Index Values
F-4E
0.8 M at 15,000 ft

t_s		Thrust (1 Engine)	w_f (1 Engine)	PI_1 $\frac{T}{w_f}$	PI_2 $\frac{\dot{E}}{w_f}$
Idle	20	400	400	1	–
	32	400	1219	0.328	–0.00041
	43	2020	3219	0.628	–0.00620
	49	3635	4350	0.836	–
	50	3860	4500	0.858	0.00360
	56	5610	5500	1.025	0.00920
	61	7070	6240	1.130	0.01280
Mil Pwr	75	7810	8312	1.080	0.01150
	78	10300	16360	0.610	0.00890
	88	11400	20758	0.550	0.00810
	100	12800	25157	0.510	0.00780
Max A/B	115	13700	29558	0.465	0.00725

perturbation frequency must be such that ϕ is not near a zero of the cosine function. For the purposes of this study the two lags constituting ϕ were considered to yield sufficient accuracy. A more detailed analysis should include additional lag components such as that due to instrumentation, fuel pumps (perhaps even aircraft dynamics depending on the performance index chosen).

Performance Index One - Results

The performance index gradient gain was selected as KMTC = 1 for this case and it gave reasonably good results. Graphs of the throttle setting and performance index, PI_1, versus time are shown in Figures 43 and 44, respectively. The throttle setting was changed by the optimizing algorithm from its initial trimmed setting of 49.1° to approximately 57.5° in 20 seconds. However, because the performance index is relatively flat near its optimal value (61°), the small resultant gradient in this region yields slower convergence. The convergence may be made more rapid by selecting larger values for KMTC as is described for the case involving the performance index PI_2.

Performance Index Two - Results

Because the "slope" of PI_2 is flatter than that of PI_1, the gradient gain was initially selected as KMTC = 4. Graphs of the throttle setting and performance index PI_2, versus time are shown in Figures 45 and 46, respectively. The throttle setting changed from its initial value of 80° to approximately 66° in 20 seconds (again the optimal value is t_s = 61°). To speed up the convergence rate, the gradient gain was doubled to KMTC = 8. The corresponding throttle setting and performance index graphs are shown in Figures 47 and 48, respectively. In this case the throttle setting converged to its optimal value in approximately 15 seconds.

A graph of the performance index gradient for the latter case (KMTC = 8) is shown in Figure 49 (actually the program prints out the negative of the gradient). A definite four cycle "noise" component to the gradient is clearly predominate in the response. It was a fortunate result in this case that the (negative) gradient had a slightly positive bias as it oscillated between positive and negative values as this oriented the throttle setting search in the correct direction. Because this could not be expected in general, attempts were made to construct the gradient without the four cycle component. Shifting the two pole Butterworth filter frequency from .2 Hz to lower frequencies provided no significant improvement as the gradient signal was also attenuated.

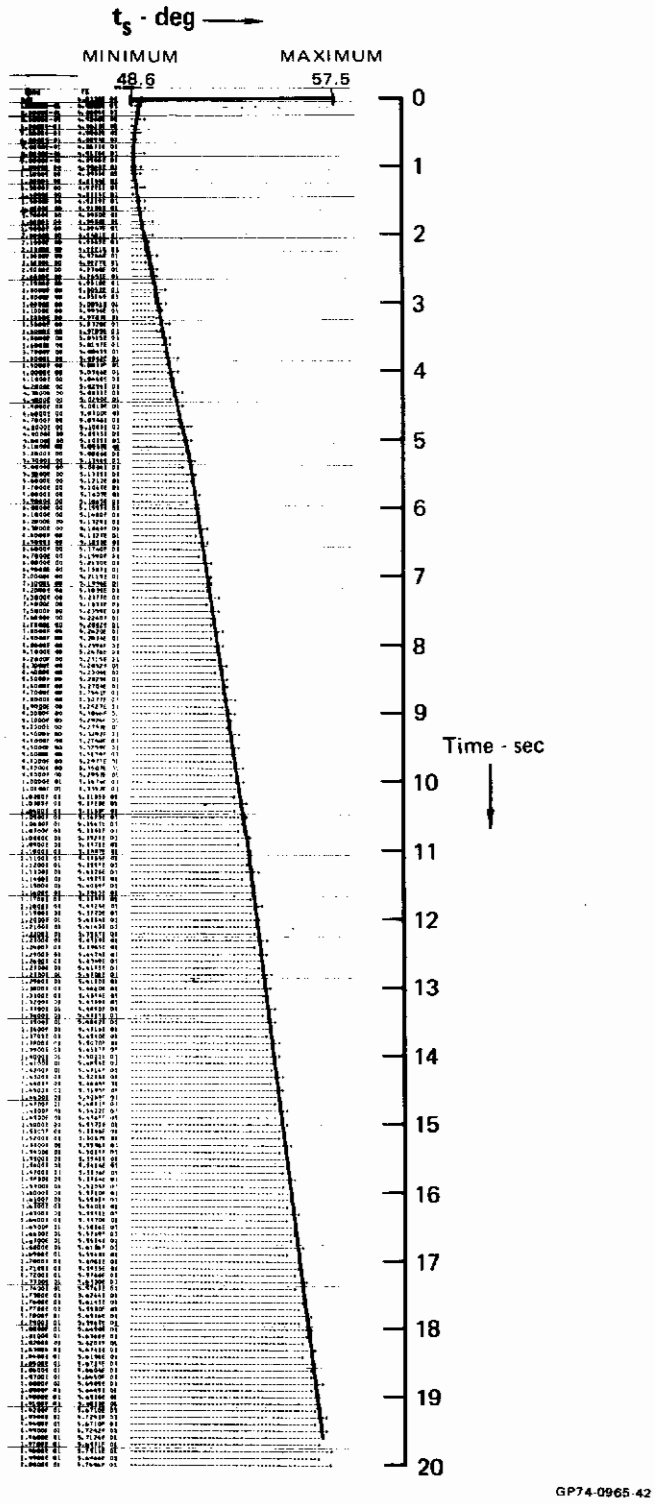

Figure 43 Throttle Setting, $PI_1 = \frac{T}{w_f}$, KMTC = 1

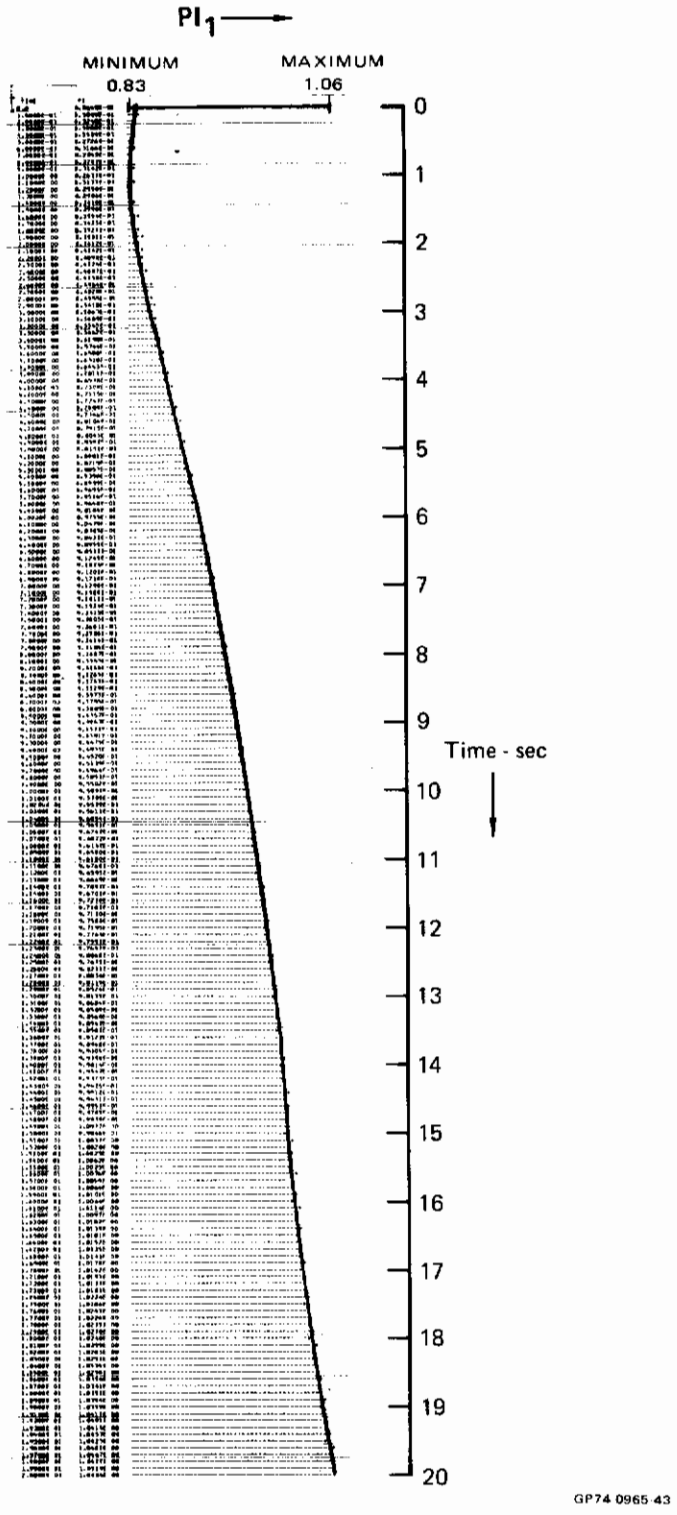

Figure 44 Performance Index, $PI_1 = \frac{T}{w_f}$, KMTC = 1

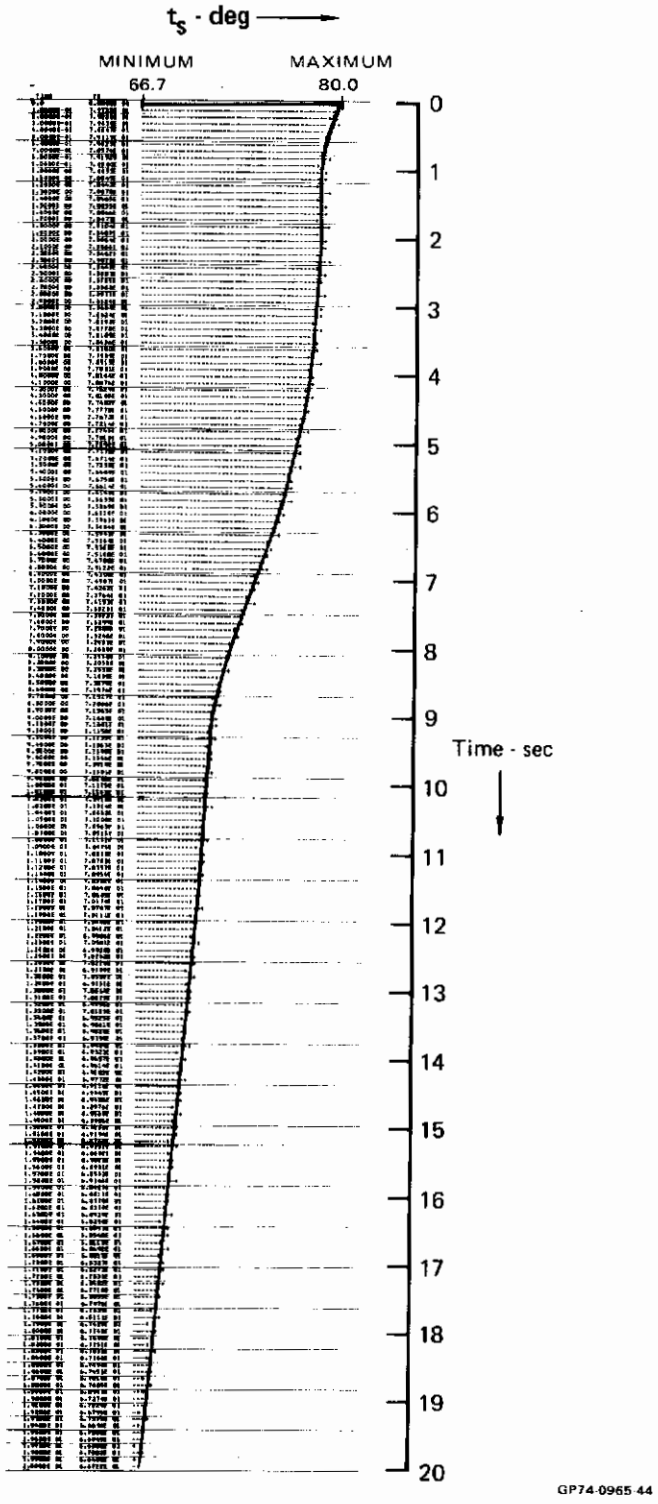

Figure 45 Throttle Setting, $PI_2 = \frac{\dot{E}}{w_f}$, KMTC = 4

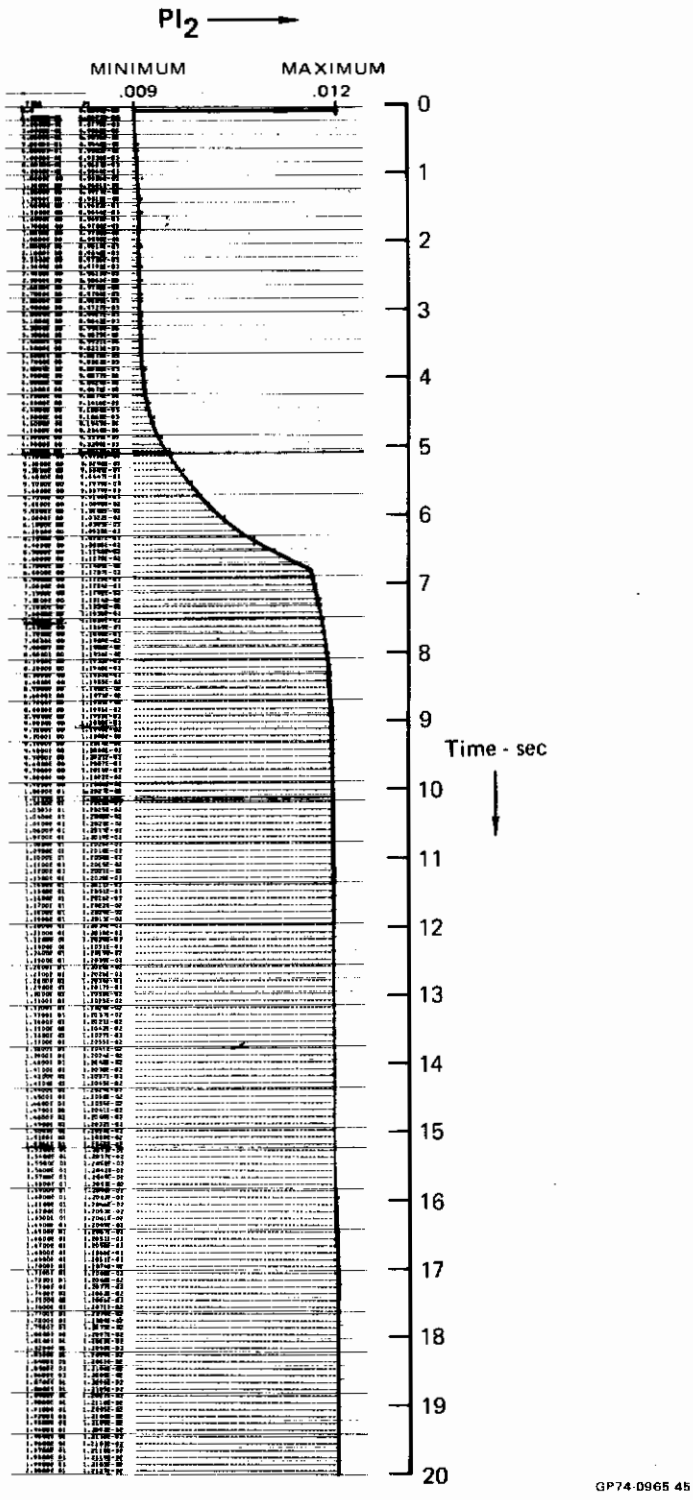

Figure 46 Performance Index, $PI_2 = \frac{\dot{E}}{w_f}$, KMTC = 4

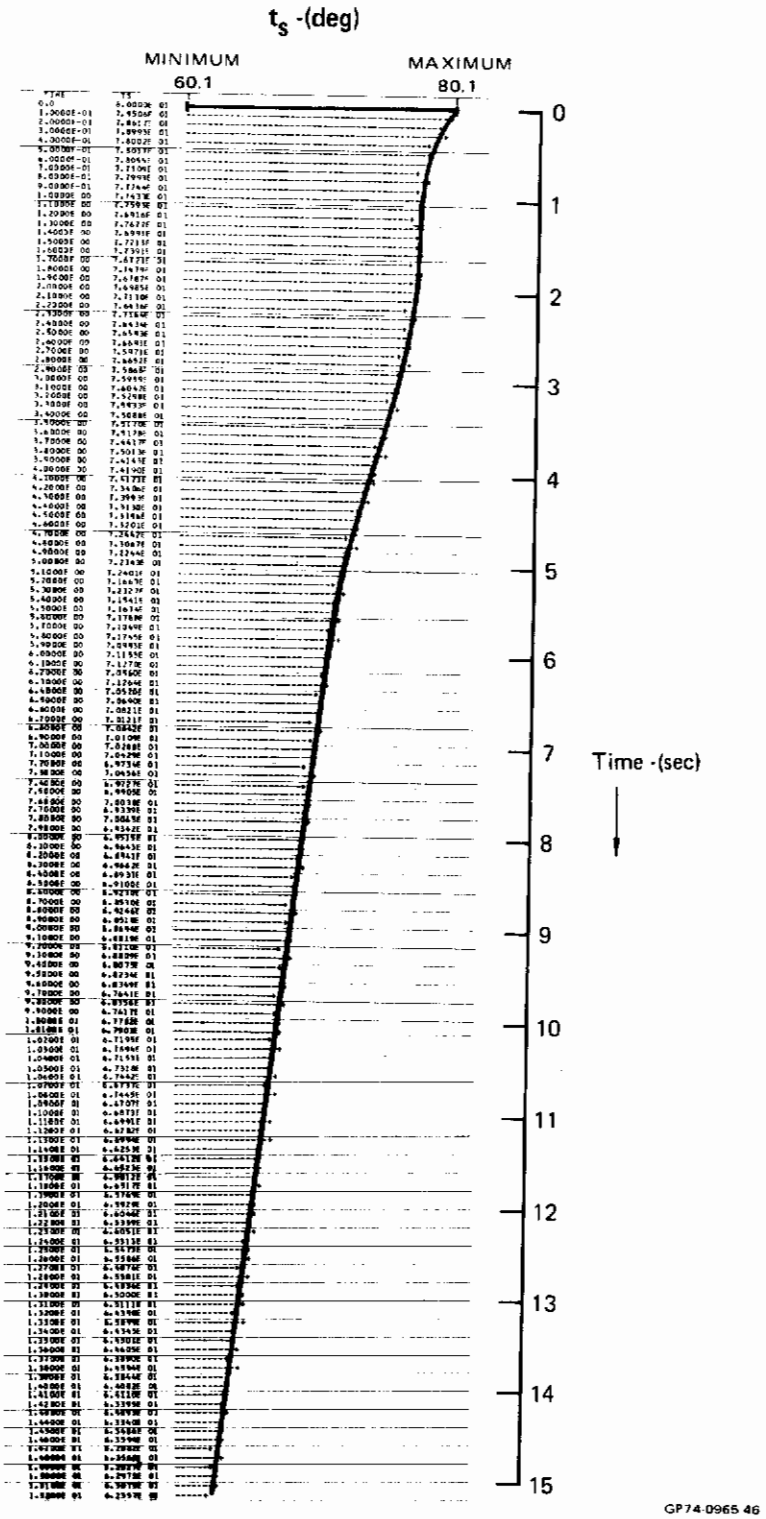

Figure 47 Throttle Setting, $PI_2 = \frac{\dot{E}}{w_f}$, KMTC = 8

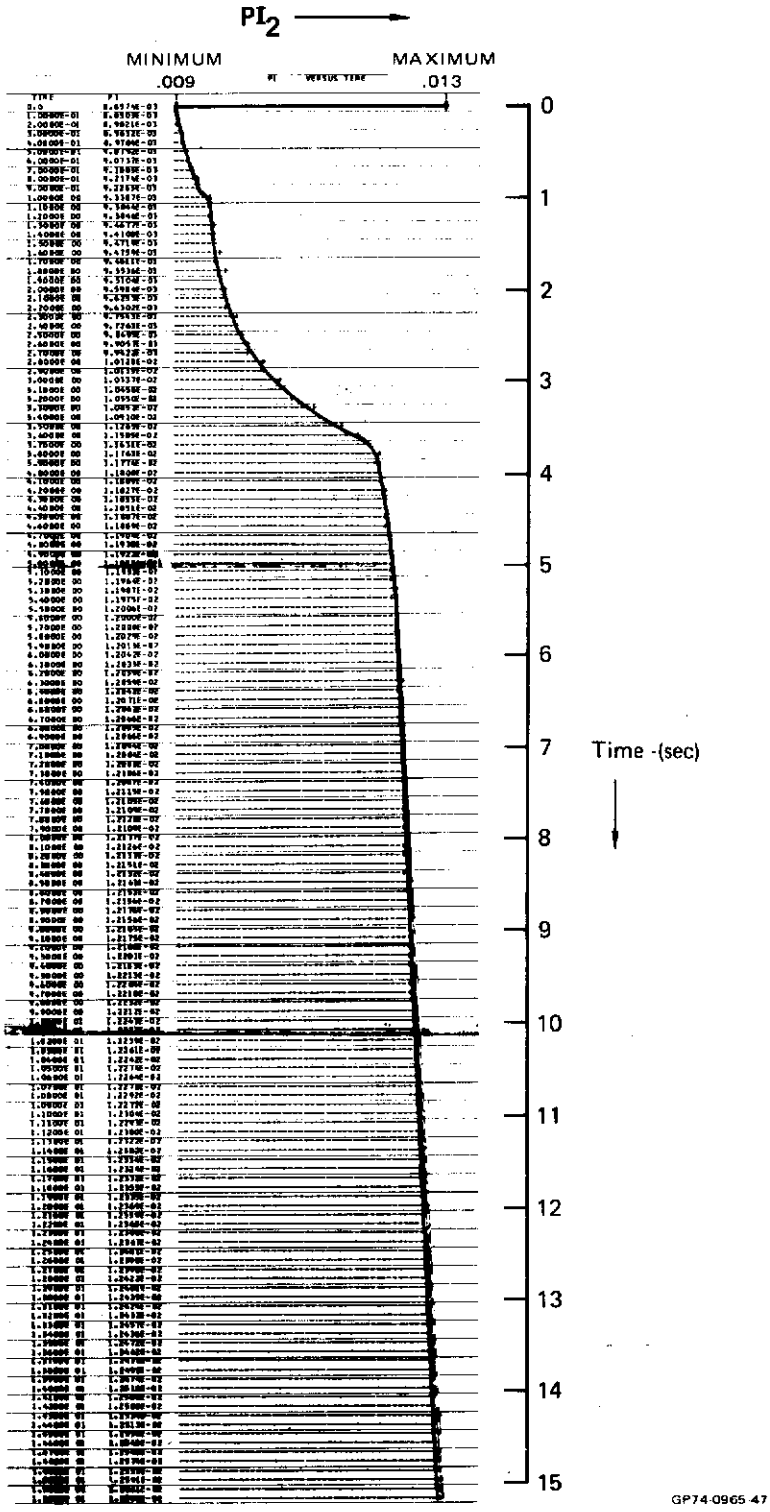

Figure 48 Performance Index, $PI_2 = \frac{\dot{E}}{w_f}$, KMTC = 8

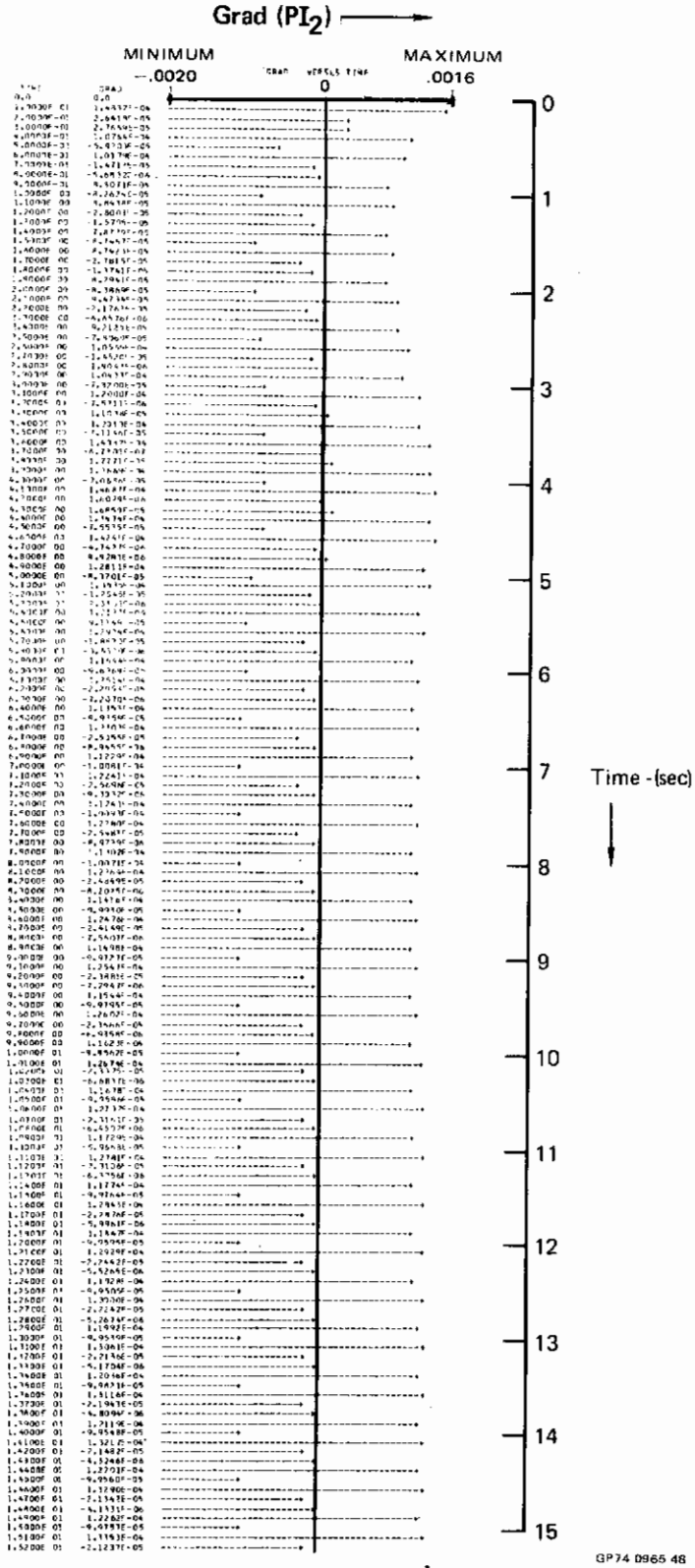

Figure 49 (Neg.) Gradient, $PI_2 = \frac{\dot{E}}{w_f}$, KMTC = 8

Butterworth filters of 3, 4 and 6 pole configurations and various frequencies were tried. These had the effect of successfully filtering the perturbation frequency (the 4 Hz component) but the gradient computation now oscillated at the filter frequency causing system instability. A 4 Hz notch filter also proved unsatisfactory.

Conclusions

While the sinusoidal perturbation method can be "tuned" to work even for certain relatively shallow gradient performance indices (such as PI_2) at a given flight condition and initial throttle setting "error", in general, phasing problems caused by both system dynamics and filter dynamics cannot be overcome to give reliable stability and safe system operation. Furthermore, the filter phasing problems are aggravated by the fact that we desire the throttle setting to converge rapidly to the optimal value. Thus, the throttle is changing quite rapidly as the method is trying to construct the gradient which results in a "smear" of gradients at various throttle settings. Because the filter delays construction of the gradient signal, overshoots and oscillation occur which can lead to instability.

Reference 16, which was discovered toward the end of the investigation described above, comes to substantially the same conclusions in regard to the phasing problems with a moving reference point (throttle setting). This reference suggests using a random perturbation method which does not have these phasing problems for peak hunting. This method is based on certain linear stochastic relationships involving the use of cross power spectral densities to construct system transfer functions. This method of peak hunting was tried but was also unable to construct the gradient correctly. Its failure was most likely due to the system nonlinearities not being sufficiently "linear" even in the small random perturbation region studied.

In conclusion, these peak hunting methods are not considered feasible for throttle control at this time. Much more investigation is required before it can be determined if these techniques can be made reliable and the stability problems overcome.

3.1.3 Linear Model with Control Law Dynamic Coupling - The linearized perturbation simulation described in Section 3.1.1 was modified to include the dependence of the control laws on the stored optimal flight path parameters

such as h_{opt}, U_{opt} and $\dot{E}_{opt}$ explicitly. This allows relaxation of the constant specific energy assumption made in Section 3.1.1. For a given optimal flight path, the path parameters are defined as functions of the aircraft specific energy so that coupling is introduced between the optimal flight path and the dynamic response of the aircraft.

Consider the aircraft equations to be linearized about a particular energy level E_o on an optimal flight path denoted as $P_o = (E_o, \theta_o, \alpha_o, U_o, h_o, \dot{U}_o, \dot{h}_o)$. For small perturbations about the point P_o we have that

$$dh_{opt} = \left.\frac{\partial h_{opt}}{\partial E}\right|_{E_o} dE = C_1\, dE$$

$$d_{\ opt} = \left.\frac{\partial \theta_{opt}}{\partial E}\right|_{E_o} dE = C_2\, dE$$

$$d\dot{E}_{opt} = \left.\frac{\partial \dot{E}_{opt}}{\partial E}\right|_{E_o} dE = C_3\, dE$$

Writing perturbations in the aircraft variables as $d(\ )_A$ where $(\ )$ is the particular variable involved and the perturbations are with respect to the point P_o, we have:

$$dh_\varepsilon = dh_A - dh_{opt} = dh_A - C_1\, dE_A$$

$$d\theta_\varepsilon = d\theta_A - d\theta_{opt} = d\theta_A - C_2\, dE_A$$

$$d\dot{E}_\varepsilon = d\dot{E}_A - d\dot{E}_{opt} = d\dot{E}_A - C_3\, dE_A$$

where the subscript ε denotes the errors in aircraft variables. To demonstrate the coupling introduced between the optimal flight path and the dynamic response of the aircraft, consider the expression for altitude error:

$$dh_\varepsilon = dh_A - C_1\, dE_A = dh_A - C_1\, (dh_A + \frac{U_o}{g}\, dU_A)$$

or

$$dh_\varepsilon = (1 - C_1)\, dh_A - \frac{U_o}{g}\, C_1\, dU_A$$

The altitude error is a function of both the perturbed altitude dh_A and the perturbed velocity dU_A. In previous linear simulations the dependency of the altitude error feedback on dE_A was not included which is equivalent to setting

$C_1 = 0$ (i.e., h_{opt} is independent of specific energy). The effect of the term in dE_A may be viewed as introducing an additional feedback loop which alters the dynamic characteristics of the aircraft response.

The coupling introduced by the specific energy terms in the expressions for $d\theta_\varepsilon$ and $\dot{E}_\varepsilon$ is negligible for optimal flight paths which are relatively smooth functions of specific energy since C_2 and C_3 are extremely small. The primary effect is the coupling introduced in the altitude error. However, under conditions where there is a significant variation in θ_{opt} and $\dot{E}_{opt}$ with specific energy such as may occur in the transonic region of an optimal flight path, the C_2, C_3 terms may become significant.

The incremental error equations above are expressed in terms of actual values of the aircraft variables. Because on-board implementation of the control laws is performed in terms of measured values, there are additional dynamics (e.g., delays, lags) introduced by the measurement process. For example, letting the subscript "m" denote measured values, we have that

$$dh_\varepsilon = G_{hm}^{-1}(P_o)\, dh_{Am} - C_1\, G_{E_m}^{-1}(P_o)\, dE_{Am}$$

where

$$dE_{Am} = G_{E_m}(P_o)\, dE_A,\quad dh_{Am} = G_{hm}(P_o)\, dh_A$$

and $G_{E_m}(P_o)$, $G_{hm}(P_o)$ are functions of the flight condition. If we assume $G_{E_m}(P_o) = G_{hm}(P_o) = G_m(P_o)$ then

$$dh_\varepsilon = G_m^{-1}(P_o)\, dh_{\varepsilon m}$$

or

$$dh_{\varepsilon m} = G_m(P_o)\, dh_\varepsilon$$

A block diagram of the linearized small perturbation system with control law dynamic coupling is shown in Figure 50. In the preliminary linear studies, $G_m(P_o)$ was modeled by a pneumatic lag with an altitude dependent time constant, τ_2, and a second order representation of the central air data computer with a natural frequency dependent on altitude and Mach number. This representation for the measurement dynamics will be denoted as $\bar{G}_m(P_o)$.

A root locus of the variation of the "phugoid" roots with C_1 as the locus parameter ($C_2 = C_3 = 0$) is shown in Figure 51 for the system block diagram shown in Figure 50 under the assumption that $G_{hm}(P_o) = G_{E_m}(P_o) = \bar{G}_m(P_o)$.

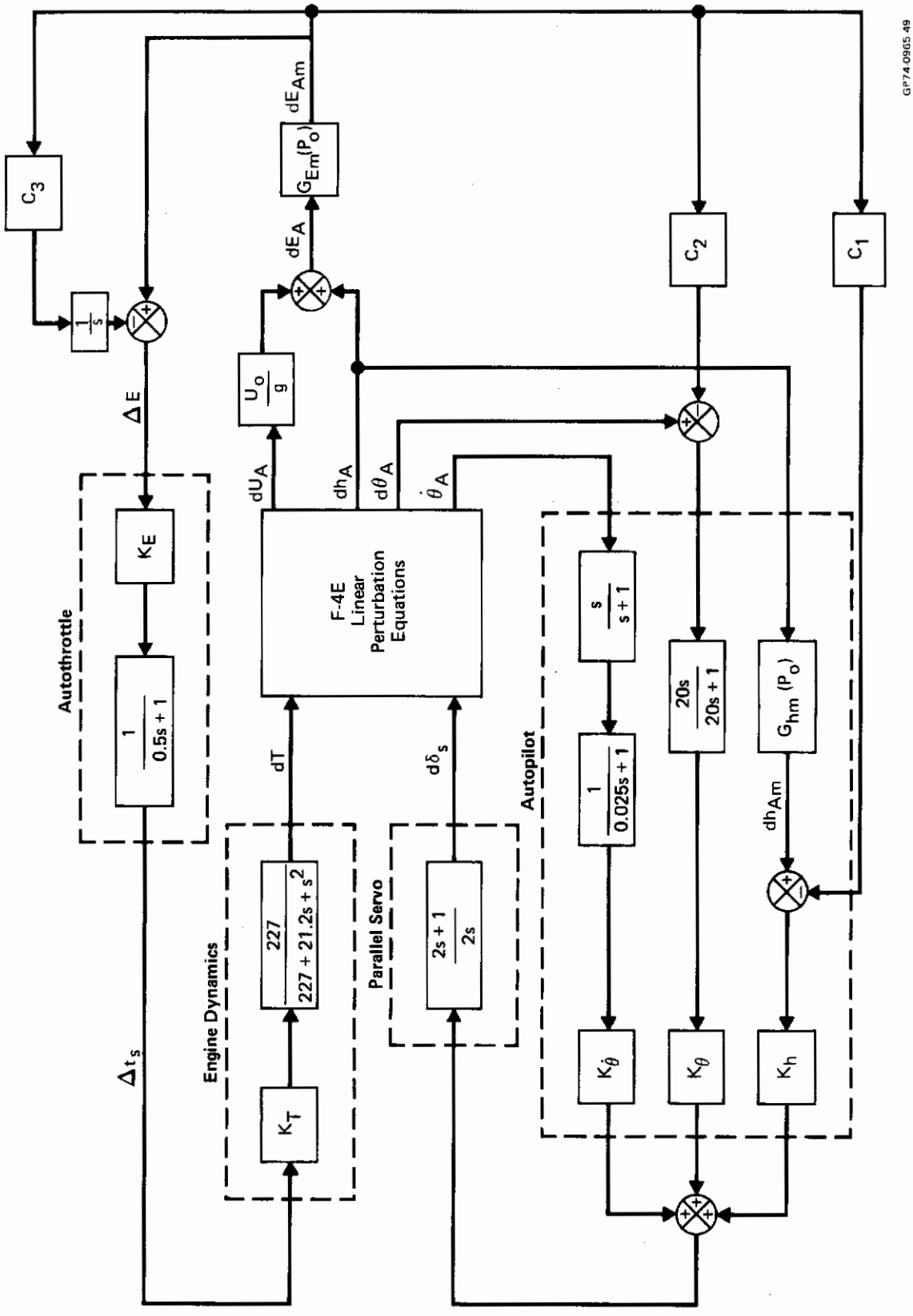

Figure 50 Control System with Energy Feedback

The flight condition is Mach = .85, h = 25,000 ft. The figure shows that negative values of C_1 cause the phugoid roots to become more lightly damped. Conversely, positive values of C_1 cause the phugoid roots to become more heavily damped. The short period roots (not shown) exhibit a similar characteristic for positive and negative values of C_1, however, with a greatly reduced degree of sensitivity. Typical values for C_1 taken from RUTO generated optimal subsonic and supersonic flight paths are in the range $0.5 \leq C_1 \leq 1.0$. These bounding values are indicated on the root locus in Figure 51. Corresponding bounds on the locus for $-1.0 \leq C_1 \leq .5$ which might occur in transonic

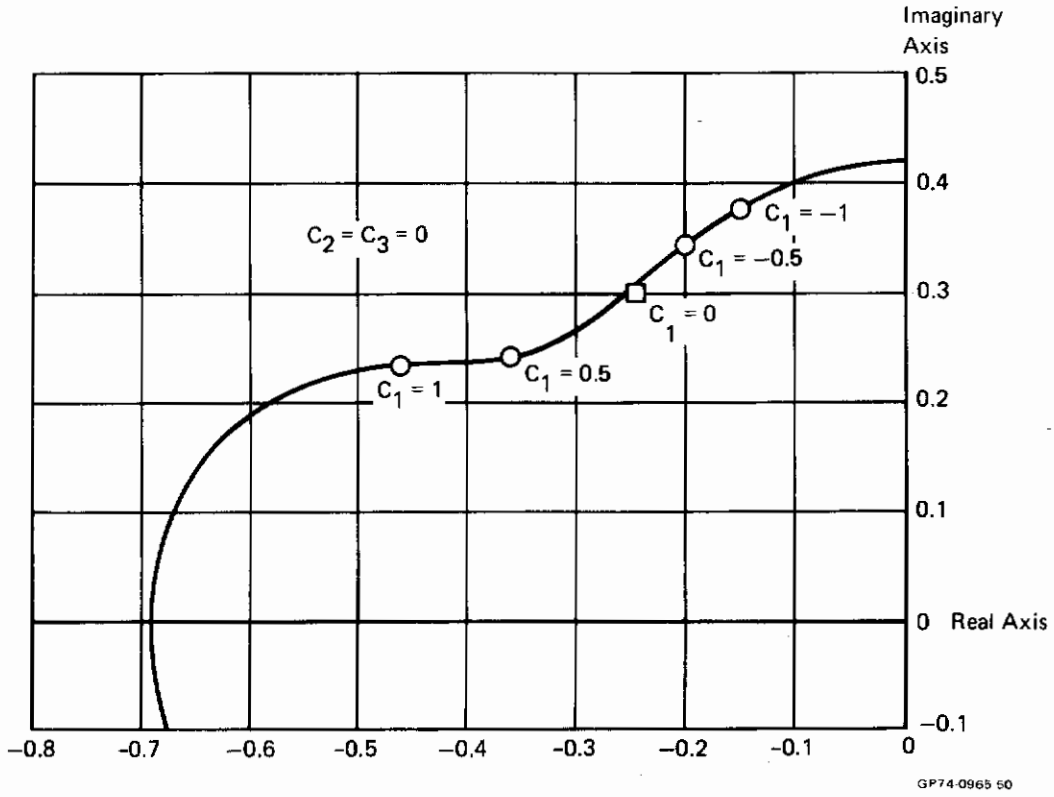

Figure 51 Phugoid Root Locus, Gain Parameter = C_1

flight are also indicated for comparison purposes.

Root locus diagrams of the phugoid roots parameterized by the altitude feedback gain, K_h, for two values of C_1 are shown in Figures 52 and 53 at the flight condition of Mach .85, h = 25,000 feet. The locus of the phugoid roots for $C_1 = 0$ shown in Figure 52 is considerably different than the locus for $C_1 = .5$ shown in Figure 53 with the more stable characteristic of the locus for $C_1 > 0$ clearly in evidence. The short period roots (not shown) are affected similarly.

Linear CSMP time simulations at the flight condition above were made for several values of C_1 and $\dot{E}_{opt}(E_o)$ in which the aircraft was initially in level unaccelerating flight (i.e. $U_A = \dot{h}_A = \dot{E}_A = 0$) at a specific energy level E_o with altitude and velocity errors. This characterizes the transition from a cruise state onto an optimal flight path. Figure 54 shows a $\Delta h - \Delta U$ plane plot of the response with $C_1 = .5$, $C_2 = C_3 = 0$ for several values of $\dot{E}_{opt}(E_o)$. Although care must be used in interpreting the validity of a linear response outside the immediate vicinity of the point about which the aircraft equations are linearized, the figure shows the stable nature of the response for three values of initial $\dot{E}$ errors where $d\dot{E}_\varepsilon(E_o) = \dot{E}_{opt}(E_o)$. In general, if $\dot{E}_A(E_o) \neq 0$, then $dE_\varepsilon(E_o) = dE_A(E_o) = \dot{E}_{opt}(E_o) - \dot{E}_A(E_o)$ which may be represented as a "step input" of magnitude $d\dot{E}_\varepsilon(E_o)$ to the integrator following C_3 in Figure 50.

3.1.4 Phugoid Approximation - The two degree of freedom (point mass) time history program simulates the phugoid motion of the aircraft when following a prescribed flight path. Because of its low frequency, the phugoid motion can be integrated with a larger step size so that this program is more economical to use than the four degree of freedom simulation. However, the equations of motion used for the linear control system design include short period as well as phugoid dynamics. In order to design control laws to be used with the point mass program it is necessary to reduce the full set of three degree of freedom equations (U, α, θ) to two degrees of freedom (U, γ). This was done by assuming that $\dot{\alpha}$ and $\ddot{\theta}$ are negligibly small. A block diagram of the control system in terms of the reduced set of equations is shown in Figure 55. The linear perturbation aircraft equations are given by:

$$(1 - \hat{Z}_{\dot{\gamma}})\, d\dot{\gamma} = \hat{Z}_\gamma \sin\theta_o d\gamma - \hat{Z}_u dU - \hat{Z}_h dh - \hat{Z}_\delta d\delta_s - \hat{Z}_T dT$$

$$d\dot{U} = -g\cos\theta_o\, d\gamma - \hat{X}_{\dot{\gamma}} d\dot{\gamma} + \hat{X}_u dU + \hat{X}_h dh - \hat{X}_\delta d\delta_s - \hat{X}_T dT$$

$$d\dot{h} = U_o \cos\theta_o d\gamma + \sin\theta_o dU$$

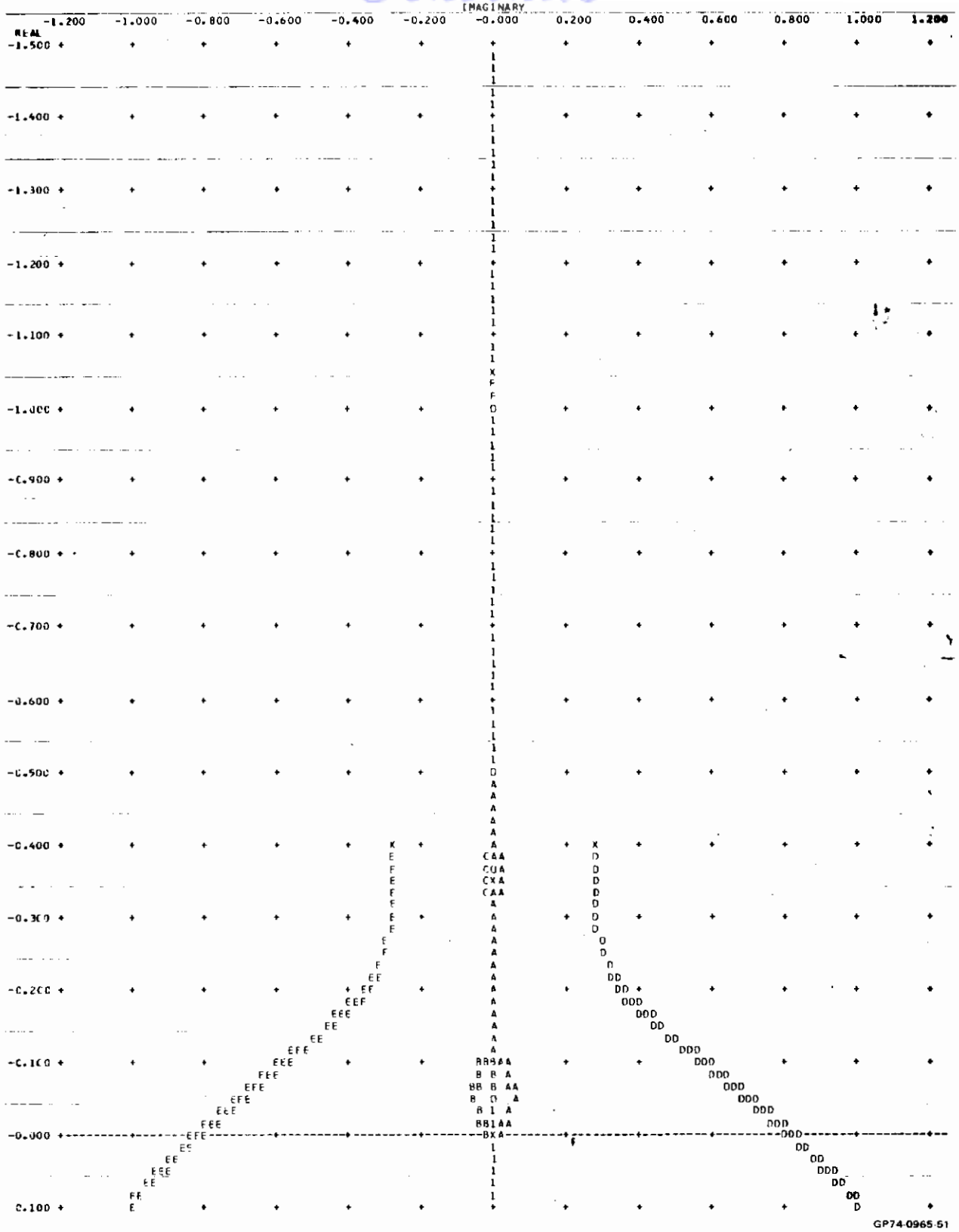

Figure 52 Phugoid Root Locus for $C_1 = 0$, Gain Parameter = K_h

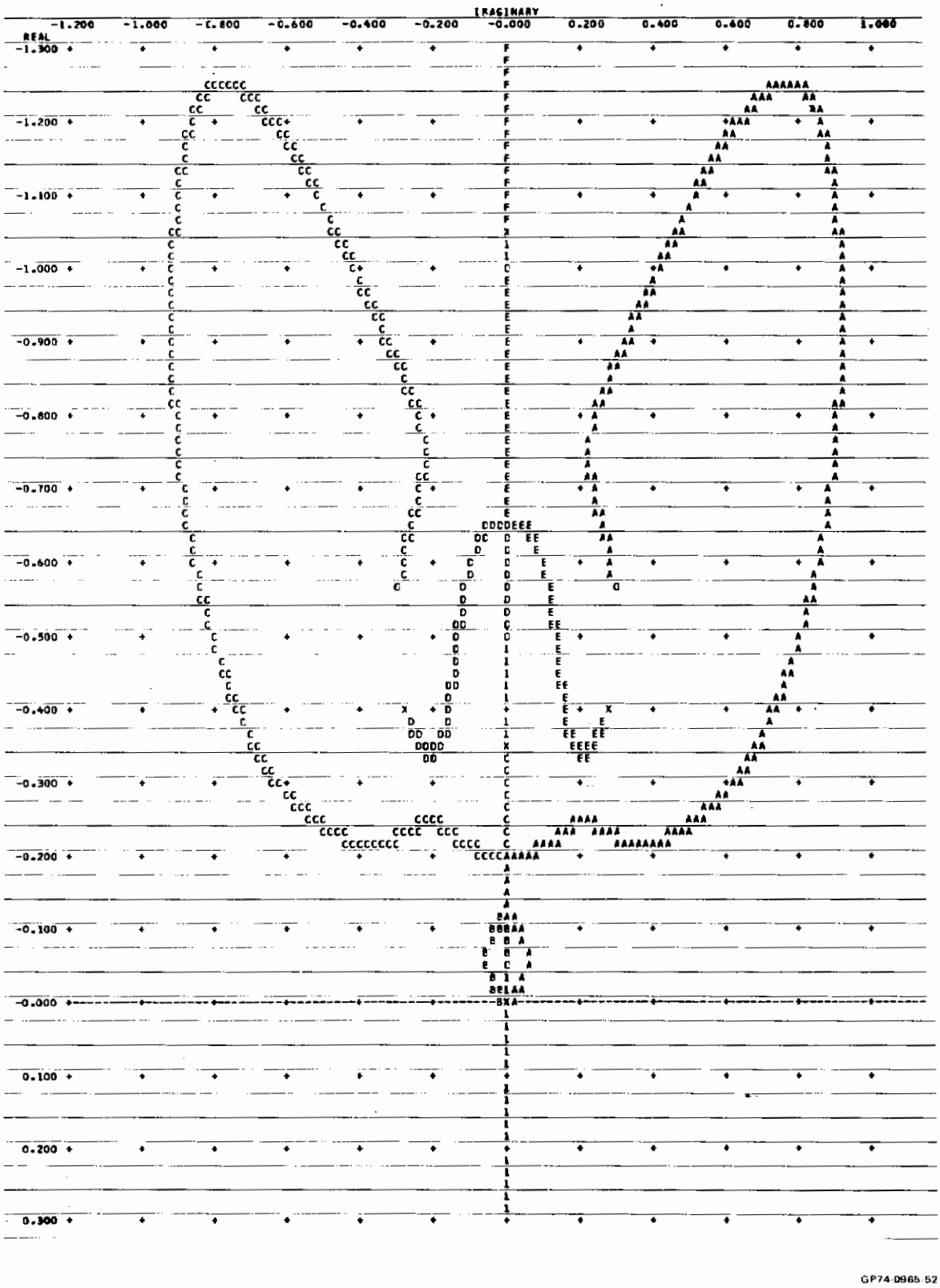

GP74-0965-52

Figure 53 Phugoid Root Locus for $C_1 = 0.5$, Gain Parameter = K_h

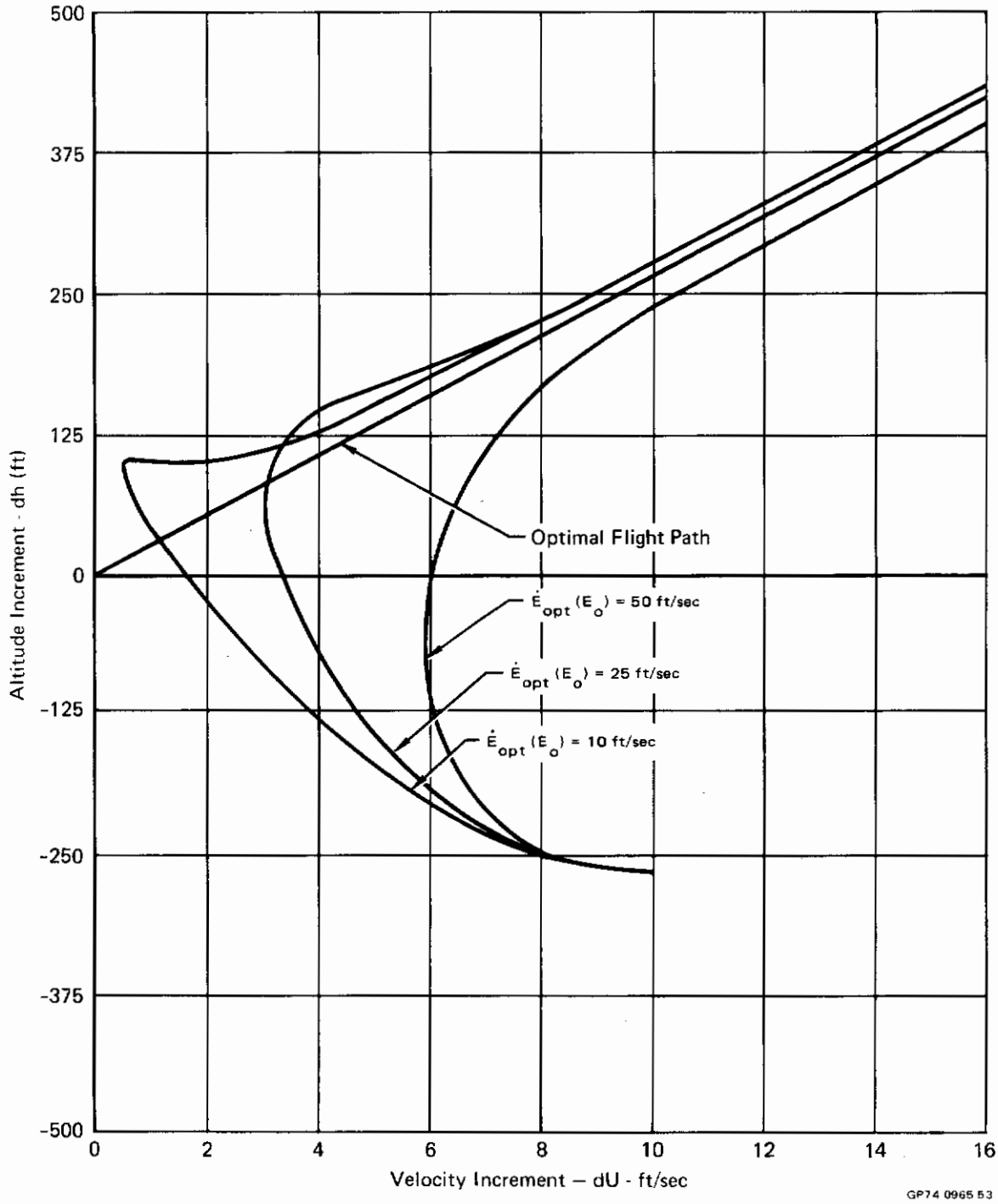

Figure 54 Linear CSMP Response for Three Values of $\dot{E}_{opt}$ (E_o)

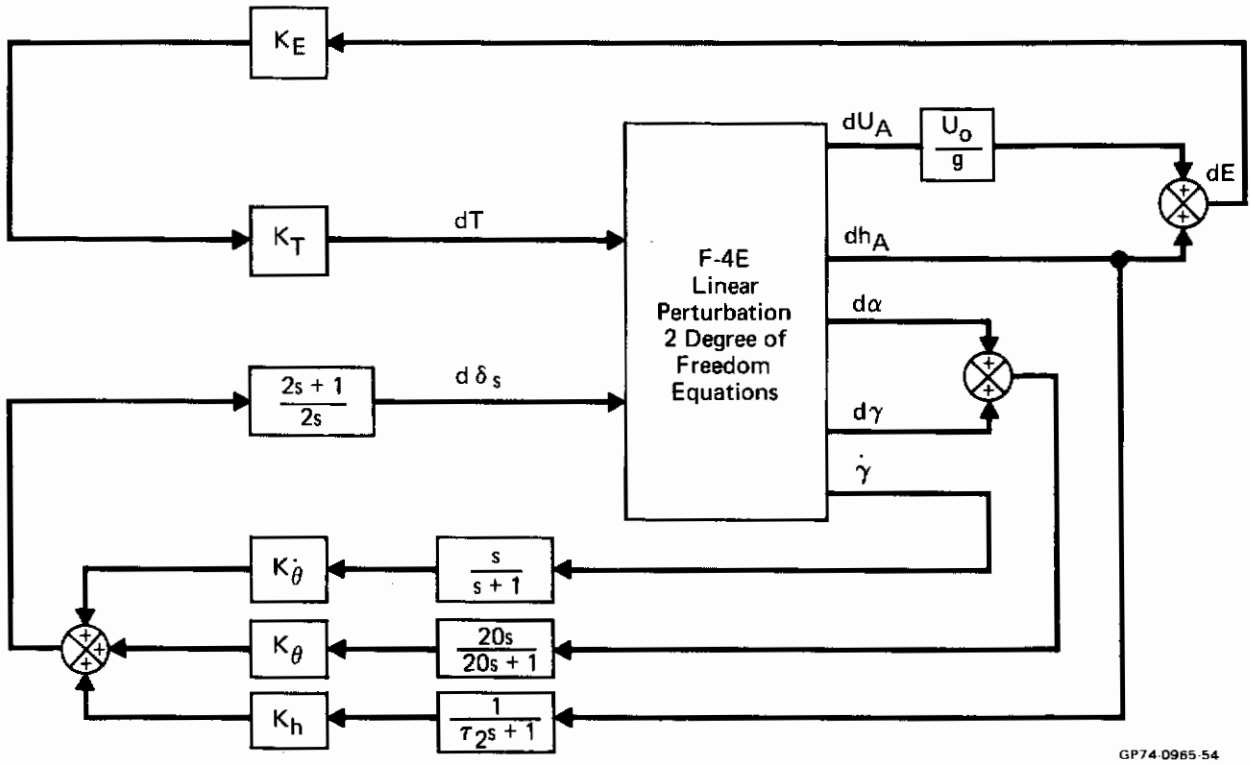

Figure 55 Control System for 2 Degree of Freedom Equations

The perturbed angle of attack is algebraically defined by the pitching moment equation as:

$$d\alpha = - \hat{M}_{\dot{\gamma}} d\dot{\gamma} - \hat{M}_u dU - \hat{M}_h dh - \hat{M}_\delta d\delta_s - \hat{M}_T dT$$

In the preceding equations the circumflex denotes coefficients defined in terms of the stability derivatives of the full set of perturbation equations as tabulated below:

$$\hat{Z}_{\dot{\gamma}} = \frac{M_q}{M_\alpha(1+Z_q)} \left(Z_\alpha - \frac{g}{U_o} \sin\theta_o\right), \quad \hat{Z}_\gamma = \frac{g}{U_o(1+Z_q)}$$

$$\hat{Z}_u = \frac{1}{U_o(1+Z_q)} \left[Z_U - \frac{M_u}{M_\alpha} \left(Z_\alpha - \frac{g}{U_o} \sin\theta_o\right)\right]$$

$$\hat{Z}_h = \frac{1}{U_o(1+Z_q)} \left[Z_h - \frac{M_h}{M_\alpha} \left(Z_\alpha - \frac{g}{U_o} \sin\theta_o\right)\right]$$

$$\hat{Z}_\delta = \frac{1}{1+Z_q} \left[Z_\delta - \frac{M_\delta}{M_\alpha} \left(Z_\alpha - \frac{g}{U_o} \sin\theta_o\right)\right]$$

$$\hat{Z}_T = \frac{1}{1+Z_q} \left[Z_T - \frac{M_T}{M_\alpha} \left(Z_\alpha - \frac{g}{U_o} \sin\theta_o\right)\right]$$

$$\hat{X}_{\dot{\gamma}} = \frac{M_q}{M_\alpha} \left(X_\alpha U_o - g\cos\theta_o\right)$$

$$\hat{X}_u = X_u - \frac{M_u}{U_o M_\alpha} \left(X_\alpha U_o - g\cos\theta_o\right)$$

$$\hat{X}_h = X_h - \frac{M_h}{U_o M_\alpha} \left(X_\alpha U_o - g\cos\theta_o\right)$$

$$\hat{X}_\delta = \frac{M_\delta}{M_\alpha} \left(X_\alpha U_o - g\cos\theta_o\right)$$

$$\hat{X}_T = X_T - \frac{M_T}{M_\alpha} \left(X_\alpha U_o - g\cos\theta_o\right)$$

$$\hat{M}_{\dot{\gamma}} = \frac{M_q}{M_\alpha}, \qquad \hat{M}_h = \frac{M_h}{U_o M_\alpha}, \qquad \hat{M}_T = \frac{M_T}{M_\alpha}$$

$$\hat{M}_u = \frac{M_u}{U_o M_\alpha}, \qquad \hat{M}_\delta = \frac{M_\delta}{M_\alpha}$$

To verify that the assumptions made to reduce the equation set did not greatly affect the location of the phugoid roots, root locus runs using the perturbation equations were made and compared with root locus runs made using the full set of perturbation equations. Typical results are shown in Table II for the flight conditions .85 Mach at 25,000 feet and 1.5 Mach at 35,000 feet. The agreement of the phugoid root locations is very good and the short period roots are missing in the reduced model as desired.

Table II Airframe Pole Positions

0.85 M at 25,000 ft		1.5 M at 35,000 ft	
2 D.O.F.	3 D.O.F.	2 D.O.F.	3 D.O.F.
0.00095+j0.02968	0.00085+j0.02964	−0.00198+j0.05375	−0.00191+j0.05376
0.00095-j0.02968	0.00085-j0.02964	−0.00198-j0.05375	−0.00191-j0.05376
−0.00644	−0.00644	−0.00606	−0.00606
Short Period	−0.75325+j2.94		−0.77144+j5.8188
	−0.75325-j2.94		−0.77144-j5.8188

A linear time history simulation at the flight condition of .85 Mach, 25,000 ft. was made in which the full set and reduced set of equations were run simultaneously and compared. The time response history of the phugoid set is shown in Figures 56 and 57 and the time history response of the difference between the three degree of freedom and the phugoid equations is shown in Figures 58 and 59. Except for an initial difference caused by the short period roots which were eliminated in the phugoid equations, the two time response histories are virtually identical.

3.1.5 Pilot Modeling and Workload Analysis - MCAIR has available a parameter optimization computer program for linear systems called MISER (Multiterm Integral Squared Error Reduction). A few runs were made using the F-4E aircraft linear perturbation equations and control system described in Figure 60 to obtain a rough estimate of what pilot dynamics (and hence workload) are required for stabilator control, assuming the throttle is controlled automatically. The pilot model chosen is a first order transfer function (gain with a lead and a lag term). This form is commonly used for modeling the pilot in a tracking task. It is postulated the pilot is given a display of the error

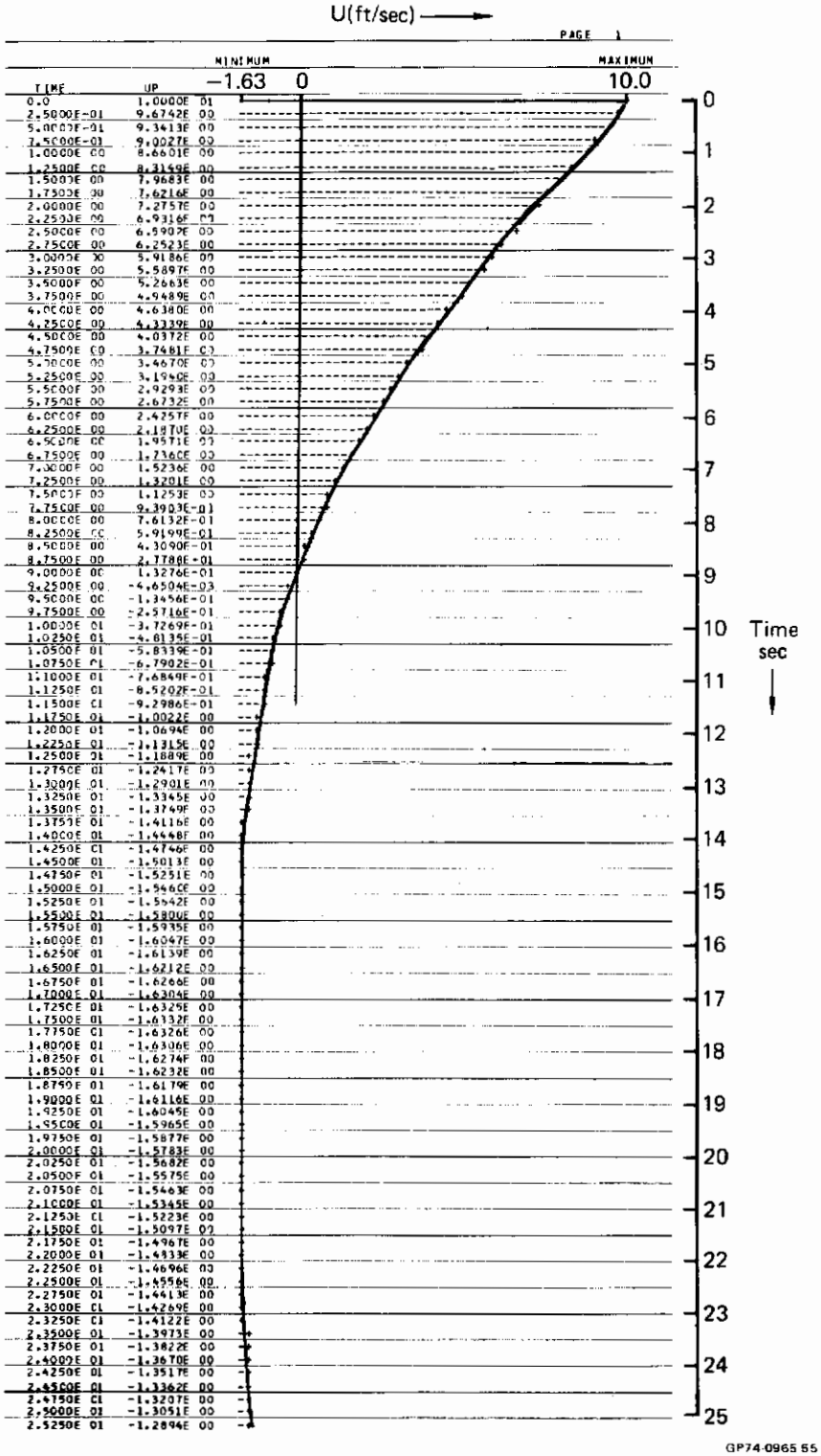

Figure 56 Phugoid Approximation - Velocity

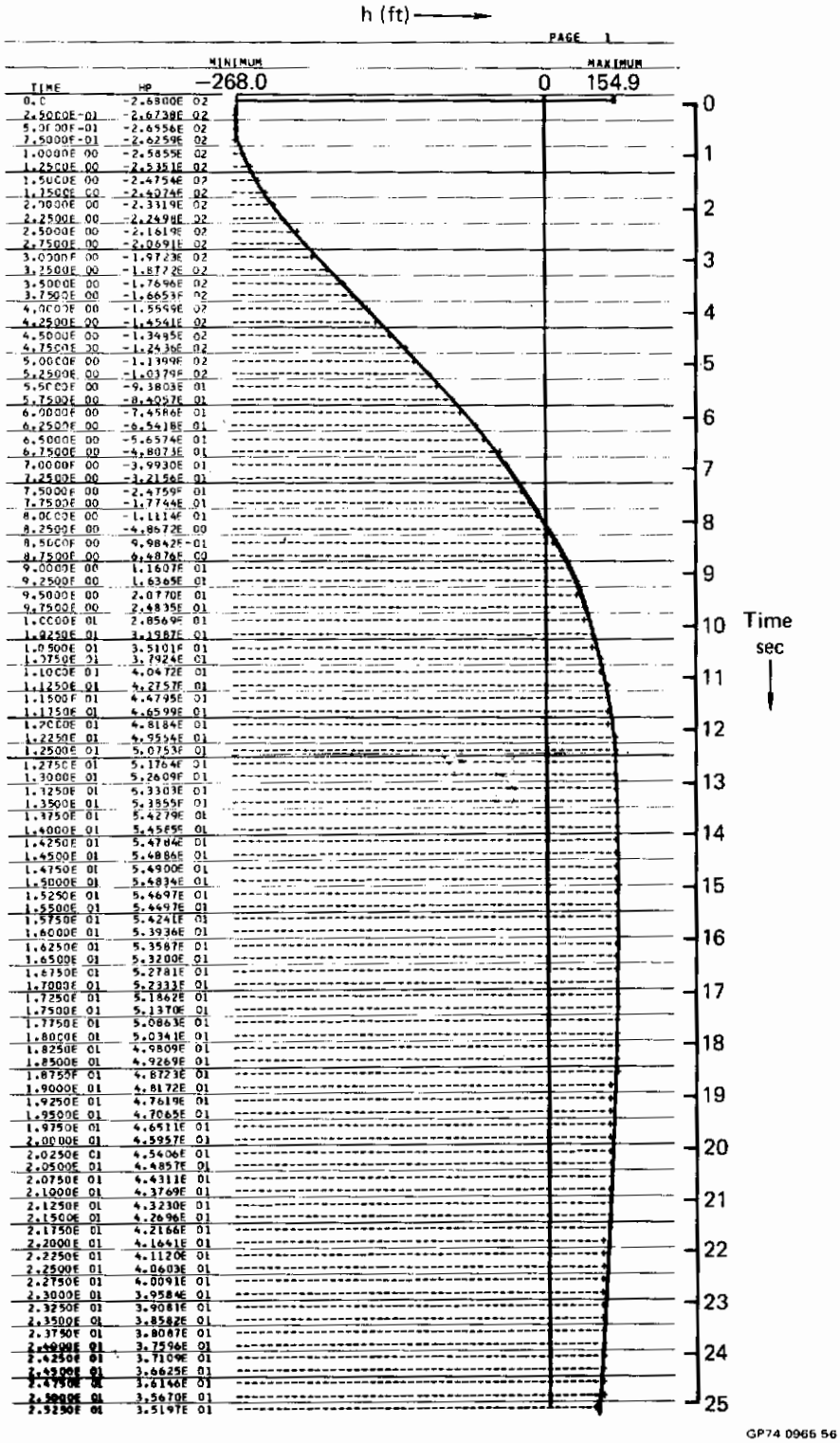

Figure 57 Phugoid Approximation - Altitude

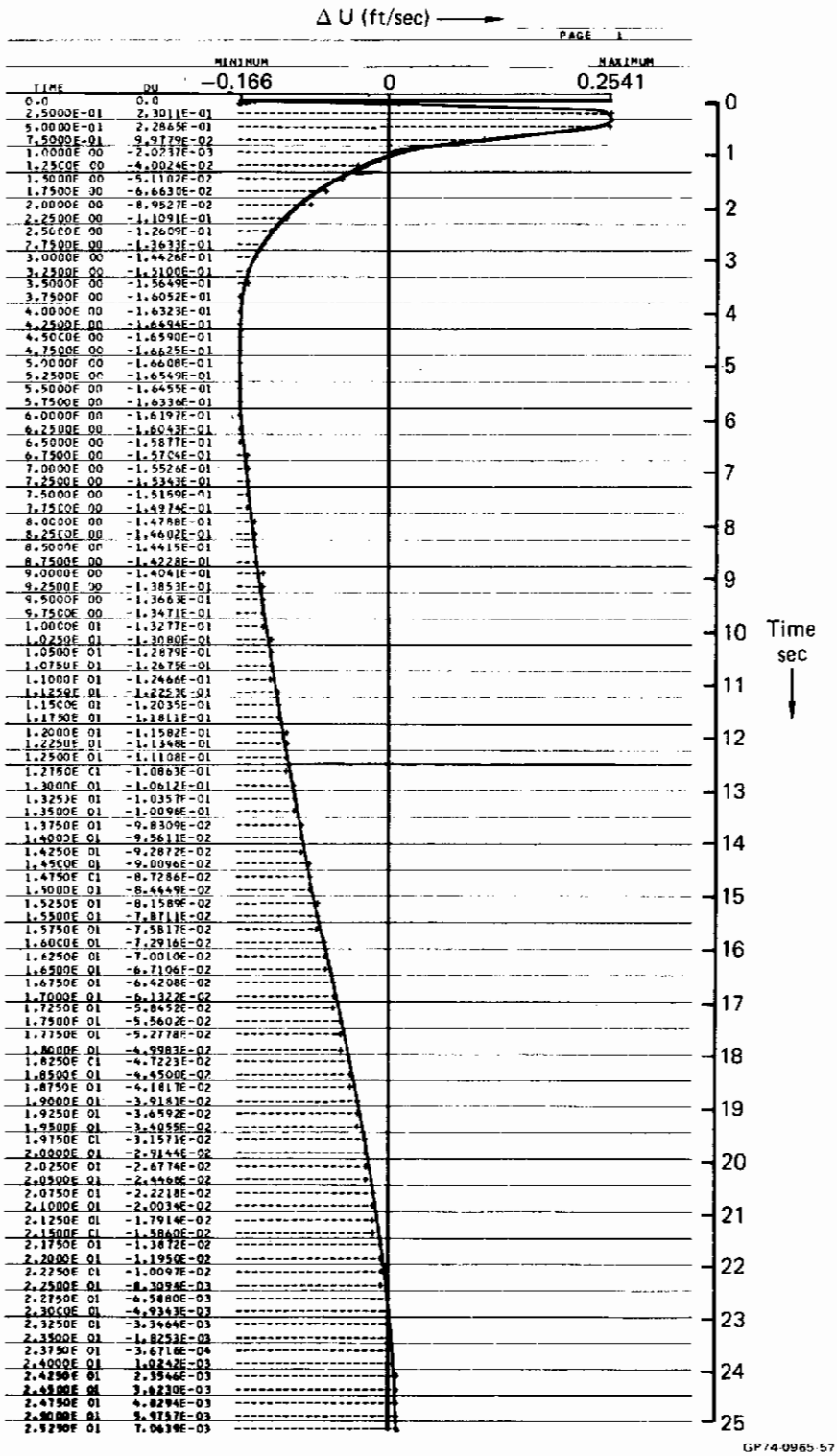

Figure 58 Phugoid Approximation - (U_{3DF} - $U_{Phugoid}$)

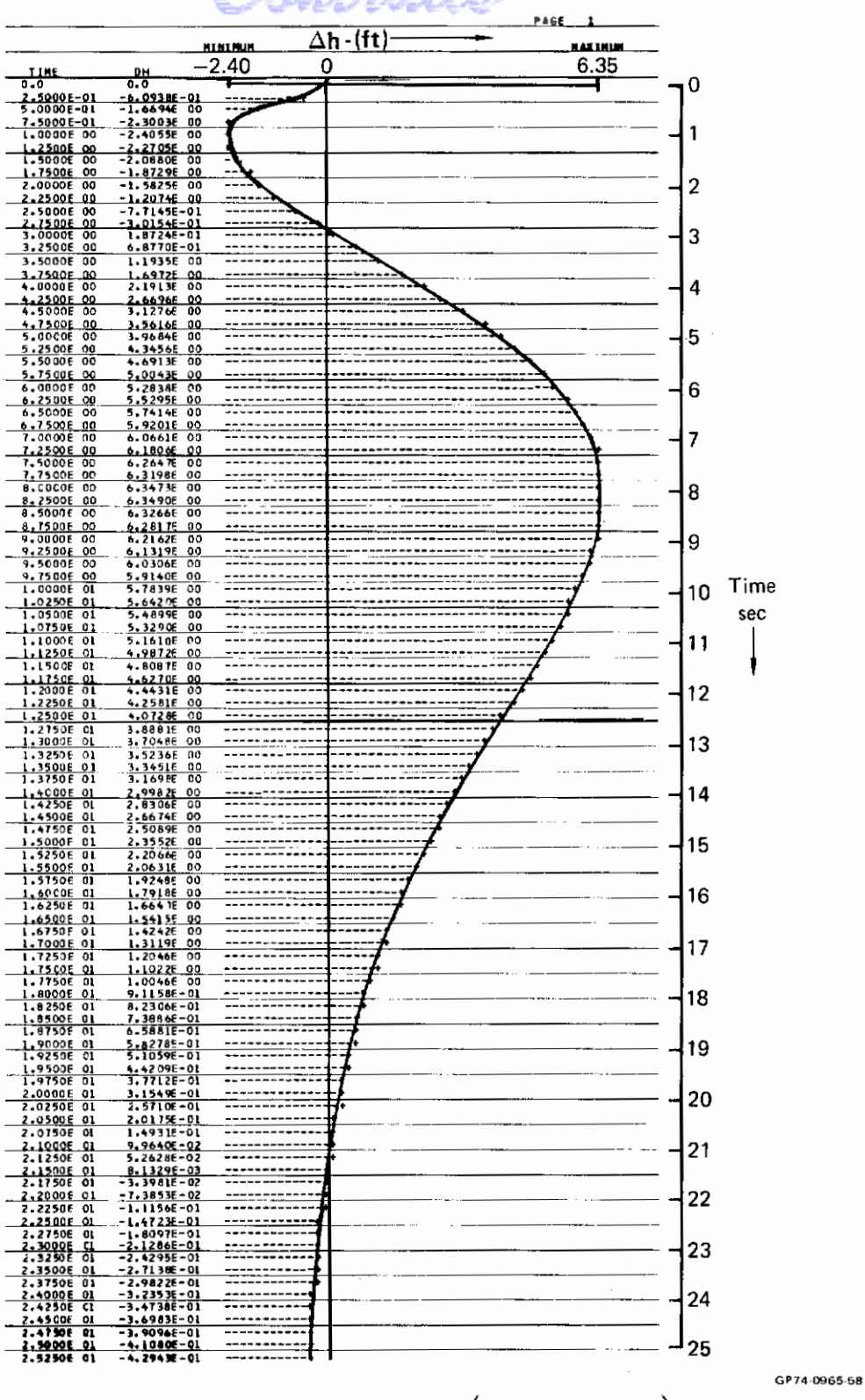

Figure 59 Phugoid Approximation - $(h_{3DF} - h_{Phugoid})$

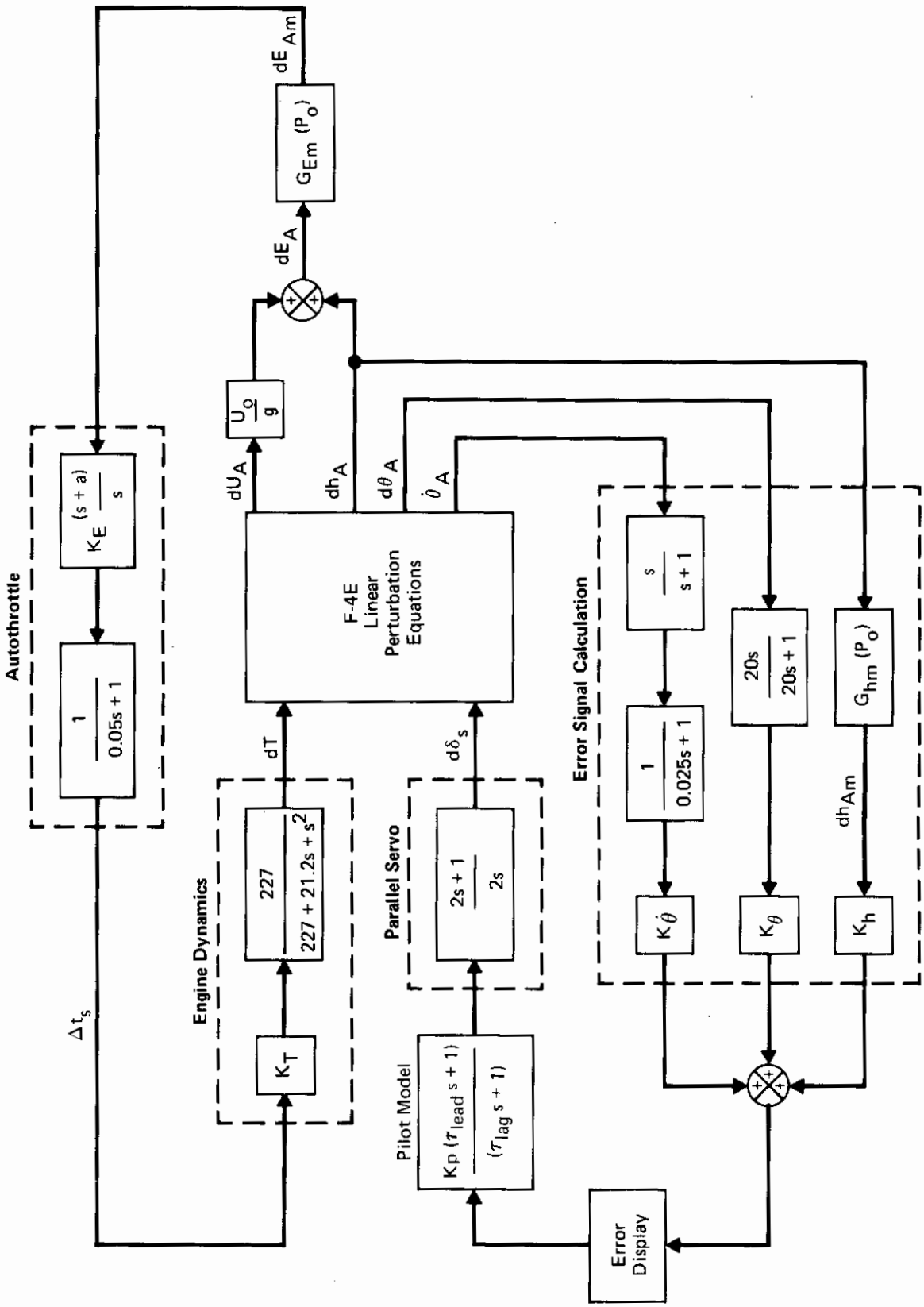

Figure 60 Pilot Model in Flight Path Control Loop

and reacts to a deviation (Δh_o, ΔU_o) from the optimal trajectory in such a manner that the following criterion is minimized:

$$\int_o^\infty [C_u \left(\frac{\Delta U}{\Delta U_o}\right)^2 + \left(\frac{\Delta h}{\Delta U_o}\right)^2 + C_\delta \left(\frac{\Delta \delta}{\Delta U_o}\right)^2] \, dt$$

The types of flight path error displays under consideration are discussed in Section 4. The choices of C_u and C_δ are arbitrary and hence the pilot dynamics found are not unique. The following gives our rationale in choosing the weighting constants C_u and C_δ. Initial flight path deviations ΔU_o, Δh_o will be considered to be related by:

$$\left(\frac{U_{nom}}{g}\right) \Delta U_o + \Delta h_o = 0$$

Therefore, in order to give approximately equal weighting to both altitude and velocity errors, C_u should be chosen as follows:

$$C_u = \left(\frac{U_{nom}}{g}\right)^2$$

C_δ was picked in order to balance the magnitudes of the three weighted terms in the performance index. One run of the MISER program with a trial value is usually required.

The F-4E linear perturbation equations were used with the control system dynamics shown in Figure 60. The two flight conditions considered, which are typical of those on an optimal path, were .85 Mach at 25,000 ft and 1.5 Mach at 35,000 ft. Table III summarizes the results.

These runs indicate that the pilot would "put in" some lead (that is, he would consider both error and error rate in his actions) to null out deviations from the desired path in order to minimize the above performance index. The amount of lead determined here is not considered unrealistic based on previous studies (Reference 17) of pilot models and ratings.

A similar study was made assuming the flight path is controlled automatically and the pilot controls the throttle by monitoring some candidate displays which are discussed in Section 4. Figure 61 shows that a first order pilot model is placed in the throttle loop. The performance function chosen is

Table III Pilot Model Results

Flight Path Loop	0.85 M at 25,000 ft	1.5 M at 35,000 ft
C_U	625	2025
C_δ	2×10^8	3×10^8
$K_{\dot{\theta}}$	0.25200	0.11000
K_θ	1.35000	0.85000
K_h	0.00028	0.00007
K_E	−0.00600	−0.00600
a	0.05000	0.05000
K_P	0.97900	2.30000
τ_{lead}	1.36000	1.11000
τ_{lag}	0	0

Throttle Loop	0.85 M at 25,000 ft	1.5 M at 35,000 ft
C_U	625	2025
C_T	0.00500	0.00020
K_P	0.03600	0.06000
$\tau_{t_{lead}}$	1.30000	0.72000
$\tau_{t_{lag}}$	0	0

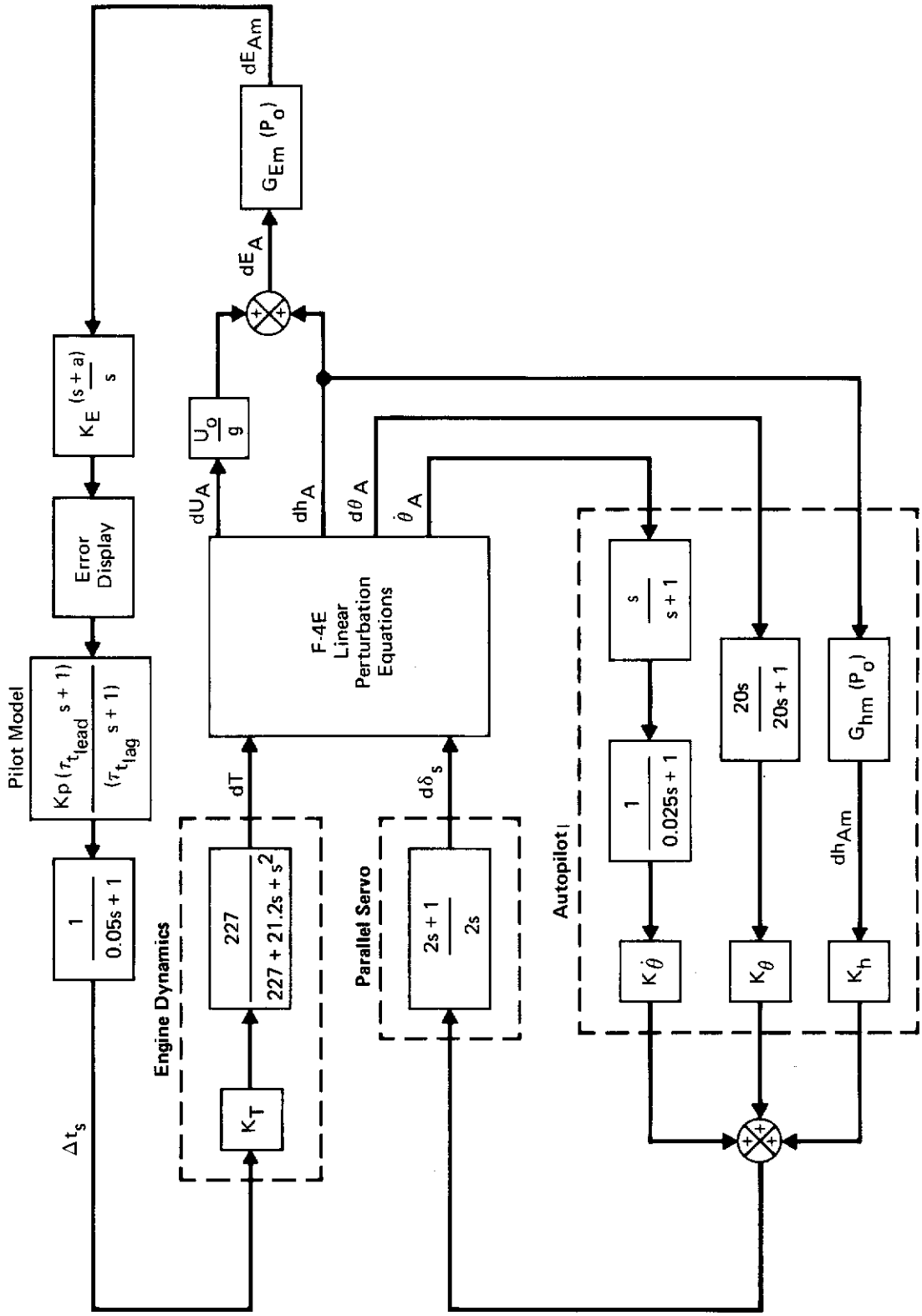

Figure 61 Pilot Model in Throttle Control Loop

$$\int_o^\infty \left[Cu \left(\frac{\Delta U}{\Delta U_o}\right)^2 + \left(\frac{\Delta h}{\Delta U_o}\right)^2 + C_T \left(\frac{\Delta T}{\Delta U_o}\right)^2\right] dt$$

As before, the weighting constants are chosen to balance the magnitudes of the weighted terms. The results for the same two flight conditions are shown in Table 3.

When the performance indices above were combined, assuming both flight path and throttle are controlled by the pilot, six parameter values were determined. The results are approximately the same as when stabilator and throttle controls are treated separately. The small pilot throttle gains have almost no effect on closed loop root locations relative to a gain of 1. The gain of 1 is preferred to handle throttle commands in a reasonable amount of time.

3.2 Nonlinear Analyses

The actual flight path/throttle control system is highly nonlinear in that it involves nonlinear airframe equations, highly nonlinear aerodynamic properties caused by optimal flight paths which range over large sets of flight conditions, and relatively rapid changes in aircraft specific energy levels. For these reasons, any final control law specification must obviously consider the effect of the system nonlinearities. The linear perturbation analyses discussed in Section 3.1 provide insight into the control problem and establish a baseline from which to initiate the nonlinear analysis.

As discussed in Section 2, the RUTO program is used to calculate the optimal flight paths and a two-degree-of-freedom program is used to calculate paths following tables of smoothed RUTO histories. The latter program provides histories of h, θ, E_s, and nominal t_s as a function of the aircraft specific energy E_s. It is assumed that, for the purpose of the nonlinear analyses, these histories have been precomputed and are available onboard in the form of stored tables of the following variables as functions of aircraft specific energy.

$\dot{E}_{opt}\ (E_s)$ = table of $(\dot{E}_{opt}, E_s)$ pairs

$h_{opt}\ (E_s)$ = table of (h_{opt}, E_s) pairs

$\theta_{opt}\ (E_s)$ = table of (θ_{opt}, E_s) pairs

$t_{s_{nom}}\ (E_s)$ = table of $(t_{s_{opt}}, E_s)$ pairs

Here the subscript "opt" denotes the value of the variable defined by the two-degree-of-freedom program and the tables range over the specific energy

levels associated with the entire path with sufficient resolution that linear interpolation provides acceptable accuracy.

Although this last assumption is by no means essential and equally suitable alternatives such as storing curve fit parameters exist, it was the one made in this study.

3.2.1 Preliminary Analysis and Design - The preliminary analysis was performed for the case where the desired path was simply a Mach/altitude hold. This corresponds to the linear perturbation analyses in that the optimal aircraft specific energy is constant, and h_{opt} and θ_{opt} are constant functions of E_s. The flight path/throttle control system used in this part of the nonlinear analysis is shown in Figure 62. Note that the initial assumption implies that $\dot{E}_{opt} = 0$.

Additional control system parameters which require definition by analysis are the gains denoted in Figure 62 as:

$$K_E,\ K_h,\ K_\theta,\ K_{\dot{\theta}}$$

These gains are flight condition dependent and are assumed to be stored on board and evaluated in terms of measured arguments.

As discussed in Section 3.1.3, the aircraft specific energy variable, E_s is assumed to be available on board in terms of a measured value which differs from the actual value. In particular, E_{meas}, (the measured value of E_s) is computed from altitude and velocity measurements as follows:

$$E_{meas} = h_{meas} + \frac{1}{2g} U^2_{meas}$$

This measured value of E_s is used as the argument of the variables $\dot{E}_{opt}$, h_{opt}, θ_{opt}, and $t_{s_{nom}}$ which define the optimal flight path. The correction to the nominal throttle setting $t_{s_{nom}}$ is given in general by

$$\delta t_s = \int_{t_o}^{t} K_E\ \delta\dot{E}\ d\tau$$

where

$$\delta\dot{E} = \dot{E}_{meas} - \dot{E}_{opt}$$

and $\dot{E}_{meas}$ is the measured rate of change of aircraft specific energy. This is equivalent to

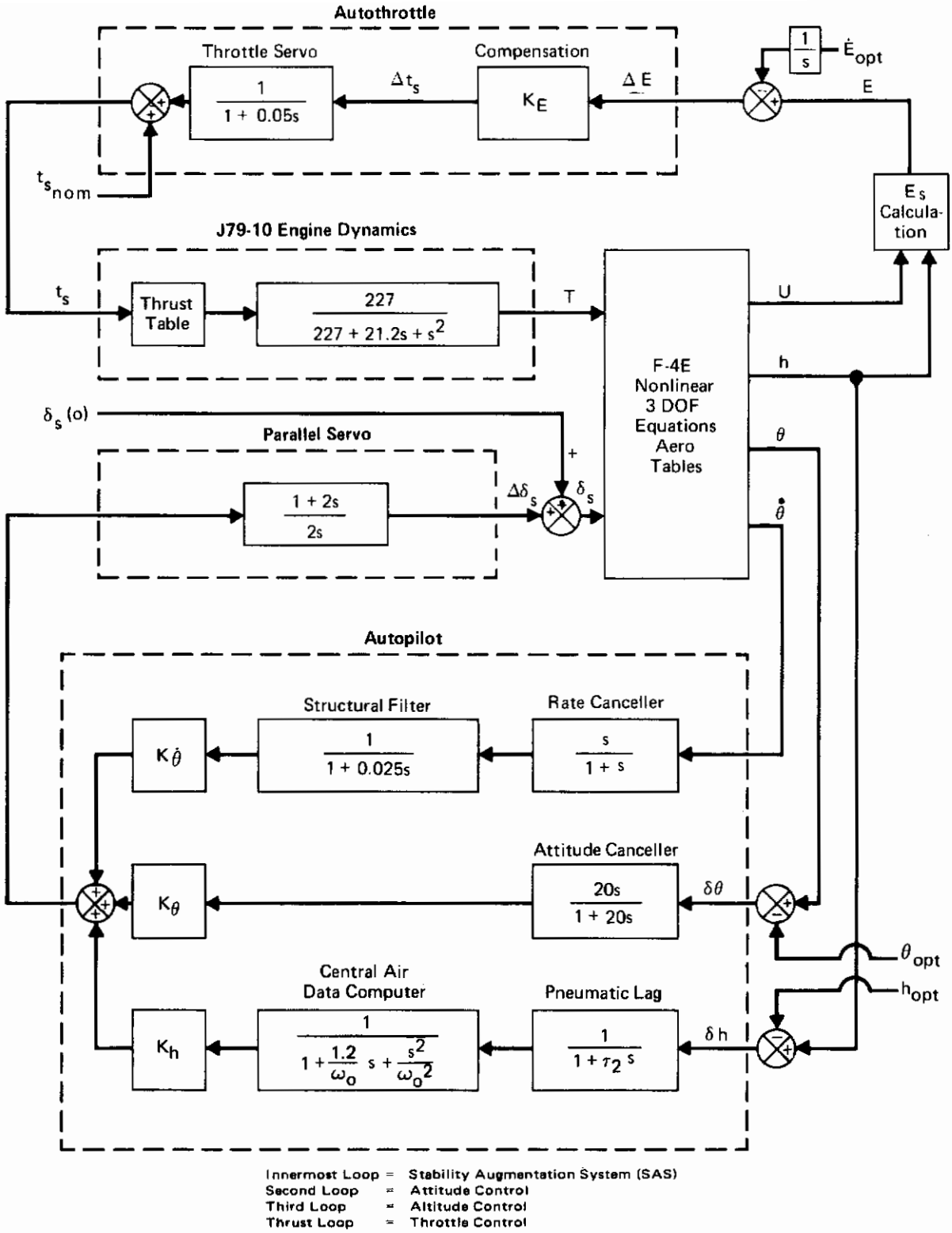

Figure 62 Nonlinear Simulation with SAS, Flight Path and Throttle Control F-4E

GP74-0965-61

$$\delta t_s = K_E \left[E_{meas}(t) - E_{meas}(t_o) - \int_{t_o}^{t} \dot{E}_{opt}\, d\tau\right]$$

so that $\dot{E}_{meas}$ is not required. In the preliminary analysis, $\dot{E}_{opt} = 0$ so that the correction to the nominal throttle setting consists only of the deviation of the aircraft specific energy from its initial value.

The control law which determines the correction to the stabilator is given by

$$\Delta\delta_s = K_\theta \left(\theta_{meas} - \theta_o\right)$$

where θ_o is a desired value of the pitch angle which will correct altitude deviations, namely:

$$\theta_o = \theta_{opt} + K_{\Delta h}\, \delta h$$

The stabilator control law may be rewritten in the form

$$\Delta\delta_s = K_\theta(\theta_{meas} - \theta_{opt}) + K_h \left(h_{meas} - h_{opt}\right)$$

where $K_h = K_\theta \cdot K_{\Delta h}$ is the effective altitude error gain which is stored on board. The gains K_h, K_θ and $K_{\dot\theta}$ were chosen to be identical to those for the existing F-4 attitude/altitude hold autopilot where K_h is a function of Mach number, and K_θ and $K_{\dot\theta}$ are functions of impact pressure.

A Mach/altitude time history (CSMP) 4-degree-of-freedom nonlinear simulation was made for the F-4E using the control system as described above. The flight condition was .8 Mach at 15,000 feet altitude. The values for the optimal path parameters were chosen as

$\dot{E}_{opt} = 0$

h_{opt} = 15,266 ft - a constant

θ_{opt} = trimmed angle of attack for straight and level flight - a constant

$t_{s_{opt}}$ = throttle setting for trimmed flight - a constant

The throttle loop gain, K_E, was fixed at -.0133. The aircraft was assumed to have an initial velocity error of 10 feet/second and an altitude error of -266 ft. which constitutes a deviation along a constant energy contour. The desired flight conditions were U_{opt} = 834.5 feet/second and h_{opt} = 15,266 feet. For computational efficiency purposes, the desired flight conditions were introduced at .2 seconds. Graphs of the time histories for altitude, velocity,

pitch angle, stabilator deflection, and thrust are shown in Figures 63 through 67. As can be seen in the figures, the velocity and altitude errors were nulled out in a reasonable amount of time. The thrust appears limited at times but this was a result of the program not accessing the thrust tables for sufficiently small changes in throttle settings in an effort to conserve computer time. This was corrected on subsequent runs.

3.2.2 Optimal Throttle/Flight Path Segments - The four degree of freedom non-linear simulation for the F-4E described in 3.2.1 was modified by eliminating the higher frequency control system, engine, and throttle servo dynamics to save computer time. This made the time simulations required to follow longer flight paths economically feasible. The resulting block diagram of the simulation is shown in Figure 68.

The control laws defined in the previous section were tested to see how well they followed typical RUTO-generated optimal (minimum fuel) flight paths. Both a subsonic and a supersonic flight path segment were used. The aircraft was given initial conditions removed from the optimal path. For the subsonic case, the aircraft was given initial conditions of M = .788 at 8,725 feet whereas the optimal conditions at that energy level were M = .745 at 9,971 feet. The results for Mach, altitude, and thrust are shown in Figures 69, 70, and 71, respectively. Errors in Mach and altitude are nulled out in approximately ten to fifteen seconds and the aircraft follows the optimal path closely out to 50 seconds. The change in throttle setting used to follow the optimal path is small (from 75.1 to 75.5 deg. ts). The aircraft pulled about 2 g's in rising to meet the optimal path. Much closer path following can be accomplished at the cost of pulling more g's and using more thrust. For the supersonic case, the control system was modified by removing the attitude canceller. The aircraft was given the initial conditions 1.27 Mach at 32,900 feet. For this energy level, the optimal conditions are 1.25 Mach at 33,800 feet. The results for Mach and altitude time histories are shown in Figures 72 and 73. Figure 74 shows that the path was followed closely in the Mach vs. altitude plane. However, there is some time lag in following the path because the thrust is limited to that corresponding to the max A/B throttle setting which limits the specific excess power below the desired value.

3.2.3 Selected Flight Path/Throttle Control System Configuration - The four degree of freedom simulation MITCON includes tables of gross thrust, ram

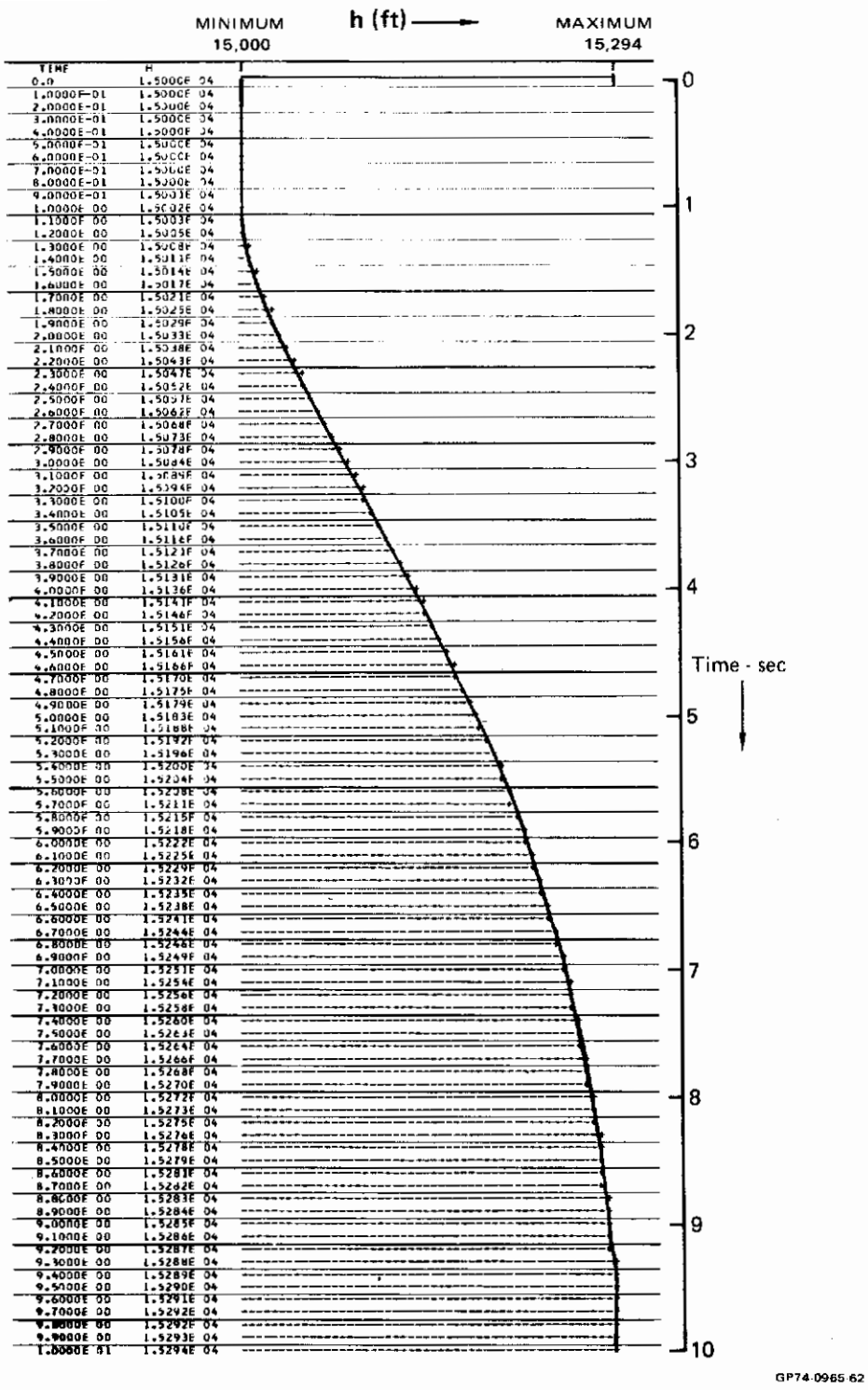

Figure 63 F-4E Mach - Altitude Hold
Altitude,0.8 Mach at 15,000 ft

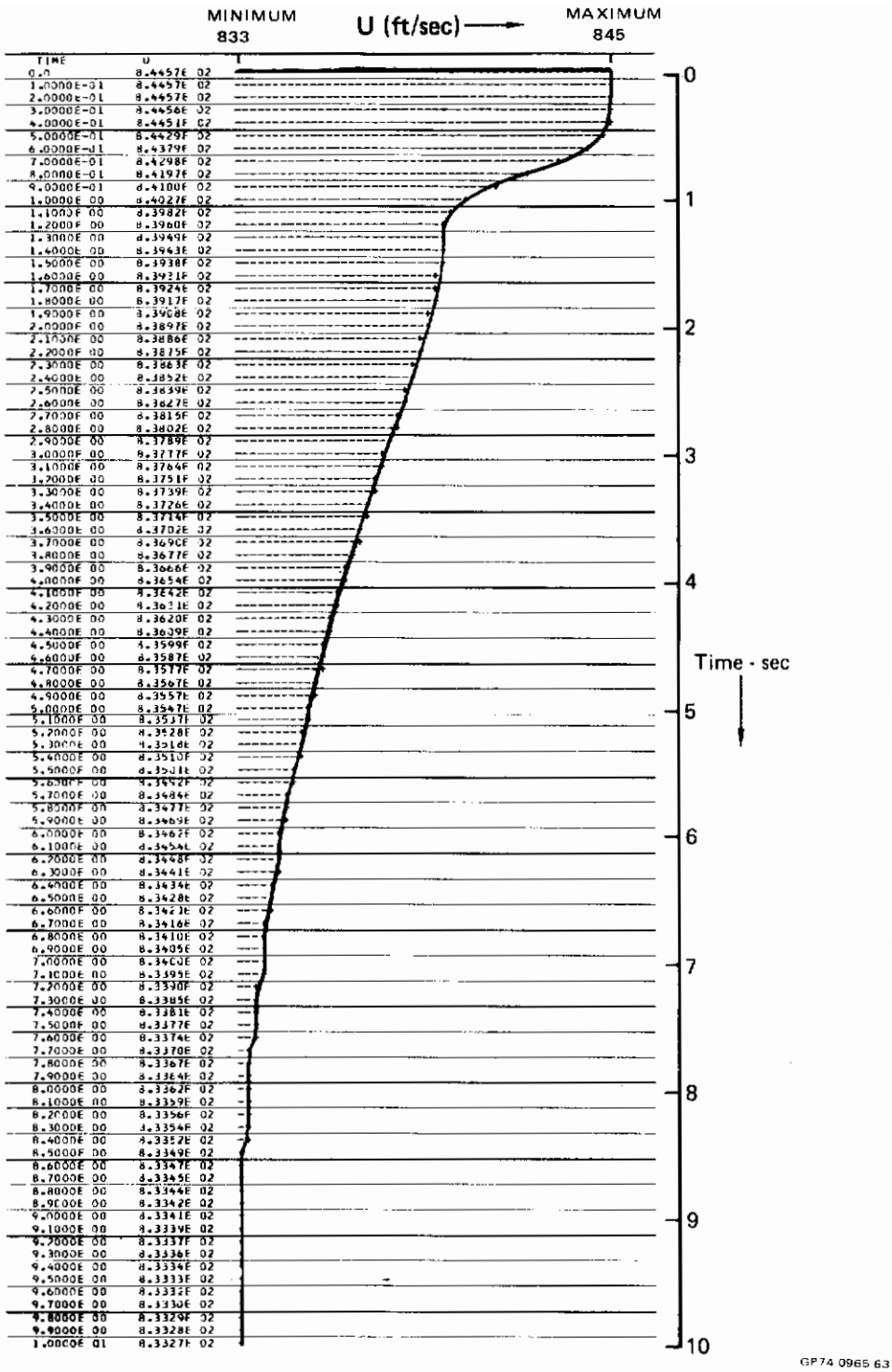

Figure 64 F-4E Mach - Altitude Hold
Velocity, 0.8 Mach at 15,000 ft

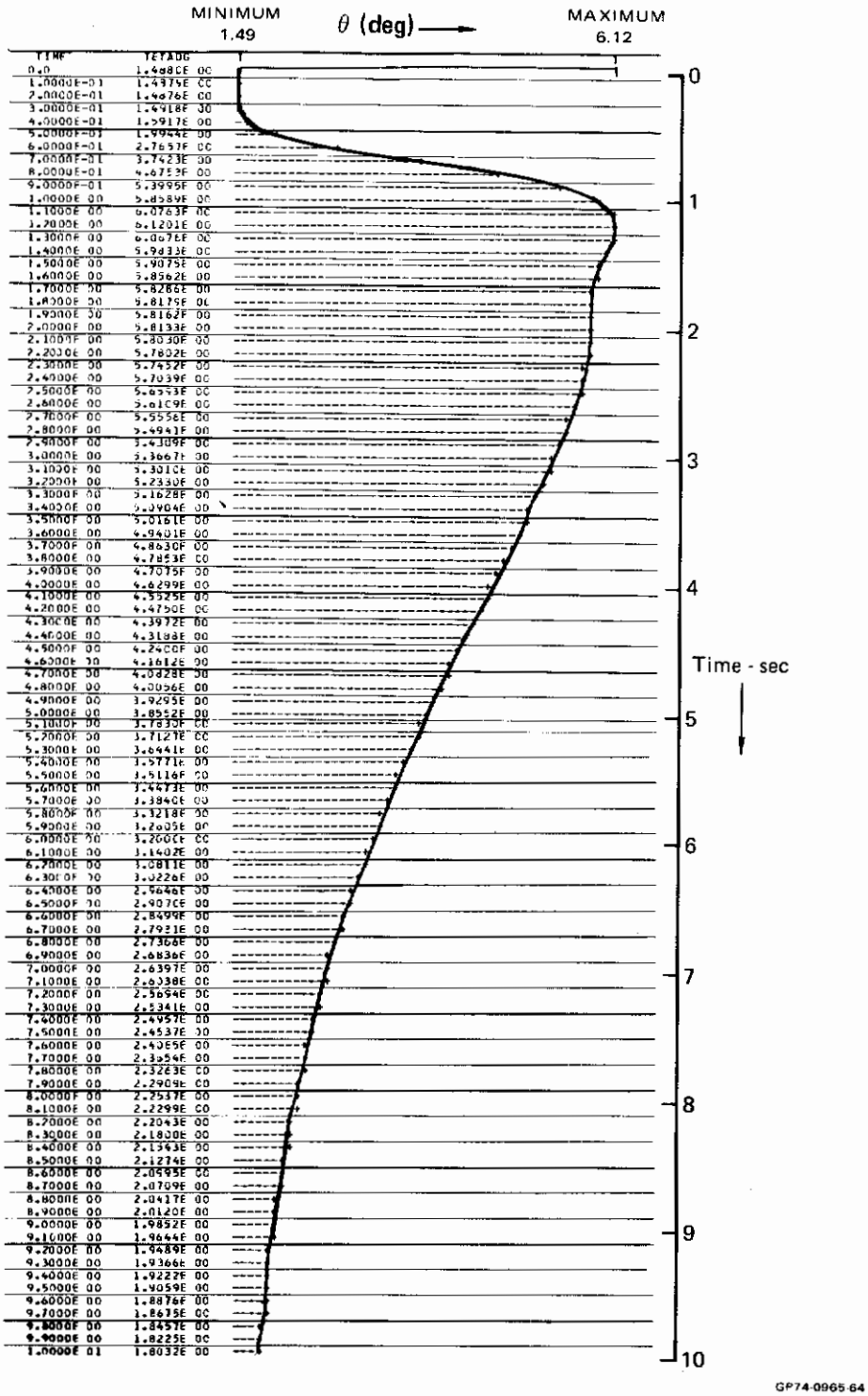

Figure 65 F-4E Mach Altitude Hold

Pitch Angle, 0.8 Mach at 15,000 ft

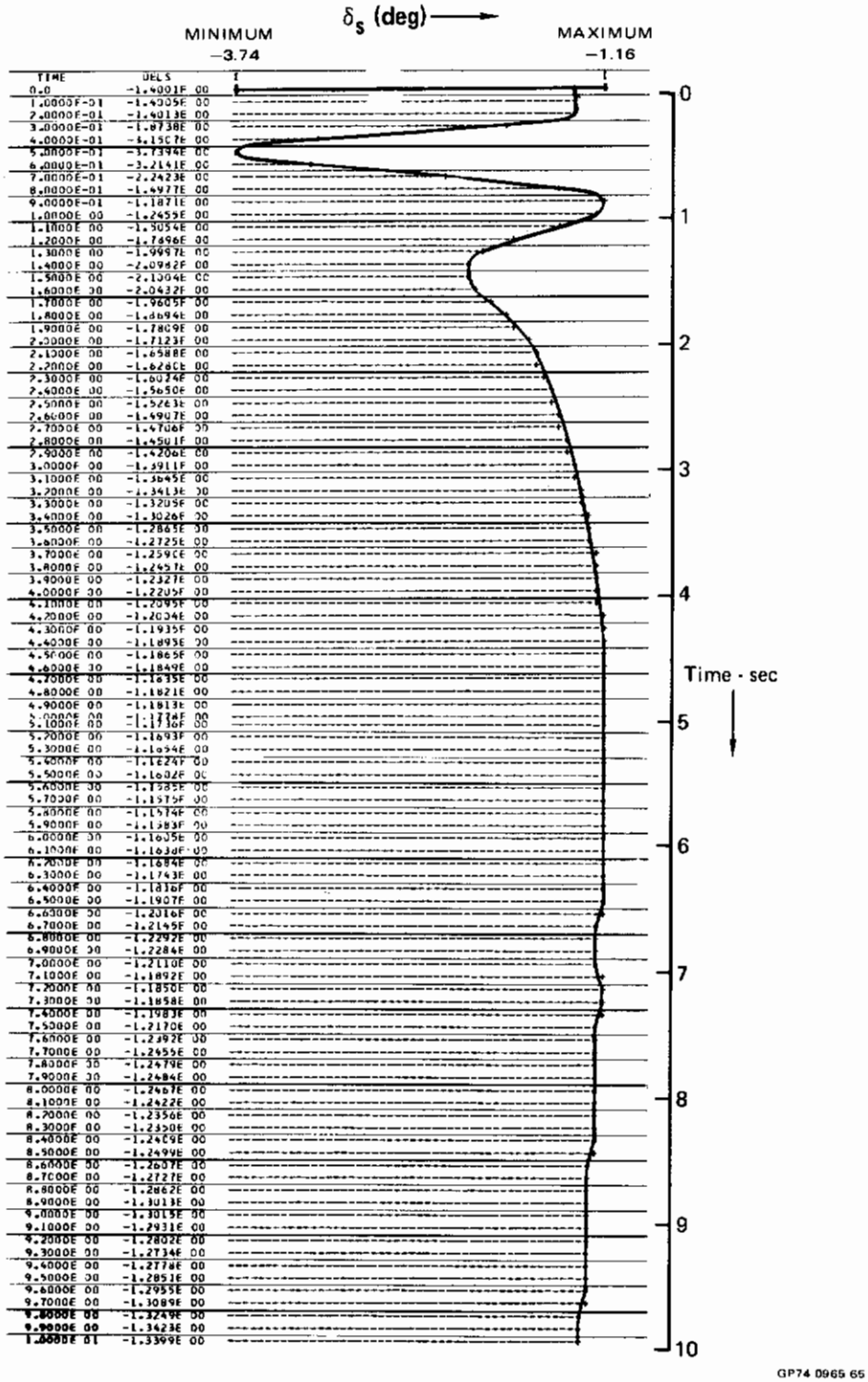

Figure 66 F-4E Mach - Alitude Hold

Stabilator Deflection, 0.8 Mach at 15,000 ft

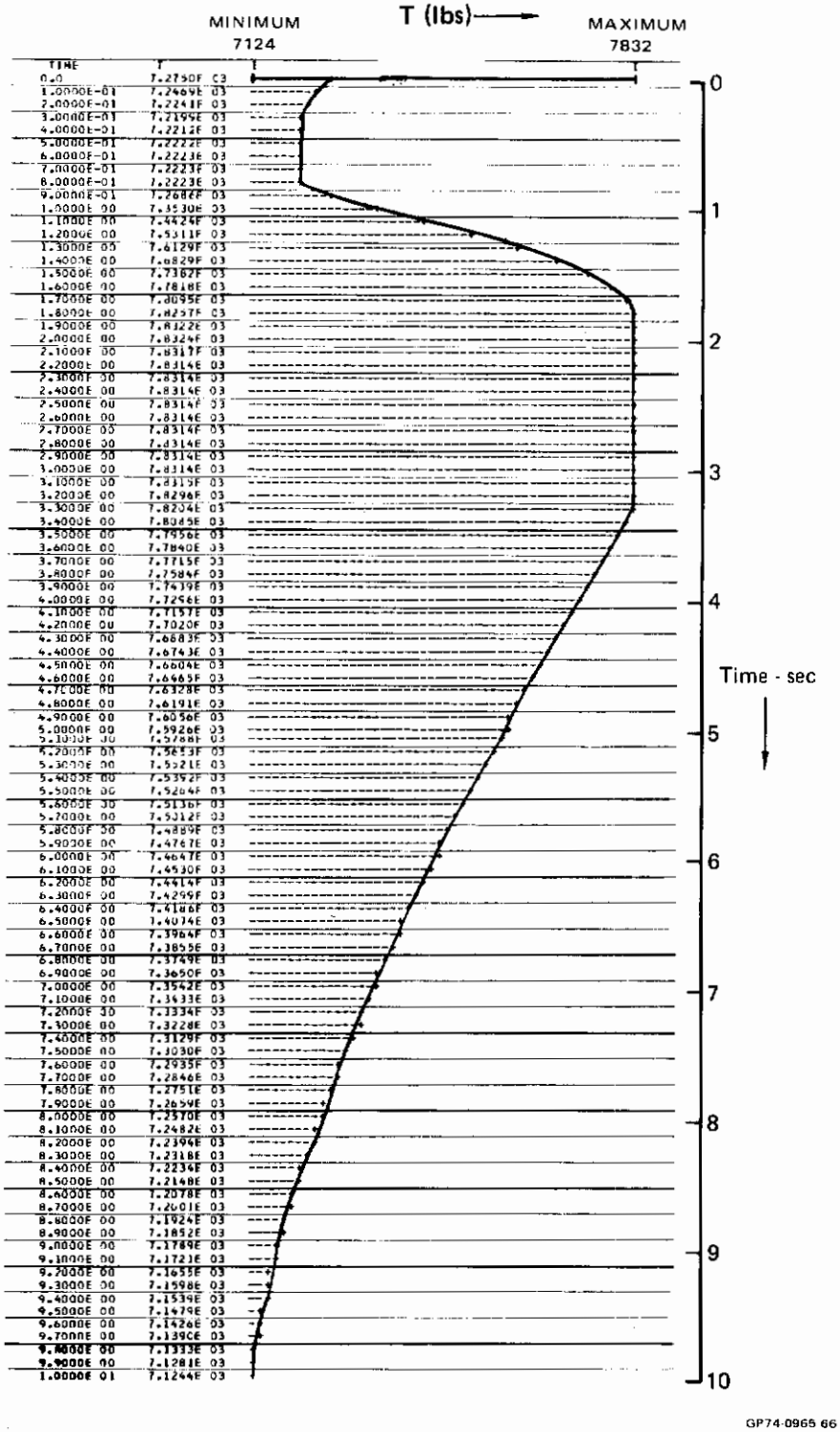

Figure 67 F-4E Mach - Altitude Hold
Thrust, 0.8 Mach at 15,000 ft

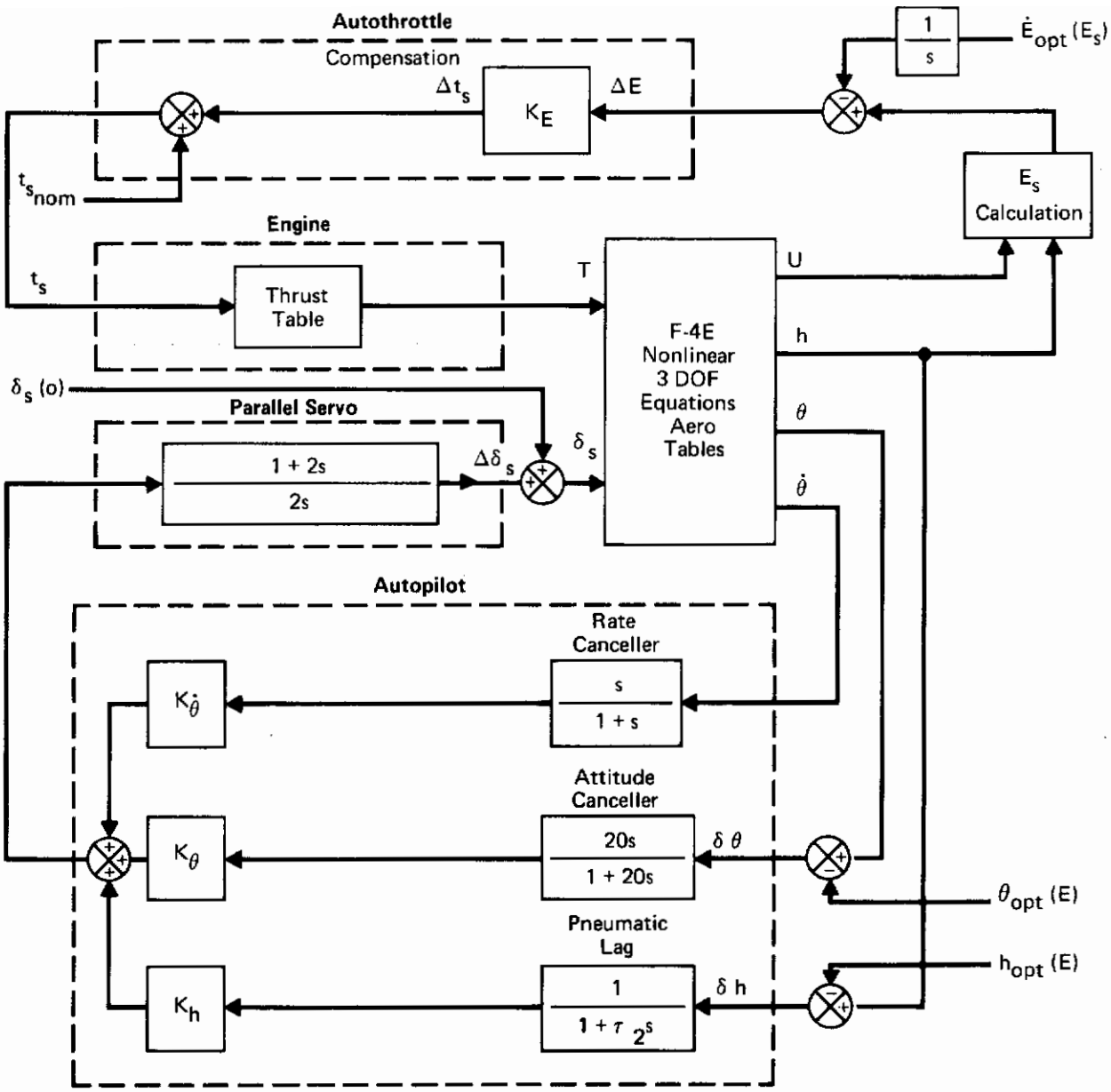

Figure 68 F-4E Nonlinear Simulation - High Frequency Terms Deleted

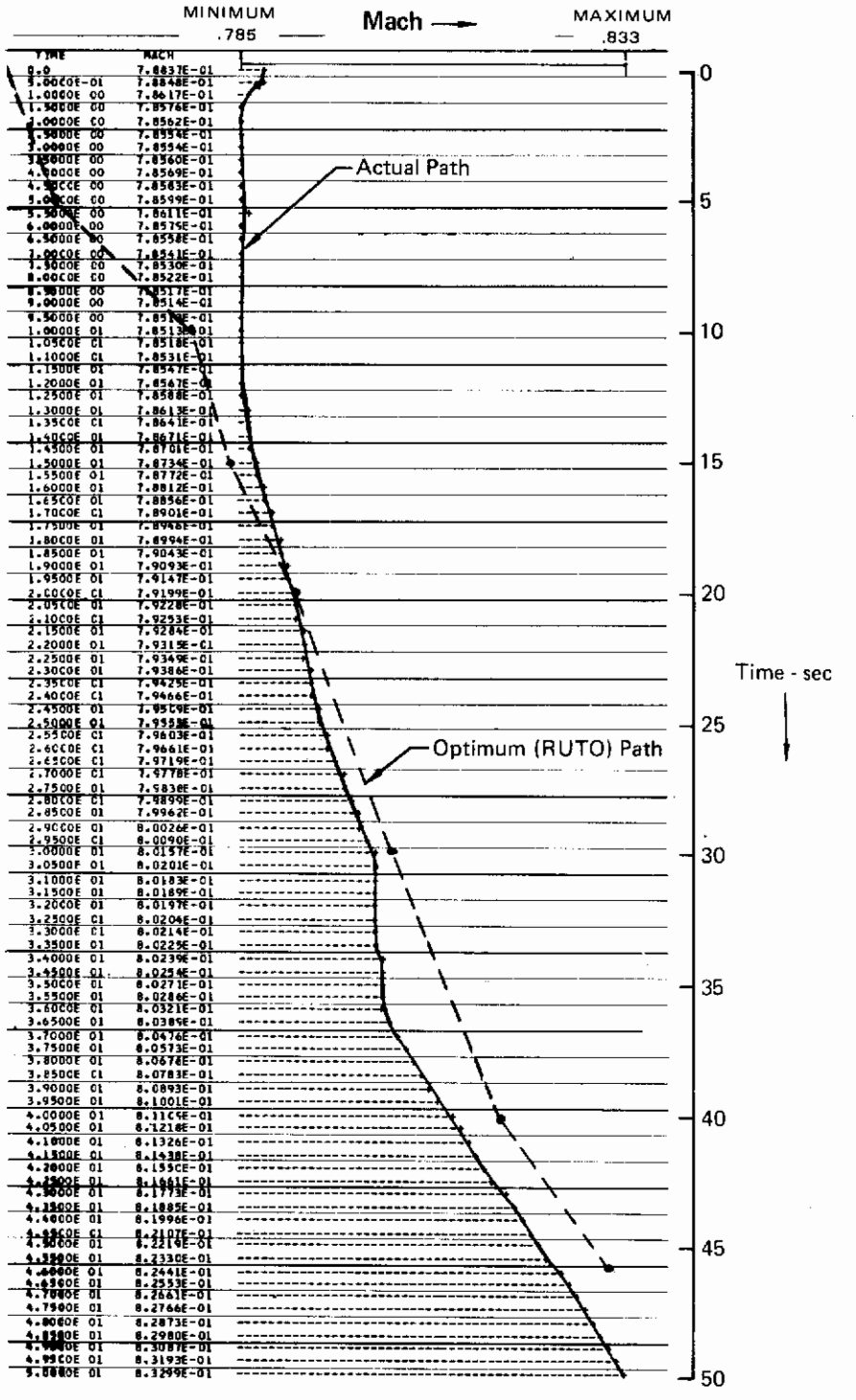

Figure 69 F-4E Subsonic Optimal Flight Path
Mach Number

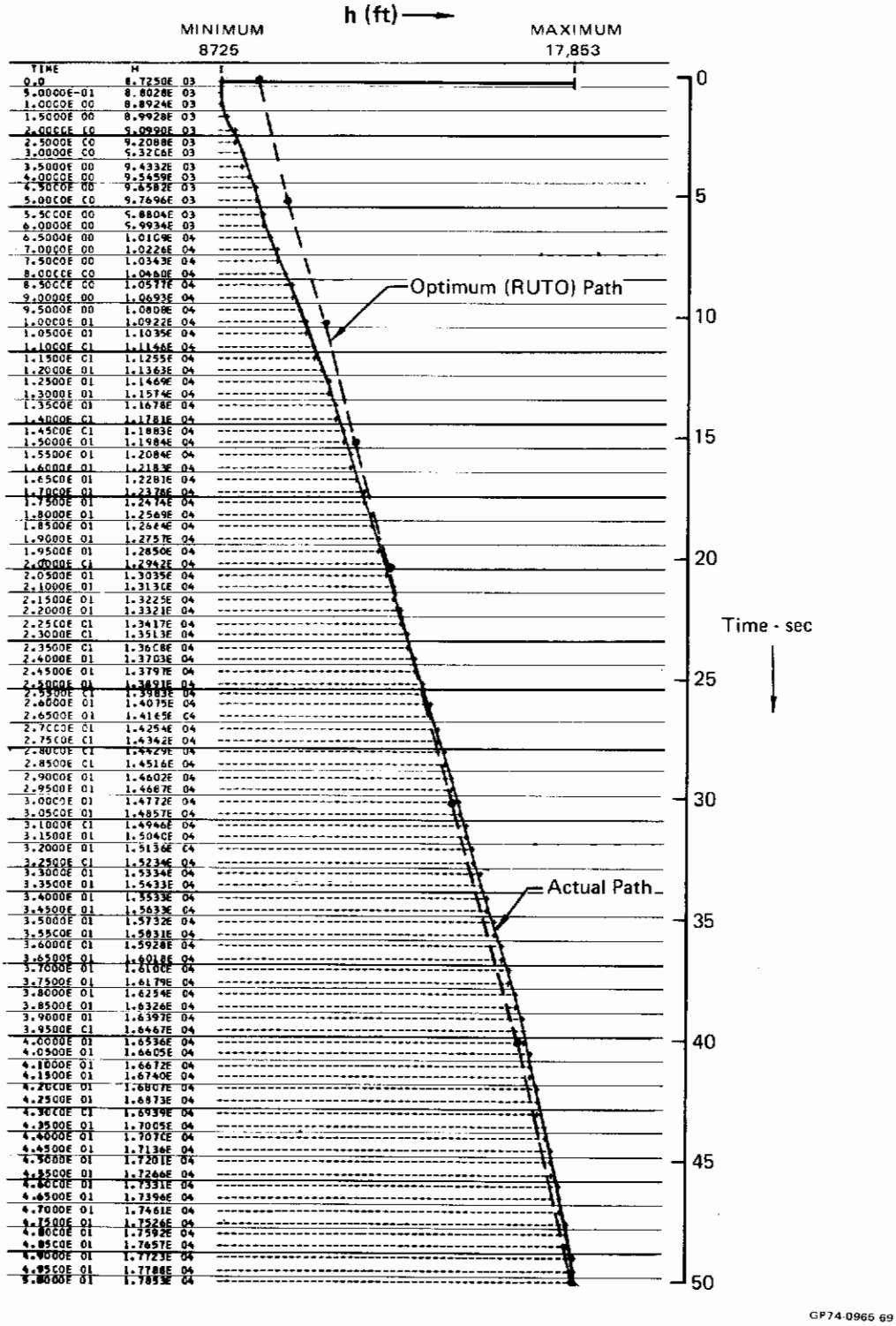

Figure 70 F-4E Subsonic Optimal Flight Path
Altitude

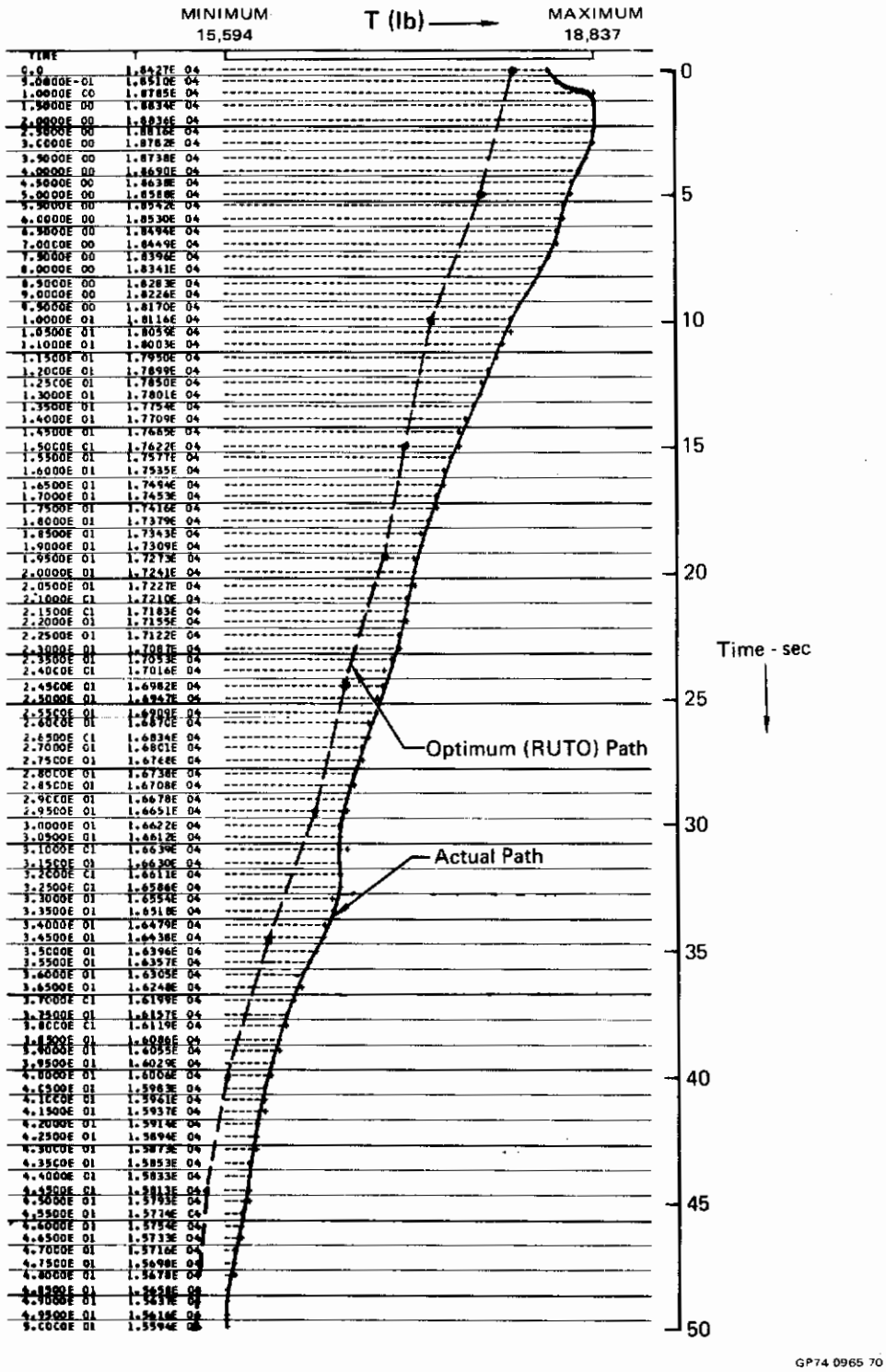

Figure 71 F-4E Subsonic Optimal Flight Path
Thrust

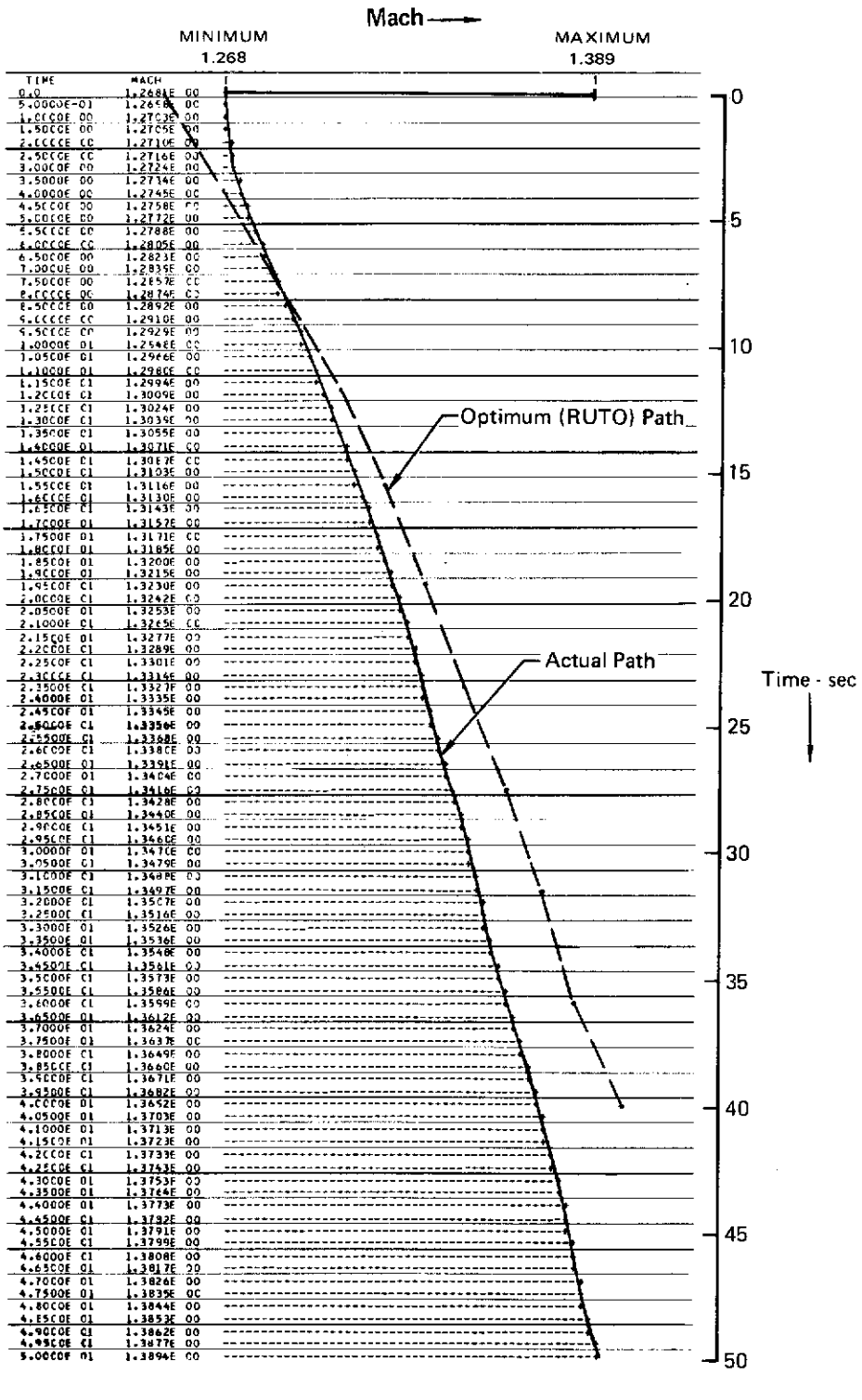

Figure 72 F-4E Supersonic Optimal Flight Path
Mach Number

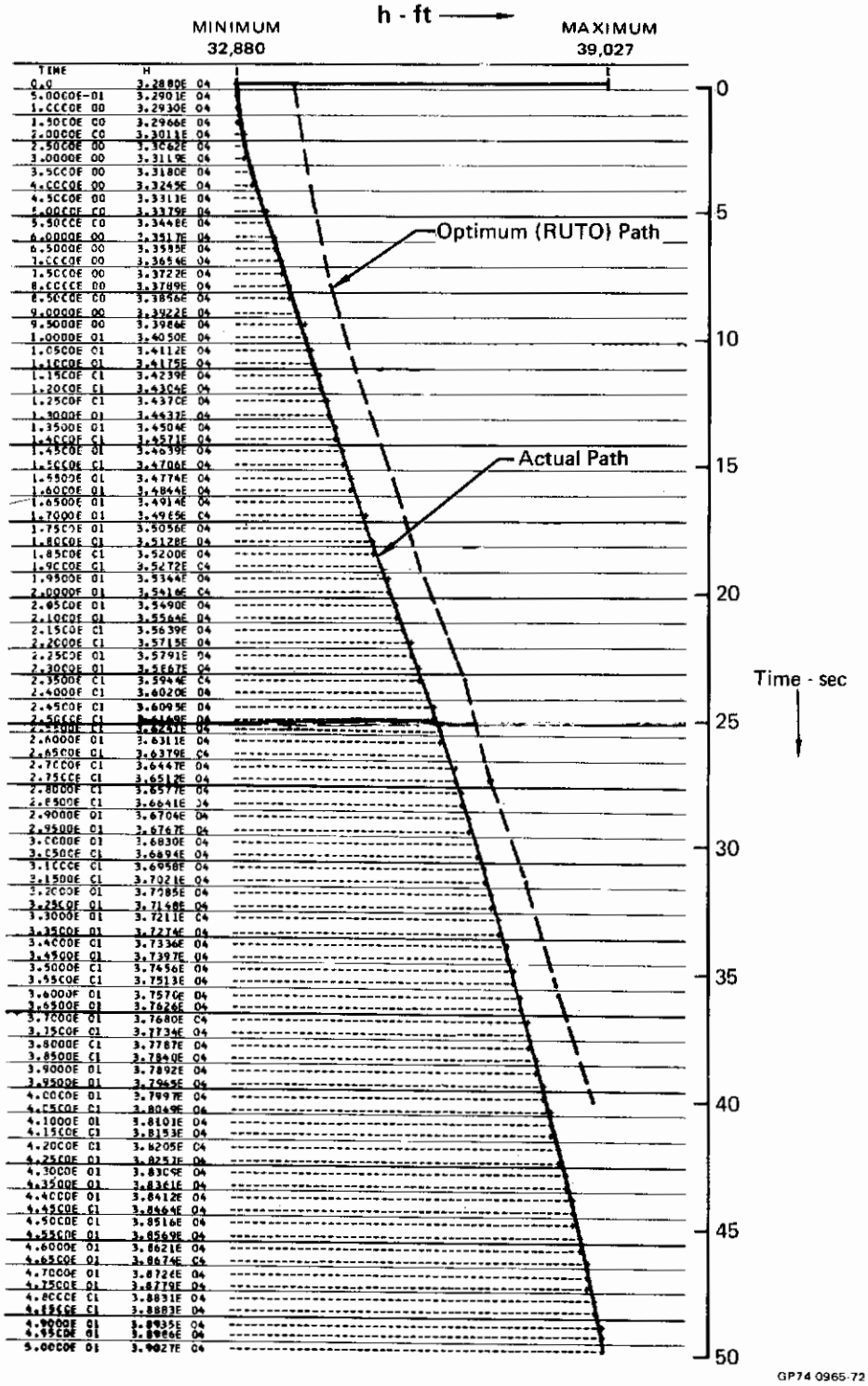

Figure 73 F-4E Supersonic Optimal Flight Path
Altitude

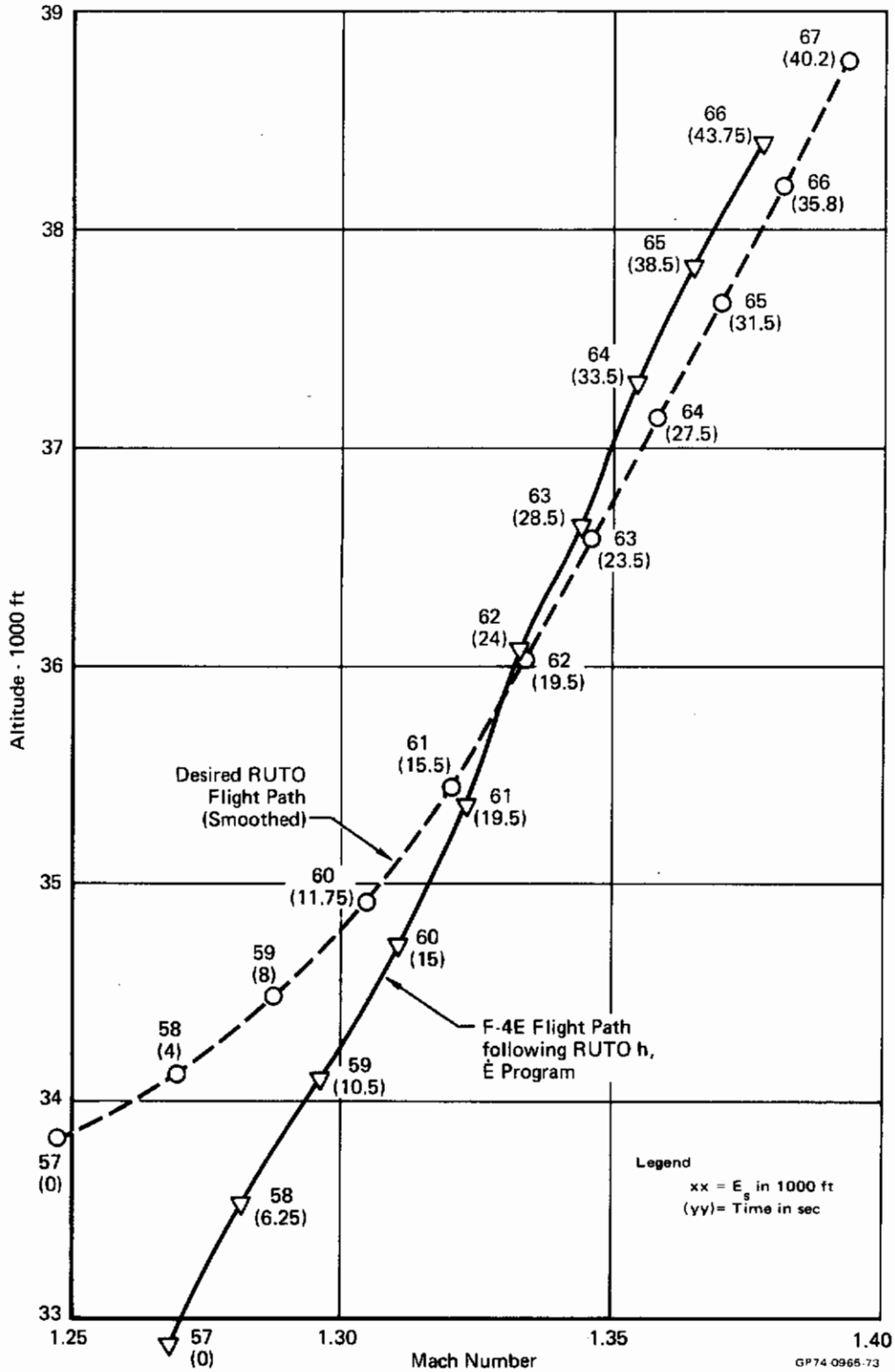

Figure 74 Comparison of Optimum Flight Path with F-4E Flight Path Following Program of Altitude and Ė with Energy

drag, fuel flow, aerodynamic derivatives and representations of measurement lags. An integral plus proportional feedback was added to the throttle control loop in order to assure a zero steady state specific energy error due to an error in the nominal throttle setting, as well as to provide improved path followings. Root locus studies were done to choose the gain and the amount of lead required for this type of compensation. The root locus for the compensation selected is shown in Figure 75. The resulting block diagram simulated in the MIMAC program MITCON is shown in Figure 76. This control system was used to follow the optimal flight path with a variable throttle as well as the optimal flight path with a fixed throttle. The results are described in the next section.

It should be noted that, while a stored table of $\dot{E}_{opt}$ versus E_{meas} worked well for these examples, a table of desired time stored versus E_{meas} appears to work equally well. In addition, it appears that flight path control can be accomplished using flight path angle, γ, feedback. The optimal flight path angle can be calculated on board from other stored information ($\dot{E}_{opt}(E_s)$, $h_{opt}(E_s)$), thus eliminating the need to store this path parameter. Since a design goal was to make as few changes as possible to the existing F-4E flight control system, pitch angle feedback was used in this study. Nevertheless, these improvements should be considered further before subsequent flight test.

3.3 Demonstration of Performance Benefits

As noted in the previous section, the MIMAC program MITCON was used for time domain simulations of the system defined by the block diagram shown in Figure 76. These simulations were used to evaluate the performance of the control system when following two optimal minimum fuel flight paths. The first was a variable throttle flight path in which there is feedback to the throttle. The second was a fixed throttle flight path in which the throttle is held at the maximum afterburner setting with no feedback except during an intermediate subsonic cruise segment discussed below. In each case the optimal flight path is defined from a sea level specific energy of 5000 feet to a specific energy of 65,000 feet by use of the RUTO Program (Reference 4) and the Point Mass Program which "smooths" the RUTO trajectory and provides connecting segments for the sea level pullup onto the path and across the RUTO discontinuity in the transonic region. A terminal time constraint is imposed on the fixed throttle case by requiring that the elapsed time at which a specific energy of 65,000 feet is reached is the same as for the variable throttle

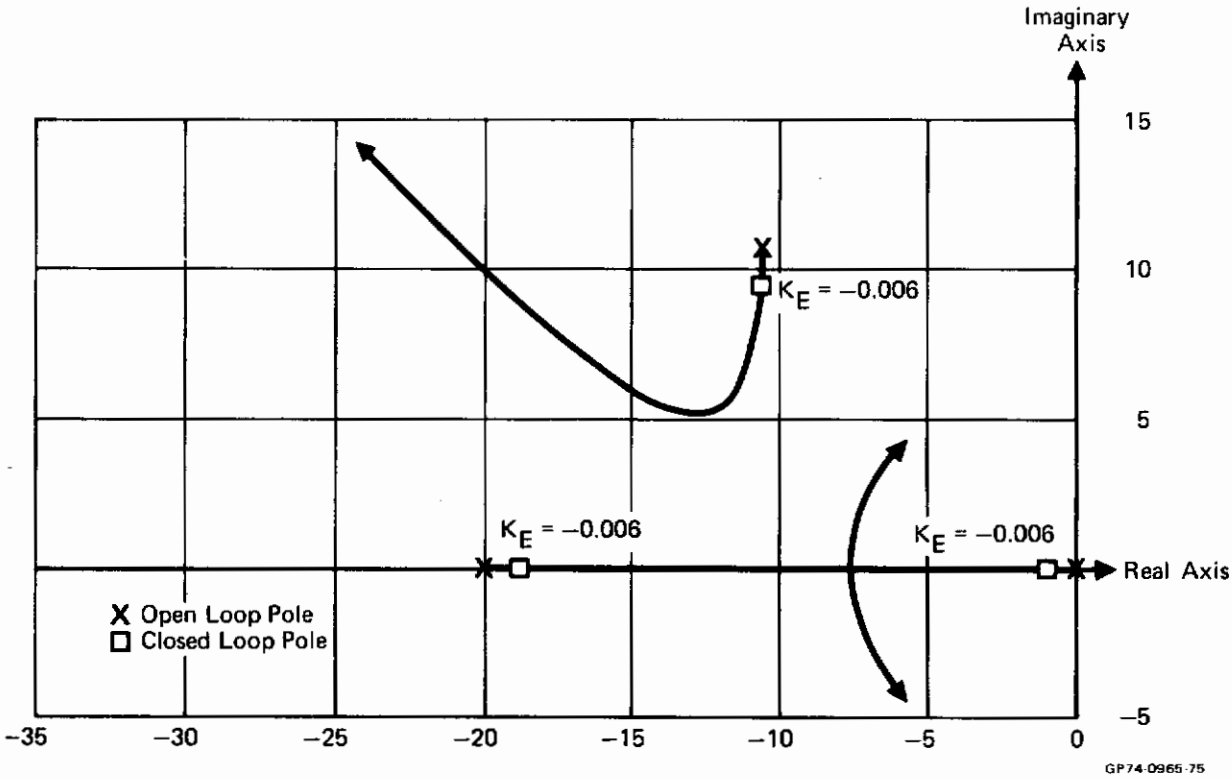

Figure 75 Root Locus for Throttle Control with Integral Plus Proportional Compensation

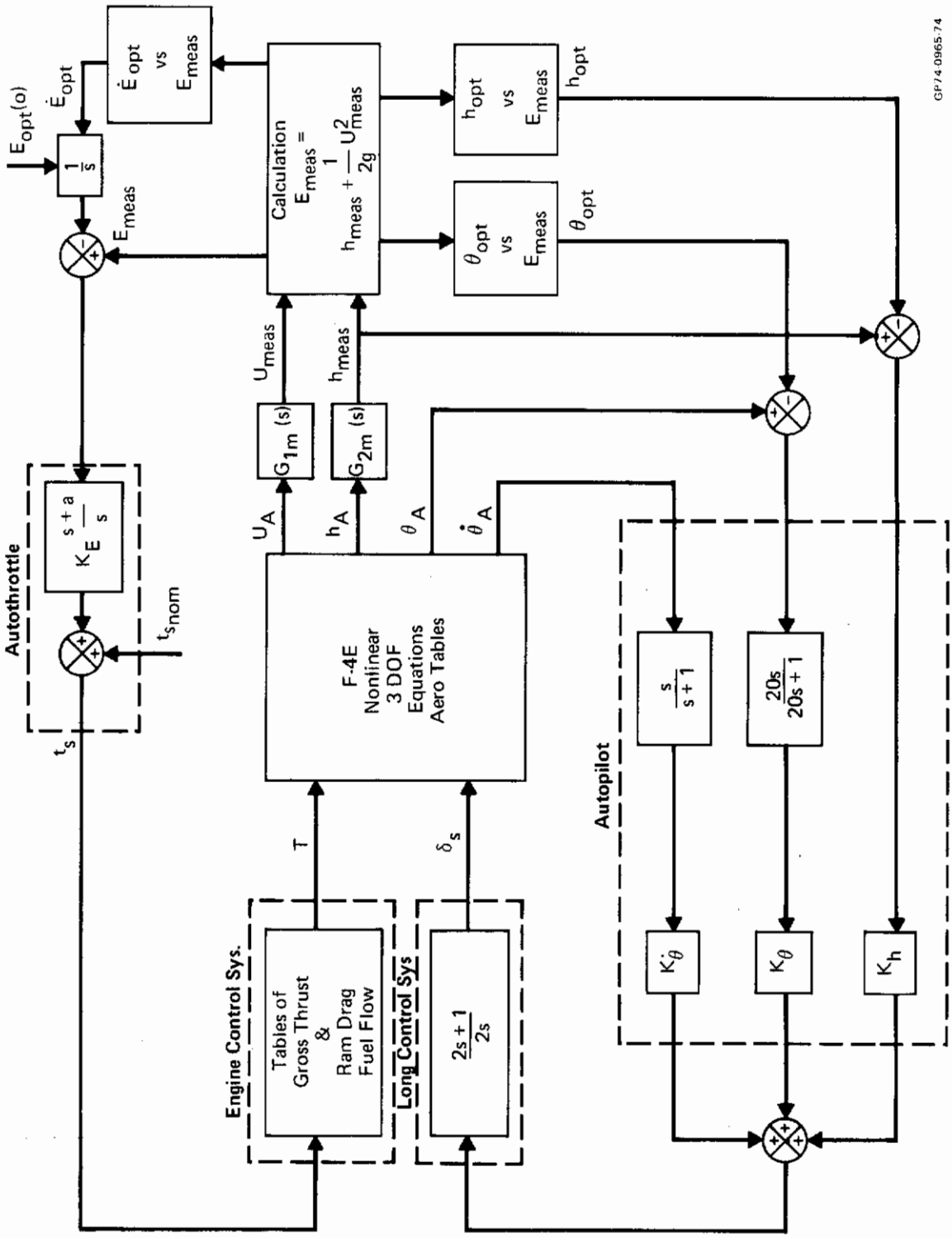

Figure 76 MIMAC Nonlinear Simulation Block Diagram

case. To accomplish this, a subsonic cruise segment is included in the fixed throttle case. During the cruise segment the throttle control system provides a feedback correction to any error in the stored cruise throttle setting and the aircraft is held at the proper Mach-altitude point. Note that without the proportional plus integral feedback in the throttle loop, an error in the stored value of the cruise throttle setting would result in a steady state error in aircraft velocity as the stabilator control system nulls out steady state altitude errors. Since the cruise velocity was selected to match the final range and time at the final specific energy with that of the variable throttle flight path, a cruise velocity error is particularly undesirable.

A Mach-altitude plane plot of the optimal minimum fuel, variable throttle flight path is shown in Figure 77 with the results of a MITCON simulation superimposed. The point denoted as "E_{sw}" in the figure is the specific energy level at which the nominal throttle setting is moved from the military power setting to the minimum afterburner setting. The control system performs very well in keeping the aircraft on the optimal path with a maximum deviation of 300 feet in altitude occurring during the transonic transition across the discontinuity in the RUTO defined trajectory. The load factor is maintained relatively close to desired limits of $\pm$ .5g about 1g during the sea level pull up and the transonic transition where deviation of +.65g occurs during the sea level pullup and -.57g occurs during the transonic pushover. Similarly, a Mach-altitude plane plot of the minimum fuel, fixed throttle flight path is shown in Figure 78 with the results of a MITCON simulation superimposed. The point denoted "C_r" in the figure is the cruise point. The control system again performs very well with a maximum deviation of -300 feet in altitude again occurring during the transonic transition region. The load factor is maintained reasonably close to the desired limits of $\pm$ .5g about 1g with nominal deviations of +.75g occurring during the sea level pull up and -.32g occurring during the transonic pushover.

Plots of time, range and fuel consumed versus specific energy are shown in Figures 79, 80, and 81, respectively. The agreement in the terminal time at a specific energy of 65,000 feet is very close, the difference being approximately .1 seconds as noted on Figure 79. The cruise segment of the fixed throttle case is terminated at 300.3 seconds and both cases achieve a specific energy of 65,000 feet at approximately 404.2 seconds. The range versus specific energy plot shown in Figure 80 also shows close agreement at the final

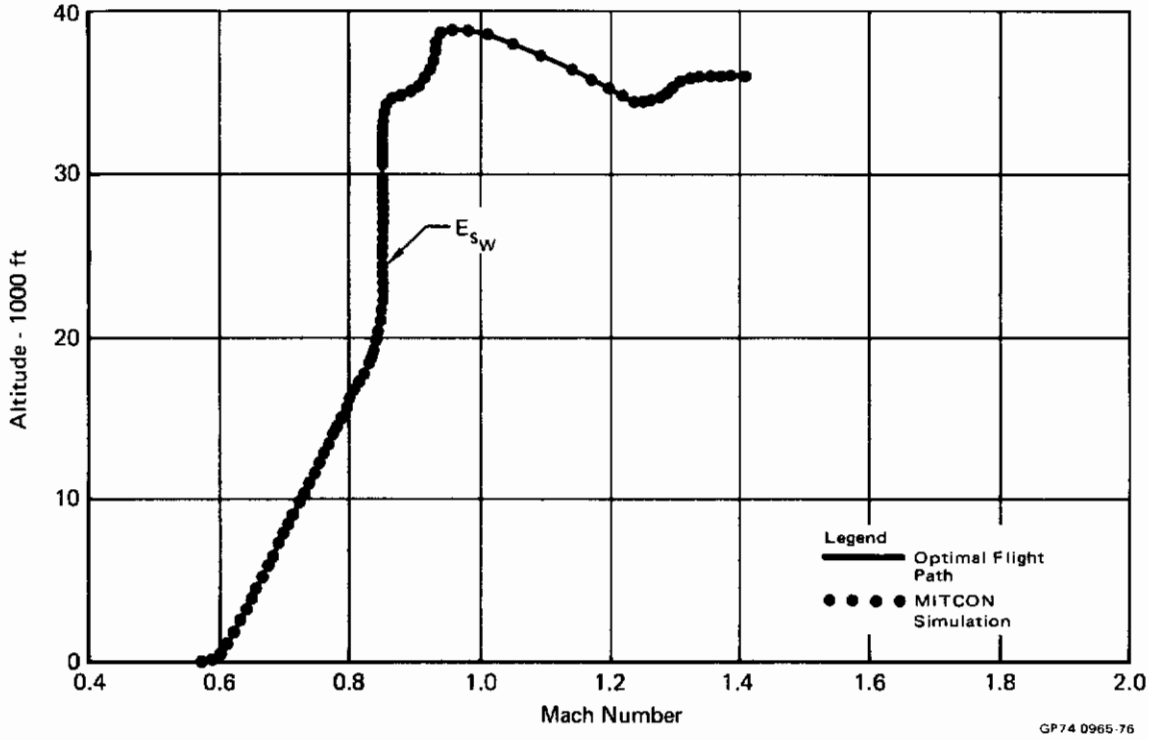

Figure 77 Variable Throttle Flight Path

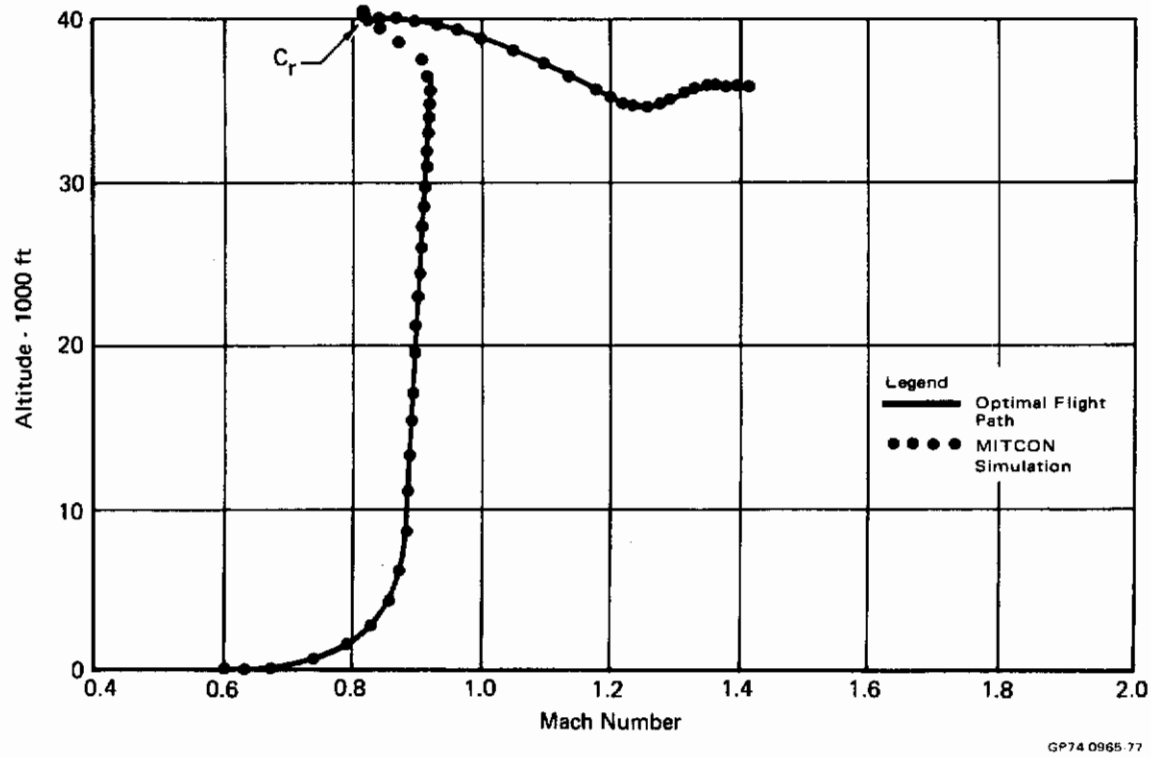

Figure 78 Fixed Throttle Flight Path

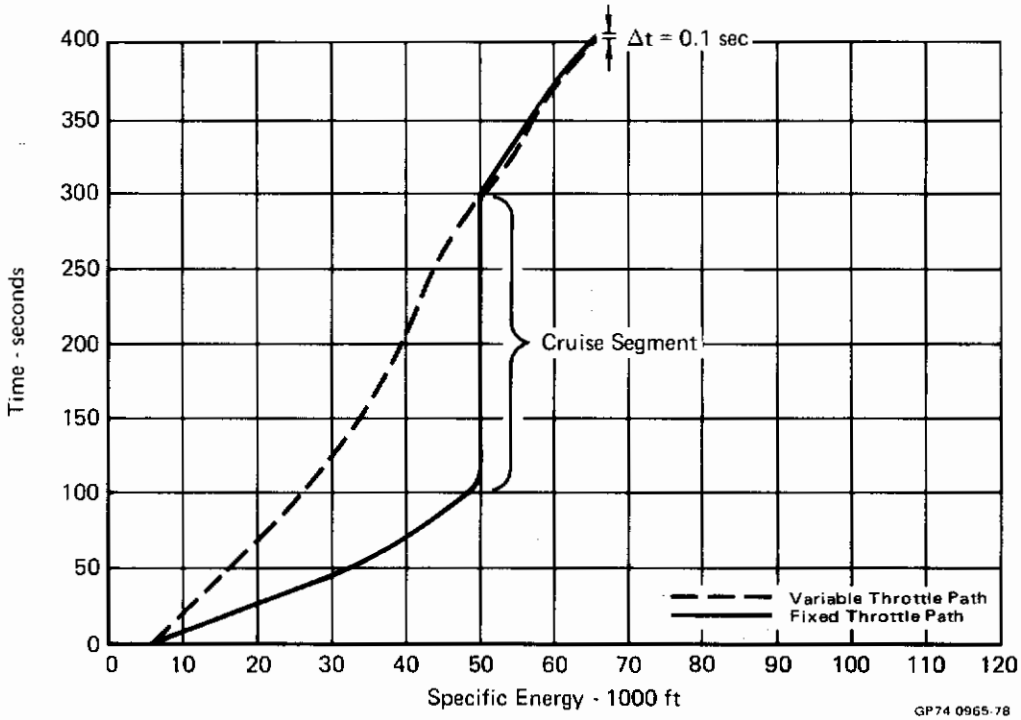

Figure 79 Time vs Specific Energy

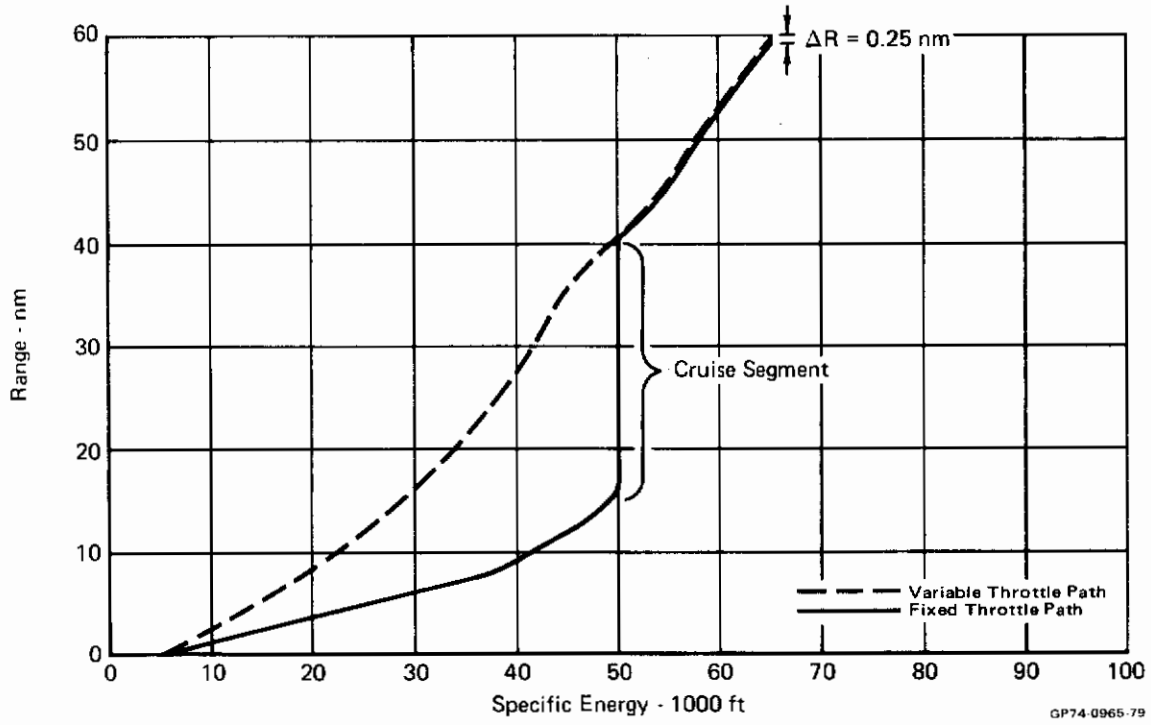

Figure 80 Range vs Specific Energy

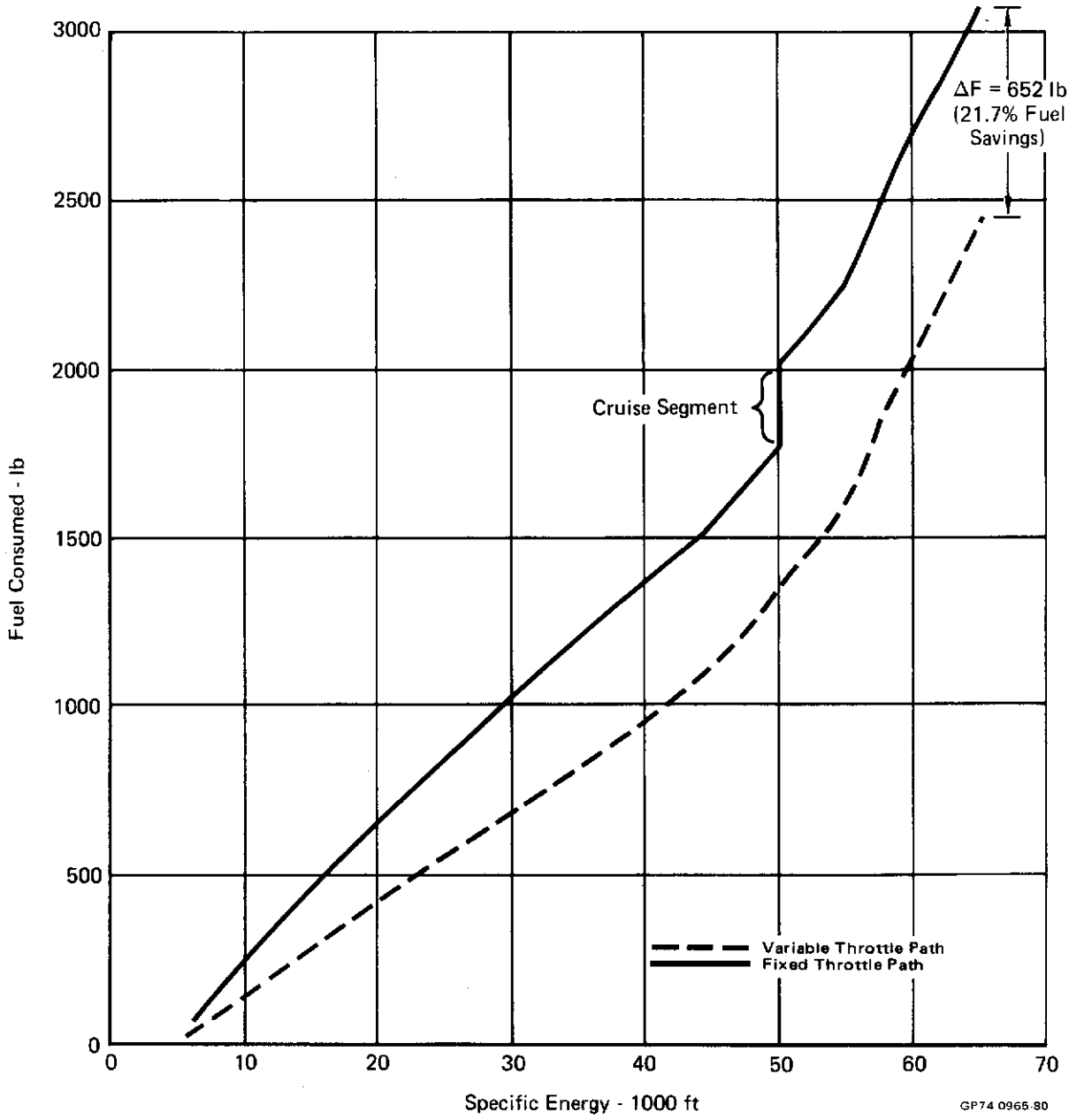

Figure 81 Fuel vs Specific Energy

specific energy. In the variable throttle case the range is 60.26 nautical miles and in the fixed throttle case it is 60.01 nautical miles which gives a difference of .25 nautical miles or about .4%. The general shape of the time and range versus specific energy graphs are very similar as would be expected. The fixed throttle case initially achieves higher specific energy levels at a much faster rate, hence, the range versus specific energy curve has a correspondingly reduced slope. The cruise segment at a constant specific energy in the fixed throttle case then yields a nearly identical time and range value for the two cases at the end of the cruise. Since the optimal flight paths are virtually identical from this point on, the two time plots as well as the two range plots lie practically on top of one another. The fuel consumed versus specific energy plot shown in Figure 81 is of particular interest as it demonstrates a significant fuel savings of approximately 21.7% for the variable throttle flight path over the fixed throttle flight path.

In each of Figures 79, 80, and 81, the data derived from the MITCON simulations begins with the specific energy level at which the pullup onto the optimal trajectories is initiated. This is E_s = 5974 feet in the variable throttle case and E_s = 7083 feet in the fixed throttle case. The initial data for specific energy levels between 5000 feet and the specific energies given above are derived from RUTO data. This was done to establish a common reference point for comparison of the two cases. The initial aircraft weight in the MITCON simulations was adjusted to reflect the difference in specific energies at the beginning of the sea level pull ups and the difference in throttle settings at which initial level flight segments from E_s = 5000 ft to the pull up specific energies are made for the two cases. The difference in time at which the aircraft reaches the sea level pullup specific energy starting from E_s = 5000 feet for the two cases is approximately .3 seconds.

SECTION 4

HYBRID SIMULATION STUDY RECOMMENDATIONS (TASK IV)

4.1 Introduction

Throttle/Energy management in the form of throttle control and flight path selection has been shown to improve performance of a mission in terms of fuel savings, time reduction, improved range or a combination of any or all three. This has been done analytically using all-digital simulations.

However, there are areas of throttle/energy management which cannot be fully explored using an all-digital simulation. A pilot in the loop hybrid simulation is required to evaluate manual versus automatic implementation of the throttle/energy management system. This includes rating the candidate display systems and determining pilot acceptance. The conclusions from this simulator study can then be used to decide the mechanization of the throttle/energy management system, to design cockpit displays and to estimate the level of performance improvement which can be expected in the subsequent flight test demonstration. There will be two options presented here, one for an F-4E simulation alone, and one for a joint F-4E, F-15 simulation.

4.2 Objective

A hybrid simulation is considered necessary to demonstrate energy management principles and to satisfy the operational and safety requirements prior to a flight test. The objective of this simulator study is to determine the best means (automatic or manual) of implementing the required flight path control and throttle control based on the throttle energy management system performance and the associated pilot ratings. Two flight paths/throttle settings will be flown. The first will follow a minimum fuel flight path/throttle setting from a given set of initial conditions to a specified set of terminal conditions. The second flight path will confirm that the first provides a significant fuel saving by flying this same transition in a more conventional manner (optimal flight path with fixed throttle).

It is desired to try the following combinations of controls for following the specified flight paths and throttle settings:

Manual flight path and manual throttle

Manual flight path and automatic throttle

Automatic flight path and manual throttle

Automatic flight path and automatic throttle (baseline)

Various types of displays will be tried with the manual system.

The above combinations would then be evaluated on the basis of the percentage of theoretical performance improvement achieved using the fully automatic system as the reference, as well as pilot ratings obtained from the questionnaires. Based on this qualitative and quantitative data, the best system would then be selected for a subsequent flight test.

4.3 Simulation Requirements

The MCAIR Manned Air Combat Simulator (MACS) or similar facility will be required (Appendix A). In order to keep program costs at a minimum, only the bare essentials would be operational on MACS for this simulation. This simulator uses the CDC 6600 computer which is adequate for this study. However, the portion of the program required for onboard calculation and storage is consistent with current state-of-the-art for onboard computers.

a) Airframe - A complete set of longitudinal nonlinear three degree of freedom equations will be used to represent the F-4E and the F-15 airframe dynamics. Aerodynamic data required to simulate these aircraft are described in Appendix B and will be supplied.

b) Engine - Engine and throttle servo dynamics will be supplied for the J79-10 and F-100 engines. Gross thrust, ram drag and fuel flow tables will be supplied as a function of Mach number, altitude and throttle setting as shown in Appendix B.

The F-4E flight path/throttle control system as well as the minimum fuel-variable throttle and minimum fuel-fixed throttle flight paths/throttle settings are described in this report. The F-15 control systems and optimal paths will have to be worked out in any subsequent simulator contract. A schedule for this is included in Section 4.6.

c) Flight Control System - The baseline F-4E and F-15 longitudinal Stability Augmentation Systems will be simulated. In addition, the flight path control system will be simulated. These control systems require scheduling gains as functions of dynamic pressure and Mach as well as certain time constants and frequencies as functions of altitude. In addition, the energy management flight path control system requires that optimal histories of altitude and pitch angle be stored as functions of aircraft specific energy.

d) Throttle Control System - The throttle control system used to follow the stored optimal throttle setting will be simulated. This involves storing specific power as a function of aircraft energy.

e) Optimal Path - The parameters defining the optimal (minimum fuel) flight path and throttle settings as well as those defining the fixed throttle flight path will be stored and the deviations from them calculated and displayed.

f) Cockpit Instruments and Displays - The following F-4E and F-15 instrumentation will be implemented in the cockpits:

1) Mach/airspeed indicator
2) Altimeter
3) Rate of climb indicator
4) Accelerometer
5) Engine RPM indicator
6) Range digital readout
7) Fuel, fuel flow indicators

For the F-15 simulation, the HUD (Heads-Up Display), VSD (Vertical Situation Display) and CCC (Central Computer Complex) hardware can be used to simulate actual flight hardware.

In addition, several throttle/energy management displays will be used. These consist of both informational and command displays.

Figure 82 shows an optimal flight path display and a throttle command bar display. It was found that this display could be used successfully by pilots in a previous simulator study (Reference 19). The optimal flight path is displayed on the cathode ray tube together with the current aircraft position and direction indicator in the Mach/altitude plane. This is an informational display. The throttle command bar display is simply a vertical bar indicator displaying the present throttle position and the optimal throttle position. This is a command display.

Figure 83 shows a flight director system (Reference 20). The error in flight path altitude and altitude rate is displayed. One side of the box corresponds to altitude error and the other to altitude rate error. This is a command display.

Figure 84 shows the pitch ladder command display. The flight path control system uses a blend of altitude error and pitch angle error to control the stabilator. This blended feedback can be considered to be an effective, commanded pitch angle and can be displayed on the cathode ray tube together with the present aircraft attitude for the pilot's use on flying the optimal path. This is a command display.

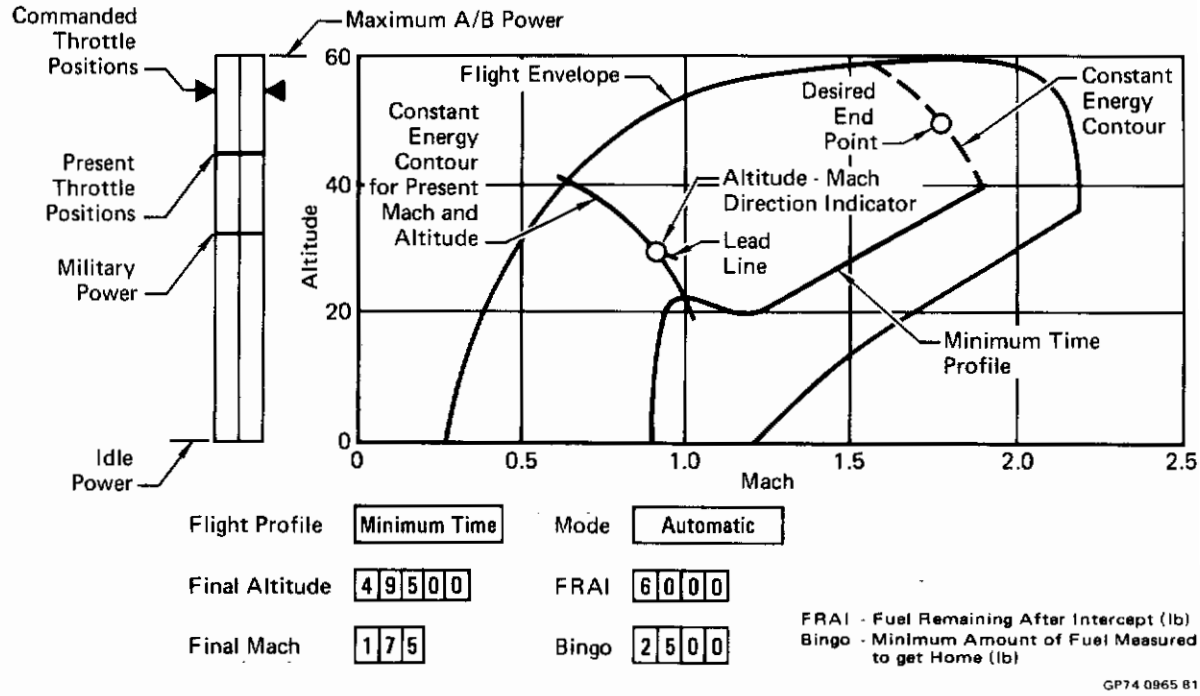

Figure 82 Energy Management Optimal Flight Path Display and Throttle Command Bar Display

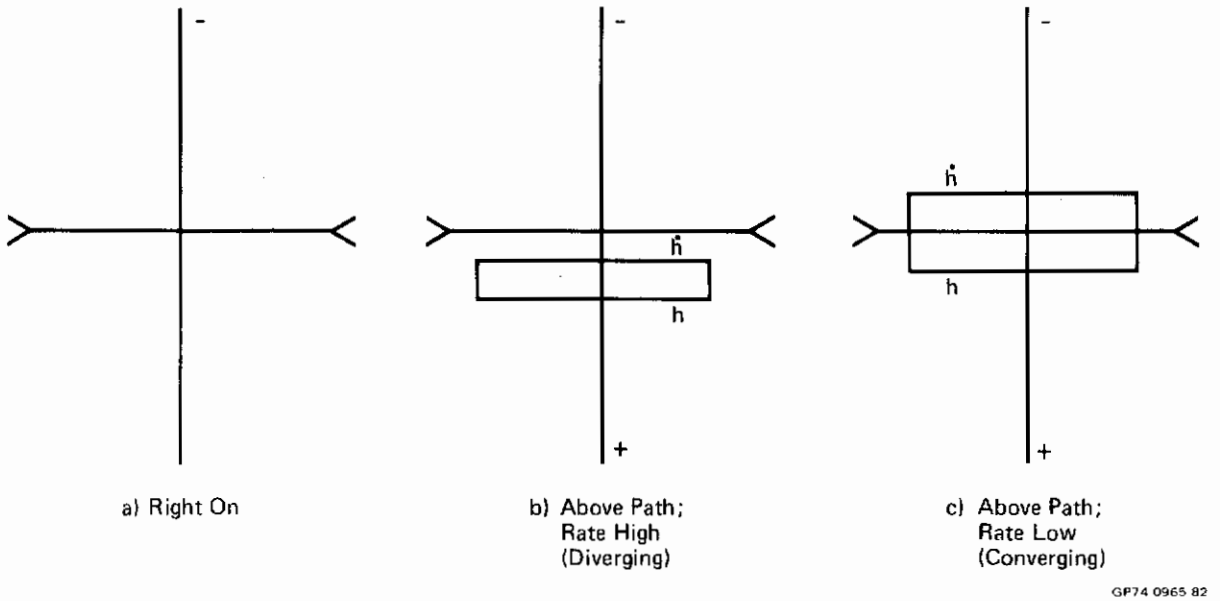

Figure 83 Flight Director in Various Modes

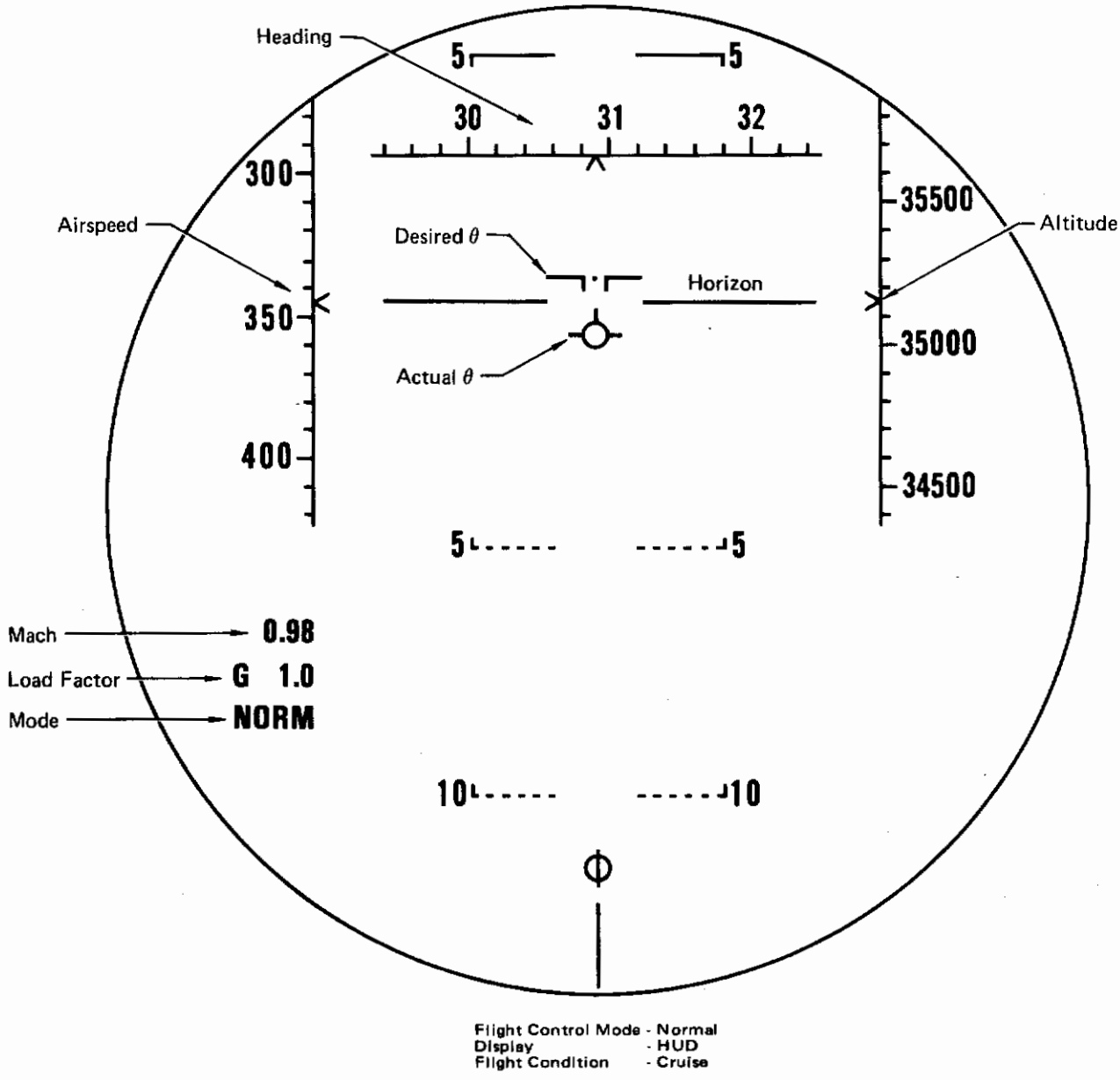

Figure 84 Pitch Ladder Command Display

Figure 85 shows a throttle command circular dial display (Reference 1) which is a circular dial that can be used to display error in thrust or throttle position which the pilot would attempt to null. Alternately actual and desired throttle settings can be displayed using both hands. This is a command display.

g) Pilot Controls - The following controls should be included:
   1) Center stick and pedals
   2) Pitch trim
   3) Throttle quadrant

h) Data Recording - Instrumentation equipment required for these tests in addition to the digital data being recorded by the CDC 6600 computer memory core and magnetic tape includes strip chart recorders, digigraphic display equipment and audio/video recording and playback facilities. The signals which will be recorded are listed in Table IV.

4.4 Simulation Test Plan

Tests will be conducted to determine the best method of mechanization (automatic versus manual) for the combined flight path/throttle control system based on the percentage of predicted performance improvement achieved and pilot ratings. Several display combinations for manual flight path and throttle control will be considered. Initial conditions both close to and far removed from the optimal path/throttle setting will be considered. We will assume that the same number and types of simulator runs will be made for both aircraft (F-4E and F-15).

The pilot or automatic system will attempt to fly the optimal as well as a more conventional flight path/throttle setting. These are the ones chosen for a flight test demonstration of performance improvements.

It is anticipated that approximately 268 simulator runs of 8 minutes duration should be made for each aircraft considering various combinations of automatic and manual systems, displays, and off-path conditions. It will be sufficient to have two pilots (either Air Force or MCAIR) make these runs. Each run should be made at least three times for statistical confidence. These display systems will be tried:

1) H-M diagram with bar throttle display (Figure 82)
2) Flight director with circular throttle display (Figures 83 and 85)
3) Pitch ladder with circular throttle display (Figures 84 and 85)

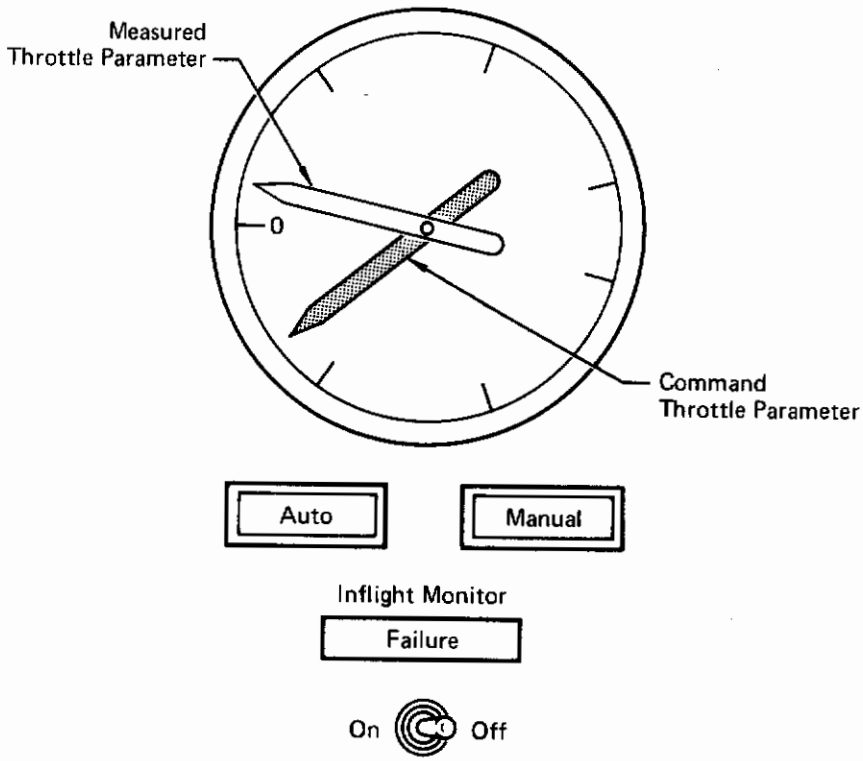

Figure 85 Circular Dial Throttle Control Display

Table IV Digital Data Output

Mach	Altitude	Pitch Angle	Specific Power	Specific Energy	Body	Load Factor at C.G.	Load Factor Pilot Seat
Command Mach	Command Altitude	Command Pitch Angle	Command Specific Energy	Measured Specific Energy	Altitude Rate	Pitch Rate	Flight Pitch Angle
Throttle Position	Fuel Flow	Gross Throttle	Ram Drag	Net Thrust	Aircraft Weight	Aircraft Airspeed	Longitudinal Acceleration
Pitch Center Stroke Force	Pitch Center Stroke Position	Stabilator Position	Stabilator Rate	Down Range	Time (Digital)	Total Fuel Used	Vertical Wind
Temperature							

The runs can be summarized in the following tables:

COMMANDED PATHS

1. Optimal (Minimum Fuel)	1
2. Conventional (Fixed Throttle)	1
	2

CONTROL MODES

Flight Path Control System	Throttle Control System	Combinations	
		Path 1	Path 2
Manual	Manual	3	3
Manual - 3 displays	Automatic	3	
Automatic	Manual - 2 displays	2	-
		8	3

Fully automatic throttle/energy management need only be made for the four sets of initial conditions and need not be repeated.

INITIAL CONDITIONS

Flight Path	Throttle	Total
1. Near Path	Near Command	1
2. Far from path	Near Command	1
3. Near Path	Far from Command	1
4. Far from Path	Far from Command	1
		4

Fully Automatic Runs = 4 Initial Conditions = 4

Path 1 Runs = 3 Control Modes x 4 Initial Conditions x 3 Runs Each x 2 Pilots = 192

Path 2 Runs = 3 Control Modes x 4 Initial Conditions x 3 Runs Each x 2 Pilots = 72

Total Runs = 4 + 192 + 72 = 268

This figure could be lowered somewhat if it is established in earlier runs that one or more of the display systems obviously does not work.

Additional studies can be done considering the effects of wind gusts, steady winds and temperature variations on the selected system(s). A problem area that exists relative to onboard energy management optimization is that of handling nonstandard day temperatures and lapse rates. MCAIR is presently conducting independent research in this area in order to provide an operationally useable energy management display system. This program is scheduled for completion in late 1974, and the results will be integrated into the simulation program.

4.5 Evaluation Criteria

Quantitative Data - The payoff functions to be evaluated will be weight of fuel used and accuracy in meeting terminal conditions in time and range. The reference (baseline) value of this performance function will be that calculated for the fully automatic throttle/energy management system. The payoff function will be calculated for each of the control modes based on its performance in flying the two specified paths from the four sets of initial conditions by both pilots three times.

Qualitative Data - For each of the control modes (display configuration), the pilot will be given a questionnaire to fill out. A candidate questionnaire is shown in Figure 86 which should determine the throttle/energy management system's flyability and stability.

4.6 Schedule

There are two options, the first is an F-4E simulation alone, the second is a joint F-4E/F-15 simulation. The F-15 simulation will involve modifying all the analysis programs (RUTO, 2 DOF, 4 DOF) to design the F-15 flight path throttle control system and the optimal flight paths proposed for a flight test. The schedule below gives a time estimate for each of the simulations. These can be run concurrently or consecutively.

There will be four phases of this simulation. The first is the simulation programming and checkout. Use of the MCAIR MACS simulator is attractive since the cost of programming will be reduced by using the F-4E and F-15 equations which are already programmed. About four weeks is estimated to add in and check out the energy management equations and the associated pilot displays, and to check out the complete simulation. The second phase is pilot training and system evaluation. It is estimated that this will take approximately 1/2 working day. A schedule for familiarizing each pilot with each combination of displays is given below.

Test Day #1	Display Configuration	
2 hrs	Optimal Flight Path Display	Bar Throttle Display
1 hr	Flight Director Display	Dial Throttle Display
1 hr	Pitch Ladder Display	Dial Throttle Display

It is estimated that the runs suggested in Section 4.4 would take approximately 2 weeks. If additional runs considering effects of wind gusts, steady winds and temperature variations are required, more time will be required.

The third phase is data reduction. It is estimated that this phase would take one month. The fourth phase is the final report which will take about two weeks to prepare.

An estimated schedule for the simulation study is presented in Figure 87.

Workload to Maintain Accuracy in Following Displays

	Excellent	Good	Average	Poor	Unacceptable
Initial Conditions 1					
Initial Conditions 2					
Initial Conditions 3					
Initial Conditions 4					

Does system degrade handling qualities: If so, how?_____

Should displays be placed elsewhere?_____

Do you feel a combination of informational and command displays would be better?_____

Other displays which may be useful?_____

GP74-0965-85

Figure 86 Throttle/Energy Management Simulation Pilot Questionnaire

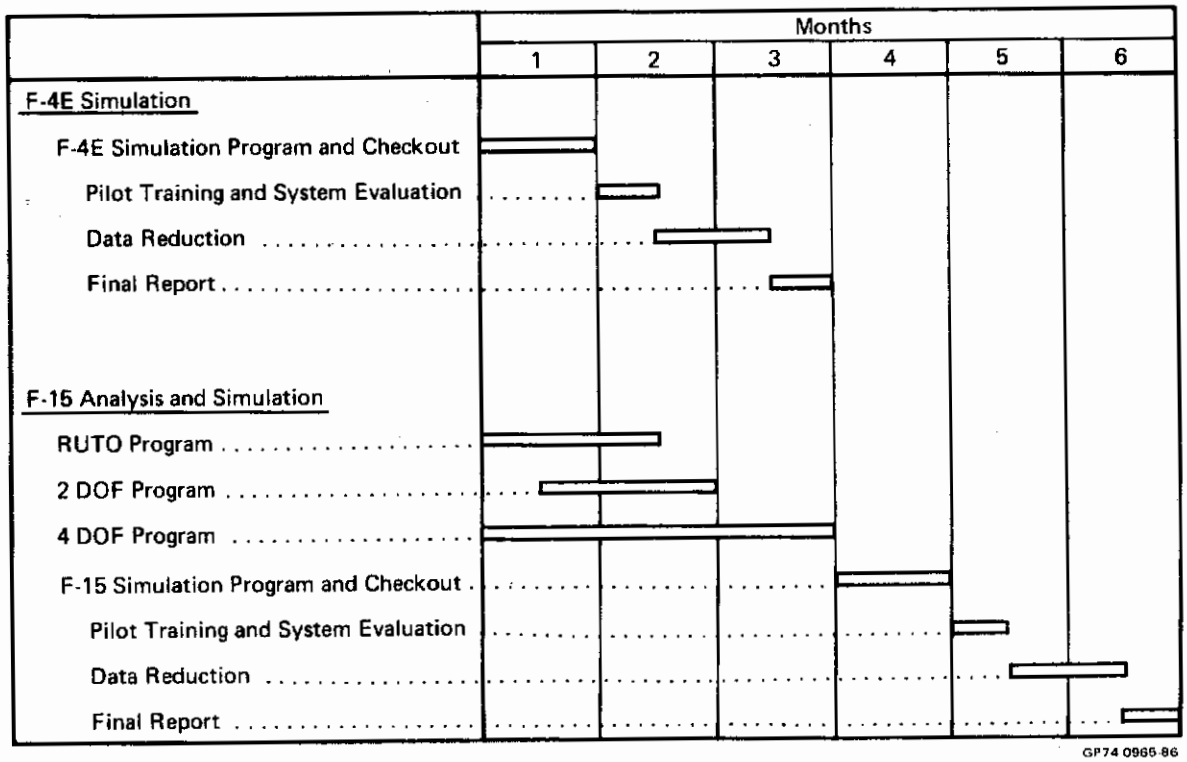

Figure 87 Simulation Schedule

SECTION 5

CONCLUSIONS AND RECOMMENDATIONS

5.1 Conclusions

5.1.1 Application of Modified Rutowski Method to Missions - The benefits of throttle/energy management, which was applied to various mission segments in a previous study (Reference 1.1), have been extended to complete missions, by adding the following capabilities to the generalized Rutowski Method (RUTO Program) for calculation of the optimum flight path and throttle control histories.

a. Descent segments and additional types of cruise segments.

b. Matching of acceleration and dash segments for the same payoff function.

c. Parameter search by the Davidon method to select a sequence of mission segments to a specified end condition.

The Generalized Rutowski method (RUTO program) can optimize a large class of missions of the "Long Range Intercept" type with a relatively small number of calculations. These missions require matching of acceleration segments and dash or cruise segments to give minimum fuel used to a specified range, time and energy. The calculations required are:

a. A curve of minimum steady cruise fuel flow versus cruise or dash velocity.

b. A family of acceleration segments with the weighting constants determined from the equations of lines tangent to the above curve at various cruise velocities, one acceleration path for each tangent point.

The family of Long Range Intercept missions includes previously studies problems as special uses. These are:

a. Minimum fuel to a specified time - loiter

b. Minimum fuel to a specified range - cruise

c. Minimum time to a specified range

A different type of mission was also found, requiring a combination of subsonic and supersonic dash segments, corresponding to average cruise velocities in the transonic region.

5.1.2 Control Concept for Flight Test Demonstration - Flight test missions were defined for the F-4E airplane for which 22 percent fuel savings can be demonstrated by using variable throttle compared to a fixed throttle mission to the same final conditions.

A stored program of flight path and throttle commands (altitude, pitch angle and specific power versus specific energy) was selected as the most practical way to add throttle/energy management capability to an F-4 airplane for demonstration purposes. A properly smoothed path based on the RUTO calculation can be followed closely by the airplane, without large load factor variations, and with performance from two degree-of-freedom trajectories very close to that estimated by the Rutowski method.

Control laws have been defined for the F-4E airplane which provide a stable response and which follow the command paths extremely close with automated control. The control logic uses inputs from existing sensors (h, θ, $\dot{\theta}$, u) and effects control through the F-4 autopilot and an autothrottle servo. The same control signals can be used to drive displays for manual control.

5.2 Recommendations

A manned simulator study should be made to determine the ability of the pilot to control the aircraft on throttle/energy management trajectories, and select the displays and controls laws for a flight test.

Either the F-4E or F-15 aircraft is suitable as a flight test aircraft to demonstrate the fuel savings available by throttle/energy management. Specific aircraft of each type exist with most of the hardware needed for a throttle/energy management control system.

Consideration should be given to definition of a Total Energy Management System for advanced fighters, integrating the Throttle/Energy Management concepts of this study (for beyond-visual-range operation) with the results of the Energy Management/Armament Display study of Reference 21 and related E/M display studies (for within-visual range combat).

Additional studies should be made to extend the present control concept (aimed at a specific flight test mission) to an operational system useable for a variety of mission requirements. It is not feasible to store data for all the paths of interest, all the important performance variables (weight, drag and engine status, winds and non-standard temperature) so methods are needed for obtaining satisfactory performance with a limited amount of stored data.

REFERENCES

1. Thomas, A. N., Porter, J. L., et.al., "Results of an Investigation of Propulsion Management Systems for Advanced Military Aircraft," AFFDL-TR-71-136, October 1971.

2. Turner, R. D., "RUTO - Mission Segment Throttle Control by Rutowski's Method-User's Manual," MDC Report A 1529, 1 February 1972.

3. Wynne, J. W., "Flight Test Plan for Demonstration of Performance Benefits of Throttle/Energy Management", MDC Report A3120, December 1974.

4. Turner, R. D., "RUTOA - Throttle/Energy Management by Generalized Rutowski Method, User's Manual," MDC Report A3065, 12 September 1974.

5. Marsh, R. G., "MITCON, A Computer Program for Time Response of an Aircraft Throttle/Energy Management Control System, User's Manual", MDC Report A3114, 14 October 1974.

6. Fletcher, R., and Powell, M. J. D., "A Rapidly Convergent Steepest Descent Method for Minimization," The Computer Journal, July 1963.

7. Hague, D. S., and Glatt, C. R., "A Guide to the Automated Engineering and Scientific Optimization Program - AESOP", NASA CR-73201, June 1968.

8. Endres, R. F., "Propulsion Data Substantiation for Standard Aircraft Characteristics and Regular Flight Manual. F-111A Numbers 31 through 159", General Dynamics Report FZA-12-065, 25 July 1968.

9. Hasenback, T. C., "Performance Data Substantiation for Standard Aircraft Characteristics Charts and Regular Flight Manual. F-111A Numbers 31 and On. Appendix A: Clean Airplane Trimmed Drag Polars", General Dynamics Report FZA-12-073-A, 18 October 1968.

10. Miles, R. B., "Model F-4E Performance Data and Substantiation", MDC Report A1158 Vols. I and II, 20 July 1971, as revised 10 June 1974.

11. Hammer, R. A., "Model F-4J Performance Data and Substantiation", MDC Report A1216 Vols. I and II, 15 July 1971, as revised 7 June 1974.

12. Anderson, R. D., "Exhaust System Interaction Program: Analysis of Wind Tunnel Data on a 5% Scale F-4 Jet Effects Model in the McDonnell Polysonic Wind Tunnel, PSWT Test 295", MDC Report A1333 Vols. I and II, 4 January 1972.

13. J. D. Roberts, "Extremum or Hill Climbing Regulation: A Statistical Theory Involving Lags, Disturbances and Noise," Proc IEE, Vol. 112, No. 1, January 1965.

14. Jacobs, O.L.R. and Shering, G. C., "Design of a Single-Input Sinusoidal Perturbation Extremum Control System," Proc IEE, Vol. 115, No. 1, January 1969.

15. Jacobs, O.L.R. and Shering, G. C., "Stability of a Sinusoidal Perturbation Extremal Control System," Electronic Letters, Vol. 5, No. 1, April 1969.

16. Bell, D., Griffin, A. W., "Modern Control and Computing" McGraw Hill, 1969, Chapter 7 "Adaptive Control Systems" (p 165-181).

17. Brulle, R. V., and Anderson, D. C. "Design Methods for Specifying Handling Qualities for CCV", AFFDL-TR-73-142, November 1973.

18. Bounds, D. C. and Michael, R. O., "Calculated Longitudinal Stability and Performance Characteristics of the F-4K/M Aircraft Plus the AN/ASA-32H Automatic Flight Control System", MCAIR Report F219, April 1967.

19. Wendl, M. J., et.al., "Flight/Propulsion Control Integration Aspects of Energy Management," SAE Paper 740480, May 1974.

20. Sederstrom, D. C., and Curtner, K. L.,"F-14 Optimum Flight Modes", Honeywell Inc. Technical Report, October 1973.

21. Pruitt, V. R., "DAIS Energy Management Display/Armament Interface," Unpublished AFFDL-TR.

APPENDIX A
MDC SIMULATION FACILITIES

Modern facilities for aerospace research, development, and testing are readily available at MDC, and trained company personnel are on hand to provide efficient operations. The principal facilities and equipment applicable to development of a Throttle/Energy Management Control System program are outlined in this section. Other McDonnell Douglas facilities, not mentioned, can be made available to the program as required.

A.1 Flight Simulation Laboratory

The Flight Simulation Facility is a unified laboratory complex, oriented primarily toward, but not limited to, manned, real-time flight simulation. It consists of a hybrid computer complex, five crew stations, (four fixed base and one motion base), a terrain map, horizon displays, airborne target displays, and associated hardware.

The facility can operate two hybrid simulations and several analog simulations (depending on problem size) simultaneously. Terrain, horizon, and target displays can be routed to any of the crew stations.

The crew stations are equipped with active primary and secondary flight controls and active flight instruments. Radar, head-up-display, and other special displays and controls are provided as required. Long term "g" effects are provided by "g" suits, "g" cushions, and blackout simulation. A wide-spectrum noise generator is used to provide sound cues of engine rpm, afterburner, speedbrake, skin noise, flaps, landing gear, buffet, tire contact, and runway rumble.

A.2 Hybrid Computer Complex

Digital - The CDC 6600 computer has 98K memory, 10 peripheral processors, 12 I/O channels, two line printers, a card reader, a dual CRT console, paper tape reader and punch, three magnetic tape units, six remote consoles, and a 75,000,000 character disk file.

Graphics - The computer graphics system consists of an Information Displays, Incorporated, Input-Output Machine (IDIIOM) with a programmable memory. It functions as an output terminal for the CDC 6600 and will produce up to six separate CRT displays for cockpit use. The principal components are three 21-inch CRT display screens, an interactive light pen, a function keyboard, and an alphanumeric keyboard and printer.

Converters - Two analog-digital and digital-analog converters (ADAGE 770 and 784) are provided for general purpose use with individual hybrid interface links provided for each simulator.

Analog - The analog computers available for hybrid operation are EAI (PACE) 231-R, an Applied Dynamics AD-4, and a MILGO 4100 analog computer.

A.3 Manned Air Combat Simulator (MACS)

The MACS is a real-time, fixed-base, three aircraft hybrid simulator that employs three piloted crew stations (MACS I, II and MACS III) with out-the-window displays. These crew stations may be linked together to provide air-to-air combat capability or used individually for air-to-ground combat studies with an unrestricted field of view and altitude variability.

The 22-foot diameter fiberglass domes house cockpits (40 foot for MACS III) which have been configured as advanced tactical fighter aircraft. The cockpits are complete with active flight instrumentation, such as a three-axis attitude direction indicator, Mach meter, airspeed indicator, angle-of-attack indicator, rate of climb indicator, altimeter, and "g" meter. Other instruments and CRT display capability for radar and moving map simulations, as well as warning lights and switches, are available in the cockpits.

The manual controls integrated into the cockpits include a two-axis column for longitudinal and lateral control which contains a feel system to provide realistic force response to pilot input and rudder pedals for directional control. Both the longitudinal and lateral free systems can be manually trimmed by the operational switch on the control stick. A throttle quadrant and speed brake switch are provided.

Physiological cues in the crew stations give the pilot additional flight information. These include the use of "g" cushions and "g" suits to indicate load factor, buffet simulation by high-frequency square-wave oscillations input to the stick servo, wide-spectrum noise generators to provide sound cues, and a grayout-blackout simulation by dimming cockpit and out-the-window displays.

The equipment for simulated air combat includes a Control Data Corporation (CDC) 6600 digital computer system, hybrid interface link, three separate cockpits, an IDIIOM Graphics Display System, and visual display equipment such as cameras, aircraft models, and TV projectors. The rotational six-degree-of-freedom equations of motion, Euler angles, flight control system,

thrust and drag definitions, aerodynamic model, atmospheric model, missile and gun models, scoring models, and visual display drive equations are simulated on the CDC 6600. The data flow between the CDC 6600 and the crew stations is accomplished via the hybrid interface link.

Testing Capabilities - This facility allows evaluation of the manned performance of proposed weapon systems. It is used to evaluate flight controls, cockpit arrangement and displays, fighter gun and missile effectiveness, and to develop new tactics for fighter aircraft. In addition, it is used to evaluate handling qualities, establish control system design goals, and assess dynamic wing and tail loads.

APPENDIX B

AERODYNAMIC AND ENGINE DATA FOR HYBRID SIMULATION

The following F-4E and/or F-15 aerodynamic data will be provided for the hybrid simulation study.

$C_{L_{RIGID}}$ (M, α, δ_s)

$C_{m_{RIGID}}$ (M, α, δ_s)

$C_{D_{RIGID}}$ (M, α, δ_s)

$\Delta C_{L_{FLEX}}$ (M, h, α, δ_s)

$\Delta C_{m_{FLEX}}$ (M, h, α, δ_s)

M = Mach Number

α = Angle of Attack

δ_s = Stabilator Deflection

h = Altitude

S = Throttle Parameter

$\Delta C_{D_{THRUST}}$ (S, M)

C_{m_q} (M, h)

C_{z_q} (M, h)

$C_{m_{\dot{\alpha}}}$ (M, h)

$C_{z_{\dot{\alpha}}}$ (M, h)

The range of the independent variables for which the aero data is stored should be

Mach Number .2 to 2 Mach

Altitude 0 to 60,000 ft

Stabilator -16 to +12 degrees

Angle of attack -4 to +24 degrees

The following J79-10 and/or F-100 engine data will be provided for the hybrid simulation:

Gross Thrust (M, α, S)

Ram Drag (M, α, S)

Fuel Flow (M, α, S)

M = Mach number

α = Angle of Attack

S = Throttle Setting

The range of the independent variables for which the above tables are stored is:

Mach Number (M) .2 to 2.3 Mach

Altitude (h) 0 to 60,000 ft

Throttle Setting (S) 20 to 115 degrees

LIST OF SYMBOLS

A_{ref}	- Aerodynamic reference area
C_L	- Lift coefficient
C_1, C_2, C_3	- Constants
C_{1_E}, C_{2_E}, C_{3_E}	- Constants
C_U, C_δ, C_T	- Weighting coefficients used in pilot modeling criterion
D	- Total drag
E_s	- Specific energy
E_{s_F}	- Final or combat specific energy
E_1, E_2, E_3, E_4	- Specific energy levels in Davidon option
$\dot{E}$	- Energy rate
$\dot{E}_{opt}$	- Optimal flight path specific excess power
$\dot{E}_{s_c}$	- Commanded energy rate
FPA	- Flight path acceleration
F_G	- Gross engine thrust
G_{E_m}	- Specific energy transfer function model
G_{hm}	- Altitude measurement transfer function model
K	- A constant
K_{cr}	- A constant
K_E,K_h,K_θ,$K_{\dot{\theta}}$	- Control system gains
K_T	- Net thrust versus power lever angle gradient
L/D	- Lift-drag ratio
N_{z_c}	- Commanded normal load factor, body axes
P_s	- Specific power
PAY_E	- A pay-off function
R_{Final}	- Final range in Davidon option

R_T	- Target range
R_{T_0}	- Initial target range
S	- Throttle setting index
S_c	- Commanded throttle setting
T	- Net thrust
T_{Final}	- Final time in Davidon option
U	- Velocity
U_{cr}	- Velocity at cruise
U_{max}	- Maximum velocity
U_T	- Target velocity
W	- Aircraft gross weight
W_{cr}	- Weight at cruise
W_{Final}	- Final weight in Davidon option
dh_ϵ, $d\theta_\epsilon$, $\dot{E}_\epsilon$	- Control law coupled dynamic errors in linear perturbation analyses
g	- Acceleration of gravity
h	- Altitude
h_c	- Commanded flight altitude
h_{opt}	- Optimal flight path altitude
p	- Atmosphere static pressure
q	- Dynamic pressure
s	- Transformed variable in Laplace transform
t_s	- Throttle setting-power level angle in degrees
$t_{s_{opt}}$	- Optimal flight path throttle setting (in degrees)
w_f	- Fuel flow rate
$w_{f_{cr}}$	- Fuel flow rate at cruise

LIST OF SYMBOLS (CONTD)

α	- Angle of attack
γ	- Flight path angle
γ_c	- Commanded flight path angle
ΔF_{cr}	- Fuel consumed in cruise
ΔF_E	- Fuel consumed in energy transition
ΔF_F	- Final fuel consumed
ΔR_{cr}	- Range accomplished in cruise
ΔR_E	- Range accomplished in energy transition
ΔR_F	- Final range accomplished
ΔT_{cr}	- Time elapsed in cruise
ΔT_E	- Time elapsed in energy transition
ΔT_F	- Final time elapsed
ΔT_1, ΔT_2	- Dash duration in Davidon option
ΔU, Δh, $\Delta\theta$	- Perturbed aircraft velocity, altitude, and pitch angle
δ	- Atmosphere static pressure ratio ($p/p_{sea\ level}$)
δ_s	- Stabilator deflection
θ	- Pitch angle
θ_c	- Commanded pitch attitude
θ_{opt}	- Optimal flight path pitch angle
λ_T	- Thrust installation angle
ϕ	- Performance function
$\dot{\phi}$	- Time derivative of performance function
$\dot{\varphi}_{cr}$	- Time derivative of performance function at cruise

☆U.S.Government Printing Office: 1975 — 657-019/429